IAEA TECDOC SERIES

IAEA-TECDOC-1973

Benchmark Analysis of Numerical Models for Tsunami Simulation

IAEA
International Atomic Energy Agency

IAEA SAFETY STANDARDS AND RELATED PUBLICATIONS

IAEA SAFETY STANDARDS

Under the terms of Article III of its Statute, the IAEA is authorized to establish or adopt standards of safety for protection of health and minimization of danger to life and property, and to provide for the application of these standards.

The publications by means of which the IAEA establishes standards are issued in the **IAEA Safety Standards Series**. This series covers nuclear safety, radiation safety, transport safety and waste safety. The publication categories in the series are **Safety Fundamentals**, **Safety Requirements** and **Safety Guides**.

Information on the IAEA's safety standards programme is available at the IAEA Internet site

www.iaea.org/resources/safety-standards

The site provides the texts in English of published and draft safety standards. The texts of safety standards issued in Arabic, Chinese, French, Russian and Spanish, the IAEA Safety Glossary and a status report for safety standards under development are also available. For further information, please contact the IAEA at: Vienna International Centre, PO Box 100, 1400 Vienna, Austria.

All users of IAEA safety standards are invited to inform the IAEA of experience in their use (e.g. as a basis for national regulations, for safety reviews and for training courses) for the purpose of ensuring that they continue to meet users' needs. Information may be provided via the IAEA Internet site or by post, as above, or by email to Official.Mail@iaea.org.

RELATED PUBLICATIONS

The IAEA provides for the application of the standards and, under the terms of Articles III and VIII.C of its Statute, makes available and fosters the exchange of information relating to peaceful nuclear activities and serves as an intermediary among its Member States for this purpose.

Reports on safety in nuclear activities are issued as **Safety Reports**, which provide practical examples and detailed methods that can be used in support of the safety standards.

Other safety related IAEA publications are issued as **Emergency Preparedness and Response** publications, **Radiological Assessment Reports**, the International Nuclear Safety Group's **INSAG Reports**, **Technical Reports** and **TECDOCs**. The IAEA also issues reports on radiological accidents, training manuals and practical manuals, and other special safety related publications.

Security related publications are issued in the **IAEA Nuclear Security Series**.

The **IAEA Nuclear Energy Series** comprises informational publications to encourage and assist research on, and the development and practical application of, nuclear energy for peaceful purposes. It includes reports and guides on the status of and advances in technology, and on experience, good practices and practical examples in the areas of nuclear power, the nuclear fuel cycle, radioactive waste management and decommissioning.

BENCHMARK ANALYSIS OF NUMERICAL MODELS FOR TSUNAMI SIMULATION

The following States are Members of the International Atomic Energy Agency:

AFGHANISTAN
ALBANIA
ALGERIA
ANGOLA
ANTIGUA AND BARBUDA
ARGENTINA
ARMENIA
AUSTRALIA
AUSTRIA
AZERBAIJAN
BAHAMAS
BAHRAIN
BANGLADESH
BARBADOS
BELARUS
BELGIUM
BELIZE
BENIN
BOLIVIA, PLURINATIONAL STATE OF
BOSNIA AND HERZEGOVINA
BOTSWANA
BRAZIL
BRUNEI DARUSSALAM
BULGARIA
BURKINA FASO
BURUNDI
CAMBODIA
CAMEROON
CANADA
CENTRAL AFRICAN REPUBLIC
CHAD
CHILE
CHINA
COLOMBIA
COMOROS
CONGO
COSTA RICA
CÔTE D'IVOIRE
CROATIA
CUBA
CYPRUS
CZECH REPUBLIC
DEMOCRATIC REPUBLIC OF THE CONGO
DENMARK
DJIBOUTI
DOMINICA
DOMINICAN REPUBLIC
ECUADOR
EGYPT
EL SALVADOR
ERITREA
ESTONIA
ESWATINI
ETHIOPIA
FIJI
FINLAND
FRANCE
GABON
GEORGIA
GERMANY
GHANA
GREECE
GRENADA
GUATEMALA
GUYANA
HAITI
HOLY SEE
HONDURAS
HUNGARY
ICELAND
INDIA
INDONESIA
IRAN, ISLAMIC REPUBLIC OF
IRAQ
IRELAND
ISRAEL
ITALY
JAMAICA
JAPAN
JORDAN
KAZAKHSTAN
KENYA
KOREA, REPUBLIC OF
KUWAIT
KYRGYZSTAN
LAO PEOPLE'S DEMOCRATIC REPUBLIC
LATVIA
LEBANON
LESOTHO
LIBERIA
LIBYA
LIECHTENSTEIN
LITHUANIA
LUXEMBOURG
MADAGASCAR
MALAWI
MALAYSIA
MALI
MALTA
MARSHALL ISLANDS
MAURITANIA
MAURITIUS
MEXICO
MONACO
MONGOLIA
MONTENEGRO
MOROCCO
MOZAMBIQUE
MYANMAR
NAMIBIA
NEPAL
NETHERLANDS
NEW ZEALAND
NICARAGUA
NIGER
NIGERIA
NORTH MACEDONIA
NORWAY
OMAN
PAKISTAN
PALAU
PANAMA
PAPUA NEW GUINEA
PARAGUAY
PERU
PHILIPPINES
POLAND
PORTUGAL
QATAR
REPUBLIC OF MOLDOVA
ROMANIA
RUSSIAN FEDERATION
RWANDA
SAINT LUCIA
SAINT VINCENT AND THE GRENADINES
SAMOA
SAN MARINO
SAUDI ARABIA
SENEGAL
SERBIA
SEYCHELLES
SIERRA LEONE
SINGAPORE
SLOVAKIA
SLOVENIA
SOUTH AFRICA
SPAIN
SRI LANKA
SUDAN
SWEDEN
SWITZERLAND
SYRIAN ARAB REPUBLIC
TAJIKISTAN
THAILAND
TOGO
TRINIDAD AND TOBAGO
TUNISIA
TURKEY
TURKMENISTAN
UGANDA
UKRAINE
UNITED ARAB EMIRATES
UNITED KINGDOM OF GREAT BRITAIN AND NORTHERN IRELAND
UNITED REPUBLIC OF TANZANIA
UNITED STATES OF AMERICA
URUGUAY
UZBEKISTAN
VANUATU
VENEZUELA, BOLIVARIAN REPUBLIC OF
VIET NAM
YEMEN
ZAMBIA
ZIMBABWE

The Agency's Statute was approved on 23 October 1956 by the Conference on the Statute of the IAEA held at United Nations Headquarters, New York; it entered into force on 29 July 1957. The Headquarters of the Agency are situated in Vienna. Its principal objective is "to accelerate and enlarge the contribution of atomic energy to peace, health and prosperity throughout the world''.

IAEA-TECDOC-1973

BENCHMARK ANALYSIS OF NUMERICAL MODELS FOR TSUNAMI SIMULATION

INTERNATIONAL ATOMIC ENERGY AGENCY
VIENNA, 2022

COPYRIGHT NOTICE

For further information on this publication, please contact:

External Events Safety Section
International Atomic Energy Agency
Vienna International Centre
PO Box 100
1400 Vienna, Austria
Email: Official.Mail@iaea.org

Printed by the IAEA in Austria
February 2022

IAEA Library Cataloguing in Publication Data

Names: International Atomic Energy Agency.
Title: Benchmark analysis of numerical models for tsunami simulation / International Atomic Energy Agency.
Description: Vienna : International Atomic Energy Agency, 2022. | Series: IAEA TECDOC series, ISSN 1011–4289 ; no. 1973 | Includes bibliographical references.
Identifiers: IAEAL 21-01442 | ISBN 978-92-0-128421-1 (paperback : alk. paper) | ISBN 978-92-0-128321-4 (pdf)
Subjects: LCSH: Nuclear power plants — Natural disaster effects. | Tsunamis — Simulation methods. | Tsunamis — Mathematical models. | Earthquake hazard analysis.

FOREWORD

The 2004 Indian Ocean tsunami damaged the Madras Atomic Power Station in India and led to a new understanding of the importance of flooding hazards caused by tsunamis at nuclear power plant sites. The Great East Japan Earthquake and subsequent tsunami in 2011, which heavily damaged the Fukushima Daiichi nuclear power plant, re-emphasized the importance of tsunami hazard assessments. Recognizing the importance of this topic, the IAEA has developed guidelines and recommendations on tsunami hazard assessment, including IAEA Safety Standards Series No. SSG-18, Meteorological and Hydrological Hazards in Site Evaluation for Nuclear Installations. However, there is still a need for detailed information on the development of state of the art tsunami hazard assessments. To address this need, the IAEA developed this publication to complement SSG-18.

In recent years, there has been an evolution in numerical models used for tsunami propagation and run-up. The numerical models currently available include linear propagation models with shallow water approximations, non-linear shallow water models and Boussinesq models, which offer a wide array of choices for users. In parallel with the development of these numerical models, analysis models have also been developed that numerically simulate tsunami propagation and run-up. The 2011 tsunami, which occurred in a region well equipped with monitoring instruments, provided researchers the opportunity to verify these numerical and analysis models. Fifty specialists and regulators produced this publication from five consultancy meetings, incorporating information from cutting edge tsunami simulation techniques and measurable tsunami data.

It is important that readers of this publication use only verified and validated numerical models and relevant computer codes that have undergone a benchmark analysis. This publication provides information and benchmark problems so readers can select the most appropriate tsunami analysis software to evaluate tsunami hazards for nuclear installations. The supplementary files available on-line provide data from analytical benchmarks and laboratory experiments for comparison with numerical results.

The IAEA appreciates the contributions of all those involved in the drafting and review of this publication. The IAEA officers responsible for this publication were S. Nishizaki and S. Nomura of the Division of Nuclear Installation Safety.

EDITORIAL NOTE

This publication has been prepared from the original material as submitted by the contributors and has not been edited by the editorial staff of the IAEA. The views expressed remain the responsibility of the contributors and do not necessarily represent the views of the IAEA or its Member States.

Neither the IAEA nor its Member States assume any responsibility for consequences which may arise from the use of this publication. This publication does not address questions of responsibility, legal or otherwise, for acts or omissions on the part of any person.

The use of particular designations of countries or territories does not imply any judgement by the publisher, the IAEA, as to the legal status of such countries or territories, of their authorities and institutions or of the delimitation of their boundaries.

The mention of names of specific companies or products (whether or not indicated as registered) does not imply any intention to infringe proprietary rights, nor should it be construed as an endorsement or recommendation on the part of the IAEA.

The authors are responsible for having obtained the necessary permission for the IAEA to reproduce, translate or use material from sources already protected by copyrights.

The IAEA has no responsibility for the persistence or accuracy of URLs for external or third party Internet web sites referred to in this publication and does not guarantee that any content on such web sites is, or will remain, accurate or appropriate.

CONTENTS

1. INTRODUCTION

1.1. BACKGROUND

The tsunamis generated by the 26 December 2004 Sumatra–Andaman earthquake and by the 11 March 2011 earthquake off the Pacific coast of Tohoku are named herein the 2004 Indian Ocean tsunami and the 2011 Great East Japan Earthquake (GEJE) tsunami respectively. Those are among the biggest tsunamis recorded in human history. The 2004 Indian Ocean tsunami caused widespread destruction in several countries bordering the Indian Ocean. Similarly, the GEJE generated one of the most destructive tsunamis that occurred in the recent history of Japan. Apart from the loss of human life and property, these events affected also the sites of nuclear power plants resulting in various amounts of damage.

Owing to the importance of the flooding caused by tsunamis at nuclear power plant sites, the IAEA has embarked upon the development of detailed guidelines on tsunami hazard assessment. IAEA Safety Standards Series No. SSG-18, Meteorological and Hydrological Hazards in Site Evaluation for Nuclear Installations, was published in 2011, bringing out general guidelines in regard to tsunami hazard assessment [1]. However, there is still a need for detailed information on the development of state-of-the-art tsunami hazard assessments. To address this need, the IAEA developed this TECDOC as a supporting publication to SSG-18

In recent years there has been an evolution in numerical models used to compute tsunami propagation and run-up. The numerical models currently available include models such as linear propagation models with shallow water approximations, non-linear shallow water models and Boussinesq models. These models offer a wide array of choices to the users.

In parallel with the development of such numerical models, analysis codes that simulate numerically how tsunami propagates and run-up have been developed, it is important that the user only applies the verified and validated numerical models that have undergone a benchmark analysis.

1.2. OBJECTIVE

This publication provides information and benchmarks problems to enable nuclear installation engineers and regulators to select the most appropriate tsunami analysis software for the evaluation of tsunami hazards for nuclear installations to ensure their safety against tsunamis.

In addition, the benchmark problems will enable such users to become familiar with the limitations of the tsunami analysis modelling available in research and commercial software.

1.3. SCOPE

The scope of this publication is limited to nuclear installations subject to tsunami induced by an earthquake in their lifetime. Tsunamis induced by other mechanisms such as volcanoes and landslides are not considered in this publication.

1.4. STRUCTURE

Following this Introduction, the publication includes six sections and three annexes. Section 2 presents the information on benchmarking, such as the background, procedures and

acceptance criteria, for the validation and verification of the numerical models for the tsunami hazard assessment. Sections 3, 4 and 5 demonstrate benchmark problems including problem definition and data based on the analytical solutions, laboratory experiments and field measurements, respectively. The publication is completed by Annexes I–III, that provide case studies of benchmark problems based on the above analytical solutions, laboratory experiments and field measurements by using specific software. Also, the data for these benchmark problems are given in the link with supplementary material in Annex IV.

2. BENCHMARKING TSUNAMI MODELS

2.1. GENERAL

Numerical modelling for tsunamis was initiated in the 1980s by applying the numerical solutions of the linear form of shallow water equations. Innovations in hardware and software provided a significant evolution of tsunami models in the 1990s. Benchmarking based on analytical solutions, experimental and field data has been used in validation of models since the National Science Foundation of the United States of America funded the Catalina Workshop in 1990. Further workshops on benchmarking in tsunami numerical modelling followed in 1996 and 2004 with the National Science Foundation support in Catalina Island, United States of America.

The correctness and accuracy of the numerical results have to be validated and verified by applying to the problems in small, analytical and experimental, and geophysical field scale. Hence the level of uncertainty can be reduced. In this context, verification is the process of determining whether or not the model fulfils all the demands imposed by the model and validation is the process of ensuring that the model represents geophysical reality [2]. When coupled with real time tsunami measurements from tsunameters, validated and verified codes are the only choice for realistic forecasting of the tsunami propagation and inundation.

2.2. BACKGROUND

In 1946, a big earthquake occurred off the coast of Alaska's Aleutian Islands generating Pacific-wide tsunamis which killed many people. In 1960, another big earthquake occurred off the southern coast of Chile that generated powerful tsunamis that nearly circled the earth killing many people.

After these events, the administrative and scientific interest in tsunamis increased and efforts focused on the initiation of a Pacific Tsunami Warning System. Since there were no instrument measurements in the open ocean, the tsunami science has evolved differently from research on other extreme natural hazards [3].

Tsunami inundation models have evolved since the 1990s thanks to many validation projects considering both one dimensional and two-dimensional models in space, laboratory experiments and field simulations. A comprehensive discussion is provided in Ref. [3] on the evolution of tsunami hydrodynamics in time. The conclusion of that analysis is that numerical models in general are successful to simulate all phases of tsunami life, namely: the offshore wave propagation, the near shore dynamics and in the inundation zone. However, strict control has to be maintained on critical modelling parameters; one of them is the 'friction' factor which aims at representing the energy dissipation. It is recommended that any model be validated by

comparison with analytical solutions, laboratory measurements and field measurements [2]. It is also not guaranteed that a numerical model that has performed well in all the benchmark tests will produce realistic inundation predictions with any given tsunami source. However, the model validation can significantly reduce the variability in the computed results as a function of the modelling parameters and it is always recommended. The uncertainty in the initial conditions (i.e. wave sources) and bathymetric and/or topographic data also play an important role in the result reliability and need to be explicitly addressed. The flowchart of Fig. 1 shows a procedure for testing numerical model parameters and initial data assumptions.

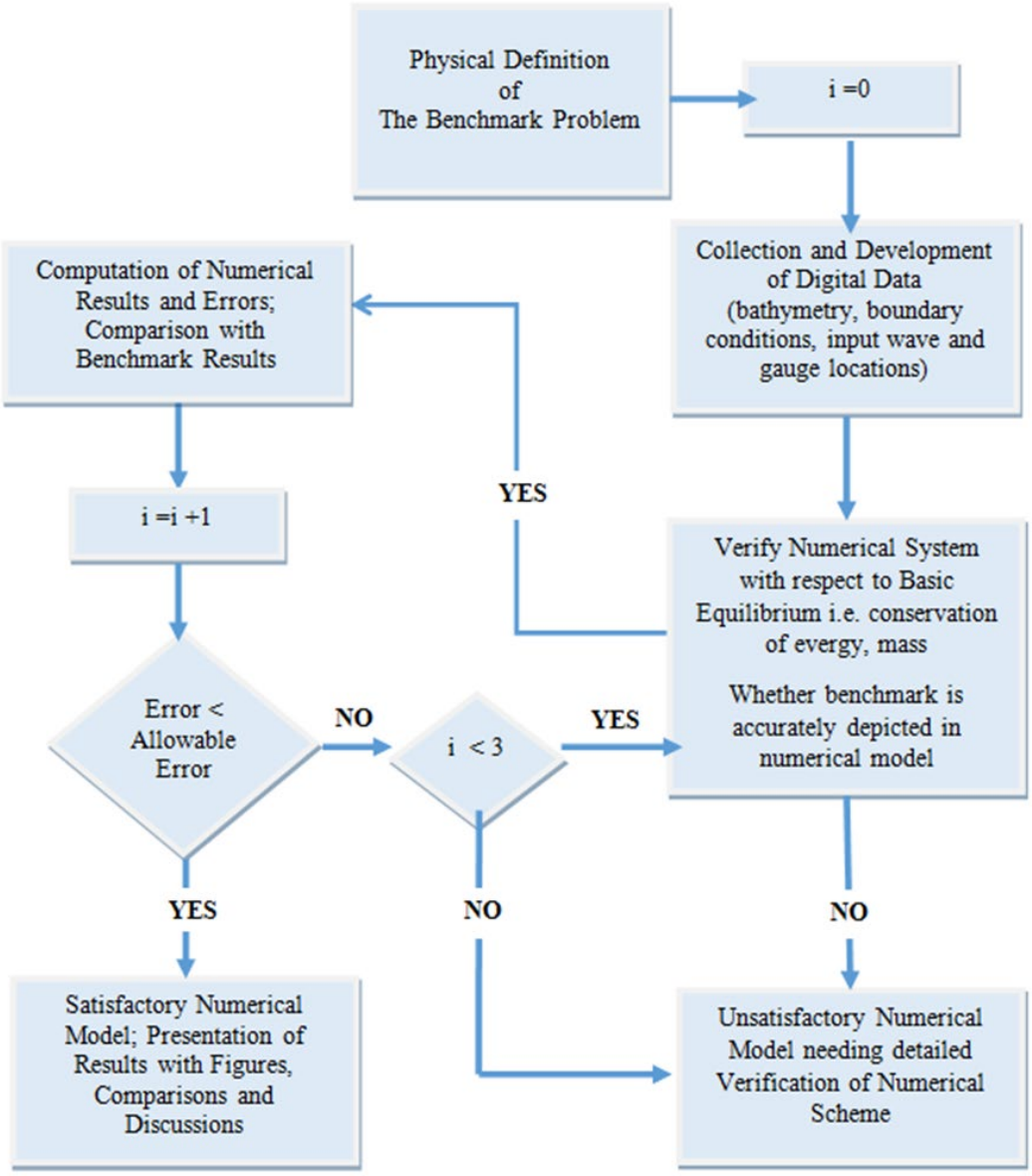

FIG. 1. Flowchart of testing the numerical model with the benchmark problem.

Considering their simplicity in modelling and evaluating the results, analytical solutions to the corresponding 1+1 hydrodynamic equations are invaluable to the process of model validation and these are covered in Section 3. The procedure for validating 2+1 codes are

discussed and the examples of various categories of benchmark problems are presented in Section 3, 4 and 5, respectively.

It has to be ensured that before taking up a code validation based on problems defined in this publication, necessary checks on numerical modelling are completed [2]. These checks include the following: (i) mass conservation, (ii) energy conservation and (iii) convergence [4].

While the conservation of mass is one of the governing equations of long wave motion solved in any numerical model of tsunamis, cumulative numerical approximations can sometimes result in the violation of mass conservation. It may occur while using friction factors, or smoothing techniques in inundation computations. Calculations of conservation of mass have to be such that the total initial displaced volume is within 5% of the total displaced volume at the end of the computation, i.e. when the initial wave is entirely reflected and outgoing to offshore [2].

The total energy input to the simulation domain has to be conserved throughout the simulation where the boundaries are closed. In the case of the sea state, the average (mean) energy density per unit area of gravity waves on the water surface is proportional to the water level squared, according to the linear wave theory (Eq. (1)).

$$E = \frac{1}{8}\rho g \eta^2 \tag{1}$$

where η is the water level, ρ is the water density and g is the gravitational acceleration. E is the mean wave energy density per unit horizontal area (J/m^2), the sum of both the kinetic and potential energy density per unit horizontal area. The potential energy density is equal to the kinetic energy density, both contributing half to the total wave energy density E as can be expected from the equipartition theorem. In ocean waves, surface tension effects are negligible for wavelengths above a few decimetres.

The energy at a certain time step can be computed by summing up the squares of the water elevations. The sum has to be conserved at any time step in simulation if the boundaries are closed in the study domain.

After satisfying mass and energy conservation, the convergence of the numerical model needs to be checked to a certain asymptotic limit, ideally the actual solution of the equations solved, if one exists. The optimal locations to check the convergence are the extreme run-up and rundown [4]. The numerical predictions need to be seen to converge to a certain value and it has to be ensured that further reductions in step sizes do not change the computed results [2].

2.3. BENCHMARK PROBLEMS

It is imperative that all numerical models used for the simulation of tsunami propagation undergo multiple stages of verification and validation. This process, in addition to basic checks, like conservation of mass and conservation of energy, needs to be checked in any numerical scheme for tsunami modelling [2].

The process of verification and validation is conducted by submitting the numerical model under consideration to a series of benchmark tests that are commonly accepted by the research community. The most important of those benchmarks with new problems are included in this publication.

Generally, three categories of data are used for defining benchmark tests for validation and verification of tsunami numerical models. These, as given before, are: (i) analytical solutions; (ii) laboratory experiments; and (iii) field measurements [2].

These problems are designed to test the accuracy of numerical models including idealized scenarios as well as actual situations. It may also be noted that analytical solutions are derived for shallow water equations in a linear form. As this does not capture the wave dispersion, one has to exercise caution while comparing these analytical solutions with the outputs from numerical models that are not bounded by shallow water approximations. However, Kanoğlu et al. [5] provide analytical benchmark of the linear form for shallow water equations with dispersion.

2.3.1. Examples of benchmarks

There are numerous benchmark problems for tsunami modelling. The most important problems are presented in Refs [2, 4, 6]. Those benchmarks have to be used as a basis in the validation procedures. In this publication four benchmark problems are presented. They are illustrated in Table 1.

TABLE 1. CURRENT BENCHMARK TESTS FOR MODEL VERIFICATION AND VALIDATION USED IN THIS PUBLICATION

No	Type of benchmark	Problem statement	Phenomenological representation	Reference
1	Analytical	Wave run-up on a plane beach	Non-linear propagation and run-up	Kanoğlu [7]
2	Analytical	Focusing on tsunami	Linear propagation and focusing	Kanoğlu, et al. [5]
3	Laboratory experiments	Run-up onto a complex three dimensional beach. Monai Valley	Non-linear propagation and run-up	Matsuyama and Tanaka [8]
4	Observed data	GEJE and tsunami	Pacific Ocean: Linear propagation, dispersion, Coriolis effects, etc. at Deep-ocean Assessment and Reporting of Tsunami (DART) locations and subsequent non-linear wave amplification and run-up in distant shores Japan coast: non-linear propagation and run-up	Ozawa et al. [9], Sato et al. [10], Kawai and Nagare [11]

Apart from the field data from the 2011 tsunami event, this publication contains two benchmark problems (one analytical and one laboratory experiment/problem) that have been recently published. It may be noted that the validation of numerical models is a continuous process. As and when new data and/or knowledge are obtained, these models need to undergo further validation exercises. Here, two new benchmark problems (one analytical and one laboratory experiment problem) are proposed in the next sections.

2.3.2. Model validation

Though it would have been ideal to obtain results that match the suggested problems, in many cases, owing to approximations incorporated during formulation of numerical schemes, the results are different from the observed data. In field benchmarks, additional issues arise owing to uncertainties in the source model, as well as in the bathymetry and topography of the observation points where the run-ups and inundation are measured. The validation, verification, standards, criteria and procedures for the National Oceanic and Atmospheric Administration (NOAA) evaluation of tsunami numerical models have been discussed in detail in the following publications [2, 4, 6]. Four different benchmark tests are used for the validation and verification of the tsunami numerical models in the National Tsunami Hazard Mitigation Program (NTHMP) [6]. These benchmark problems are: (i) analytical solution of a single wave on a simple beach (BP1 in [6]); (ii) laboratory experiments of a solitary wave on a simple beach (BP4); (iii) laboratory experiments of a solitary wave on a conical island (BP6); and (iv) field measurements of the Okushiri island tsunami (BP9). The error bounds of the run-up values for these benchmark problems are given with 5% for BP1, 5% for non-breaking waves in BP4, 10% for breaking waves in BP4, 20% for non-breaking waves in BP4 and 20% for BP6 and BP9 [6]. These bounds can be used as the acceptance criteria for the accuracy of the numerical models.

It may be noted here that different types of error can be introduced to determine the correlation between the calculated values y_i and the observed (analytical or experimental or field) values $f(x_i)$. In NOAA [6], three different types of error are presented: (i) the normalized root mean square deviations (RMS) error; (ii) the error of the maximum value (MAX) between the numerical results and the observed (analytical or experimental or field) data; and (iii) the relative error (ERR) of the multiple (minimum, average and maximum) values of the numerical and observed data that are collected in one specific location or region.

The percent normalized RMS error is applied within a space segment or time period to all observed data points. It can be defined as given in Eq. (2):

$$\text{RMS error: } 100 \times \frac{1}{f(x_i)_{max} - f(x_i)_{min}} \sqrt{\frac{\sum (f(x_i) - y_i)^2}{n}} \tag{2}$$

where the $f(x_i)$ values are the observed data and the difference between the maximum and minimum values of the observed data are used for normalization. It can be multiplied by 100 to convert into a percentage.

The main use of the RMS error is to assess the accuracy of a model in predicting the entire set of observed data, which can also be defined as overall model performance.

MAX is used to quantify each model's predictive accuracy for the maximum wave amplitude or run-up regardless of the location where or when this maximum occurs. The following formulation is used to measure the differences between the maximum computed numerical and observed (analytical, experimental and field) values (Eq. (3)):

$$\text{MAX: } 100 \times \frac{|f(x_i)_{max} - y_{i\,max}|}{f(x_i)_{max}} \tag{3}$$

where $f(x_i)_{max}$ is the maximum value of the observed (analytical, experimental, field) data and $y_{i\,max}$ is the maximum value of the computed data at the same time or location. It has to be

noted that the expression used for MAX is a relative error based on the maximum magnitude of the observed values.

ERR is used to measure the model performance. It is the relative error for multiple values that are collected in one specific location or region. This error is practically the same as MAX but it has been defined to determine the model accuracy in predicting the run-up against multiple values that have been recorded by a tsunami survey team in a region with similar inundation characteristics or geomorphology. The regional dataset is reduced to three values, minimum, maximum and average that represent the inundation at a specific location. The error is then defined as follows (Eq. (4)):

$$ERR = \begin{cases} 0 & If\ f(x_i)_{\min} \le y_{i\,ave} \le f(x_i)_{\max} \\ \dfrac{\min[abs(f(x_i)_{\min} - y_{i\min}), abs(f(x_i)_{ave} - y_{i\,ave}), abs(f(x_i)_{\max} - y_{i\max})]}{D} & Otherwise \end{cases} \quad (4)$$

where the denominator D takes one of the following values: $f(x_i)_{max}$, $f(x_i)_{ave}$ or $f(x_i)_{min}$. D is selected according to the minimum value of the numerator. For example, if $|f(x_i)_{ave} - y_{i\ ave}|$ is the minimum value in the numerator, then the denominator D = $f(x_i)_{ave}$.

The MAX and ERR errors are the only formulation used for verification and validation with observed data in the model comparison and discussion. However, RMS errors further help to assess the accuracy of a model in predicting the entire set of observed data (with the correct magnitude and phase). In other words, it is a good metric tool for assessing the overall model performance.

It has to be noted here that in the calculation of the RMS error, the datasets, numerical and observed, have to be within the same intervals in the selected time or space segment.

It also has to be noted here that the RMS error deals with an error of absolute values and does not show the bias of the code's prediction (e.g. under-prediction or over-prediction). The RMS approach is based on the assumption that the error is normally distributed with no bias. Therefore, the user may need to check the bias of the code's prediction with the associated standard deviation and the normality of the error distribution.

In the benchmark problems given in this publication, there are observed (analytical and experimental) velocity values. The velocity computations in numerical models differ at shallow depth because of the nature and limit of shallow water equations. Therefore, the error limits for velocity comparisons can be large especially for the shallow depths. As a preliminary estimation, the error limits for velocity values for analytical and experimental benchmarks can be selected as 25%.

Maximum allowable errors for each type of benchmark problem are given in Table 2. These maximum allowable errors can also be used as acceptance limits for similar cases.

TABLE 2. MAXIMUM ALLOWABLE ERRORS FOR EACH TYPE OF BENCHMARK PROBLEM

	Category	Parameter		Allowable error (%)	
		MAX & ERR	RMS	MAX & ERR	RMS[a]
1	Analytical solution	Run-up or maximum/minimum water elevation	Water level time history/water level in the selected segment of the data	5 [6]	10[a]
2	Laboratory experiments	Run-up or maximum/minimum water elevation	Water level time history/water level in the selected segment of the data	10 [6]	15[a]
3	Field measurements	Run-up or maximum/minimum water elevation	Water level time history/water level in the selected segment of the data	20 [6]	25[a]
4	Analytical solution	Maximum/minimum velocity	Velocity time history/velocity in the selected segment of the data	25[a]	10[a]
5	Laboratory experiments	Maximum/minimum velocity	Velocity time history/velocity in the selected segment of the data	25[a]	15[a]

[a]: These values are the guidance for benchmark problems in this publication and may be updated based on future studies.

While evaluating the field data, Aida's indices [12] could be used as additional measures of error. The fit for the fault model as the tsunami source can be evaluated by comparing the observed and calculated tsunami heights. Aida [12] evaluated how good the fitting is on the basis of the geometric average K and the geometric standard deviation κ. These have been applied as indices of fit in space between the recorded and computed tsunami heights. The definitions of K and κ are explained in the equations below:

$$\log K = \frac{1}{N}\sum_{i=1}^{n} \log K_i \tag{5}$$

$$\log \kappa = \left[\frac{1}{N}\left\{\sum_{i=1}^{n} (\log K_i)^2 - n(\log K)^2\right\}\right]^{1/2} \tag{6}$$

where n is the number of data for evaluation, $K_i = R_i/H_i$, R_i is the recorded tsunami height at location i, H_i is the calculated tsunami height at location i. Since the estimated error of κ depends on the number of samples, the number of samples needs to be stated for reference in calculating $K$and κ.

If a widely accepted and validated fault parameter is used, it is expected that the geometric average K would be nearly 1.0 and the geometric standard deviation κ, whose

minimum value is 1, is as small as possible (close to 1). The following criteria have to be considered for achieving a reproducibility of run-up values:

(a) The distance from the site is short;

(b) The coastal and sea bottom topographies around the site are similar;

(c) The statistically sufficient number of run-up is used for calculating K and κ.

It is suggested by the Japan Society of Civil Engineers (JSCE) [13] to use the following conditions as a rule of thumb for K and κ of wide areas:

$$0.95 < K < 1.05, \kappa < 1.45 \tag{7}$$

These conditions can also be used as acceptance limits for similar cases.

3. BENCHMARK PROBLEMS BASED ON ANALYTICAL SOLUTIONS

3.1. BACKGROUND

Analytical solutions of long wave run-up on a sloping beach (2-D problem) and amplification of the long wave during propagation (3-D problem) are given in this section as two different analytical benchmark problems.

Tsunami coastal flooding occurs with the shoreline motion and run-up. This process can be computed theoretically in some special problems. One of these problems is the non-linear evolution and run-up of a solitary wave over a sloping bottom. Synolakis solved this problem as a boundary value problem considering canonical bathymetry [14].

The linear theory predicts that the maximum run-up of non-breaking waves on plane beaches is given by the run-up law [14]:

$$\frac{R_u}{d} = 2.831 \sqrt{\cot(\beta)} \left(\frac{H}{d}\right)^{\frac{5}{4}} \tag{8}$$

Where R_u is the Run-up, $\cot(\beta)$ is the beach slope, H is the height of the solitary wave at $L/2$ distance from the toe of the slope, d is the water depth at the toe of the slope. This relationship models the laboratory experimental data very well. It can be mentioned here that the analytical and experimental studies in Ref. [14] can be the first benchmark problem for long waves.

The linear and the non-linear theory, when solved with identical initial conditions, predict identical run-up. The non-linear theory models the details of the surface elevation of the climb of a long wave on a beach satisfactorily, indicating that dispersion is a much weaker process than non-linearity during shoaling.

In the analytical solution the non-linear form of shallow water equations is used without friction. In numerical simulations similar conditions are also used. But in experimental studies [14] the surface of the sloping beach has been made smooth in order to decrease the friction effect.

Kanoğlu [7] solved the non-linear evolution of any given wave form over a sloping beach as an initial value problem. Later, Kanoğlu and Synolakis [15] solved a similar problem considering more general initial conditions, i.e. an initial wave with velocity.

Kanoğlu et al. [5] introduced a new analytical solution to study the propagation of a finite strip source over constant depth using linear shallow-water wave theory. This solution is not only exact, but also general and allows the use of realistic initial waveforms such as N-waves which are defined in [16]. The effect of focusing from a strip source is explained using linear non-dispersive and linear dispersive theories analytically and is explored using non-linear non-dispersive and weakly non-linear weakly dispersive theories, numerically.

These sample problems of (i) long wave run-up on a sloping beach and (ii) focusing of a strip source are given in the following sub-sections.

3.2. ANALYTICAL BENCHMARK PROBLEM 1 (RUN-UP OF LONG WAVES)

3.2.1. Problem definition

This problem is a simple setup for a run-up modelling exercise: a uniformly sloping beach with no variation in the lateral direction as a 2-D problem in the vertical plane. The initial-value-problem technique introduced by Carrier, Wu and Yeh [17] is used to produce the benchmark data. For the analytical benchmark problem, the beach slope is extended to infinite and fixed at 1/10. The 2-D channel cross-section and the initial free surface elevation as a certain wave with specific shape are given in Figs 2 and 3. The initial wave profile is selected to be similar with [17]. The free surface and velocity profiles at t = 0 s, 160 s, 175 s and 220 s are computed and plotted in the Figs 3 to 6.

The detailed shoreline trajectory is the primary theme. The algorithm used to calculate the motion of the shoreline (the air–water–beach interface) is important in the numerical model. Specifically, it is needed to present the temporal variations of the shoreline location and shoreline velocity from t = 100 s to t = 280 s.

Run-up onto a plane beach is solved theoretically by Kanoğlu [18]. The profile of the initial wave and sloping beach, snapshots of water surface and velocity distribution and shoreline position and velocities are shown in Figs 4 to 6. In these figures, the thick black line is the cross-section of 2-D channel and the blue line is either the water surface elevation or the velocity magnitude in the direction of the wave. Time change of shoreline distance from the original position and shoreline velocity are shown in Fig. 7. In numerical solutions, it is suggested by Horrillo et al. [19] that the grid size be selected to satisfy at least ten grids along the inundation distance for reliable model outputs.

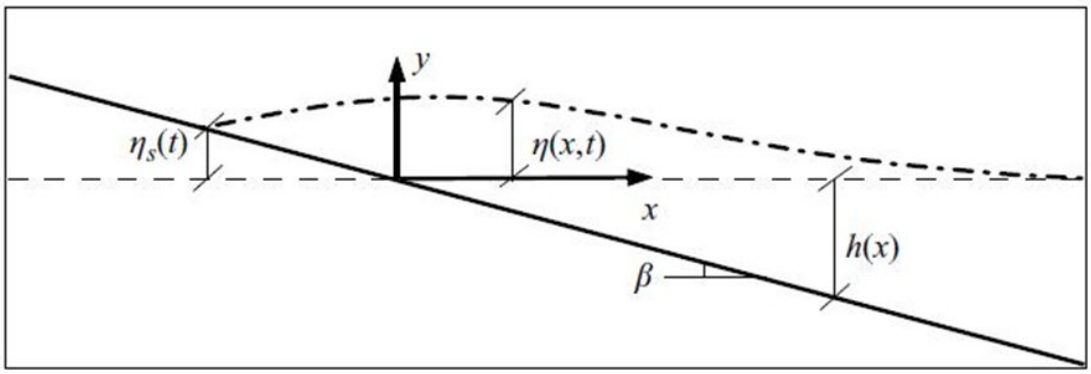

FIG. 2. Definition sketch of sloping beach which is used in analytical benchmarking (reproduced with permission of Cambridge University Press [7]).

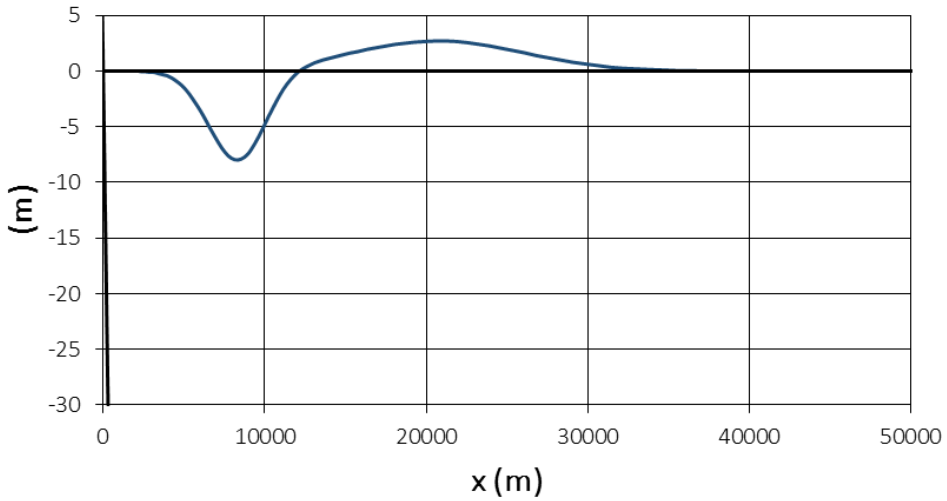

FIG. 3. Problem of run-up on a 1/10 sloping beach (distorted cross-section of the 2-D channel - thick black line and the initial wave - blue line).

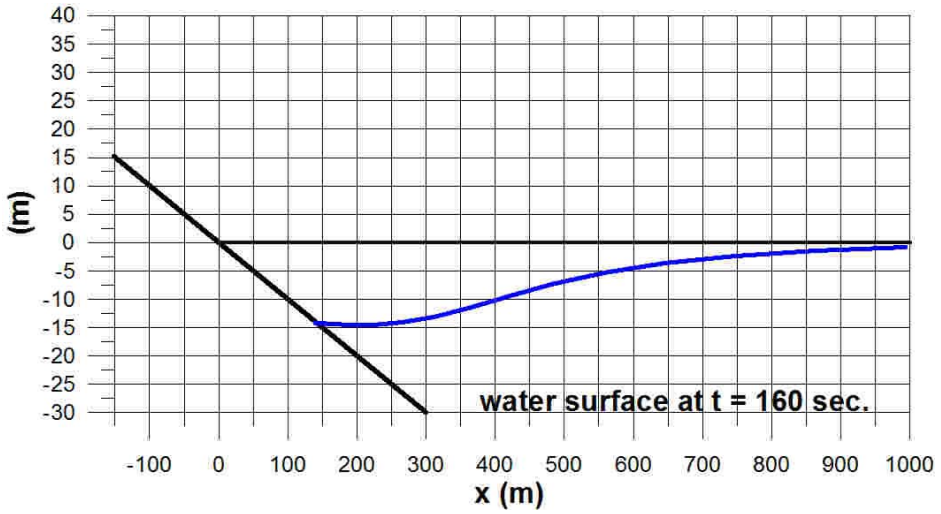

(a) Water surface elevation

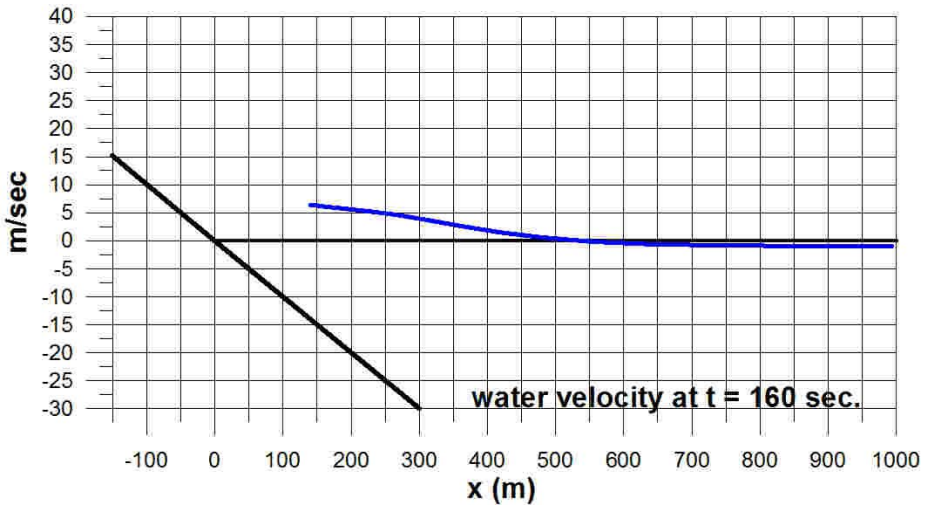

(b) Water particle velocities

FIG. 4. Water surface elevation (a) and water particle velocities (b) at the time of 160 s.

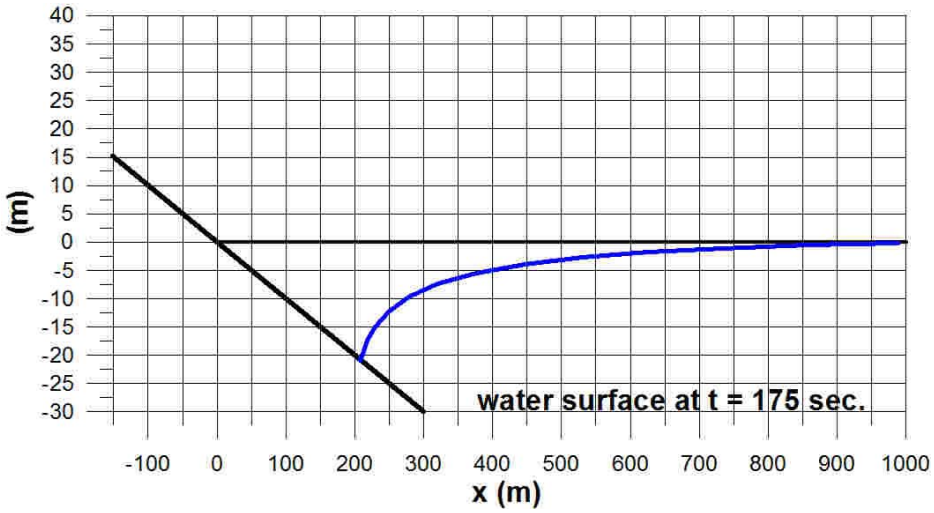

(a) Water surface elevation

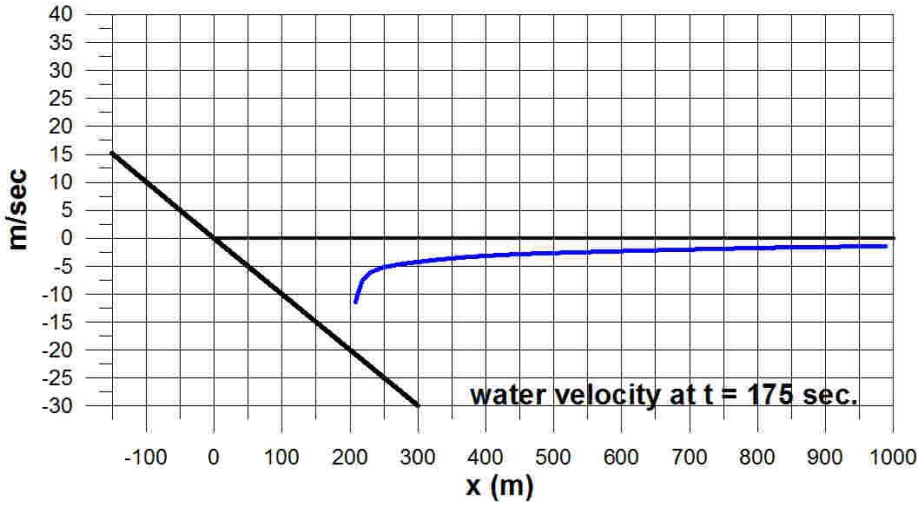

(b) Water particle velocities

FIG. 5. Water surface elevation (a) and water particle velocities (b) at the time of 175 s.

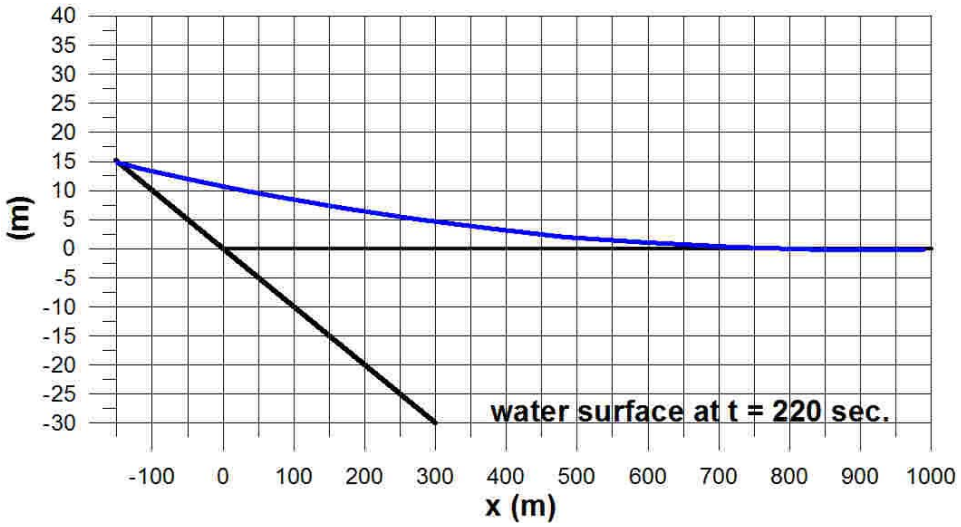

(a) Water surface elevation

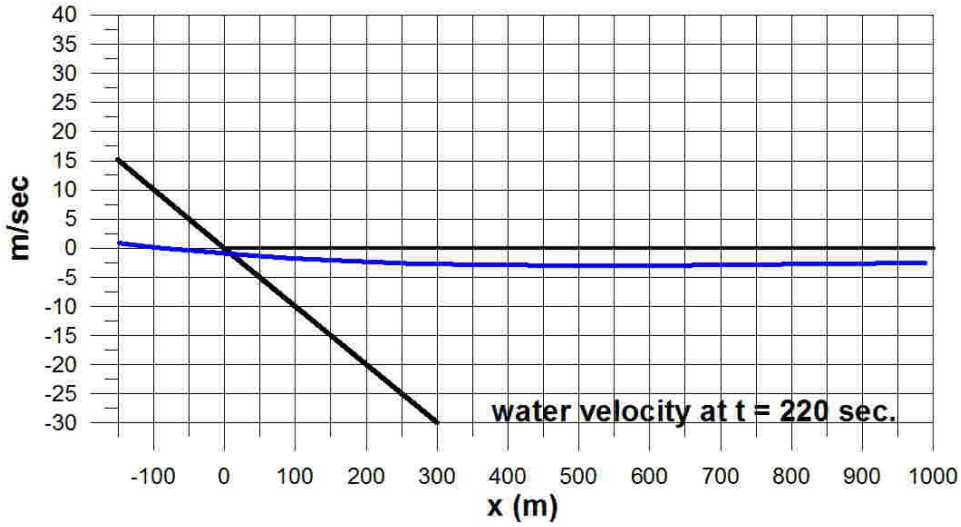

(b) Water particle velocities

FIG. 6. Water surface elevation (a) and water particle velocities (b) at the time of 220 s.

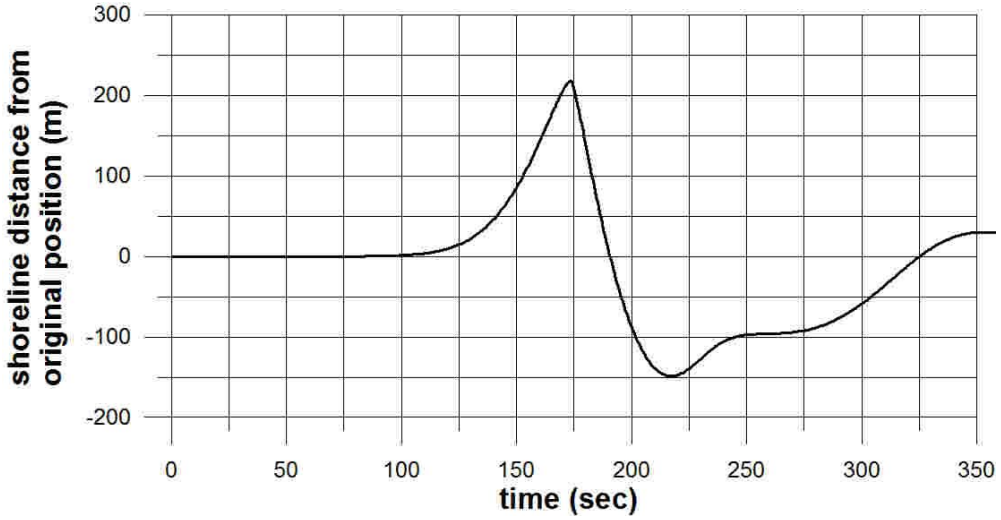

(a) Time change of shoreline distance from the original position

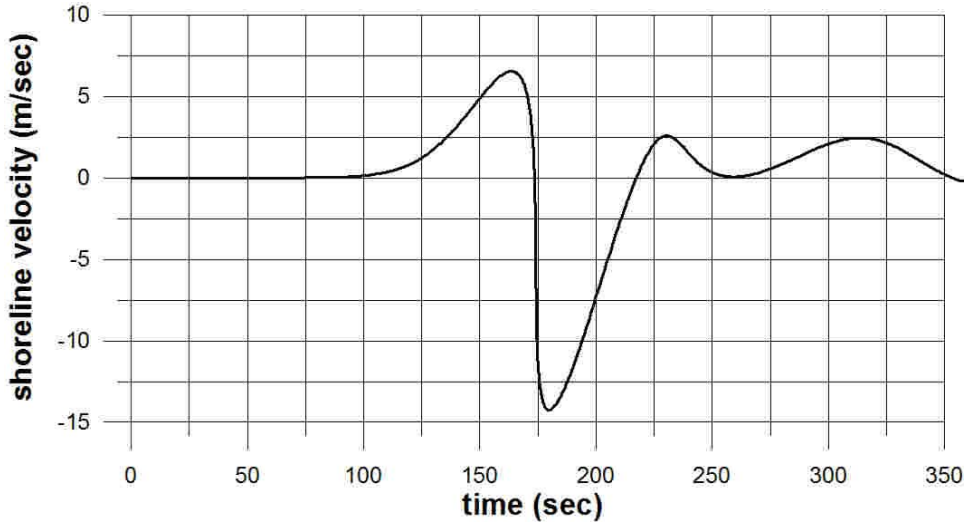

(b) Temporal variation of shoreline velocity

FIG. 7. Time change of shoreline distance from the original position (a) and temporal variation of shoreline velocity (b).

3.2.2. Data

The data (bathymetry, input wave, water surface elevations and velocities along the channel at the time 160 s, 175 s and 220 s) and the time history of shoreline coordinate and shoreline velocity are given in a single excel file "Analytical solution-1.xlsx" enclosed in the link with supplementary material (Annex IV).

3.3. ANALYTICAL BENCHMARK PROBLEM 2 (STRIP SOURCE)

3.3.1. Problem definition

This problem is about evolution and focusing of long waves with finite crest over constant depth. The problem focuses on finite strip source over constant depth using linear shallow-water wave theory.

Evolution of a finite-crested long wave over constant depth d is considered (Fig. 8). Kanoğlu et al. [5] provide an analytical solution of the problem using the linear shallow-water wave equation as field equation. The dimensional equation is:

$$\tilde{\eta}_{\tilde{t}\tilde{t}} - gd\left(\tilde{\eta}_{\tilde{x}\tilde{x}} + \tilde{\eta}_{\tilde{y}\tilde{y}}\right) = 0 \tag{9}$$

in terms of free surface elevation $\tilde{\eta}(\tilde{x}, \tilde{y}, \tilde{t})$, where g is the gravitational acceleration and d is the depth. The following dimensionless variables can be introduced:

$$(x, y) = \frac{\tilde{x},\tilde{y}}{d}, \eta = \frac{\tilde{\eta}}{d}, t = \frac{\tilde{t}}{\sqrt{\frac{d}{g}}} \tag{10}$$

The dimensionless form of Eq. (9) then reads

$$\eta_{tt} - \eta_{xx} - \eta_{yy} = 0 \tag{11}$$

Kanoğlu et al. [5] suggest an initial value problem solution for Eq. (9) with given initial surface profile:

$$\eta_0(x, y) = \frac{\varepsilon H}{2}[\tanh\gamma(x - x_0) - \tanh\gamma(x - x_0 - L)](y - y_2)sech^2\gamma(y - y_1) \tag{12}$$

having zero initial velocity, $\eta_t\ (x, y, t = 0)$. In Eq. (12), ε is a scaling parameter and the points y_1 and y_2 locate elevation and depression parts of the dipolar initial wave, respectively. x_0 is the starting point of the wave on the x-axis (see Fig. 8). The parameter γ is defined to be $\gamma = \sqrt{3Hp_0/4}$ in which p_0 is a parameter employed to adjust the steepness of the wave. Here it has to be noted that the water surface elevation is represented by the symbol η and the maximum water level is represented by the symbol H. The initial wave defined in Eq. (12) is an N-wave type initial condition first proposed by Tadepalli and Synolakis [16], but it has finite crest length (L) along the x-axis.

Maximum wave envelope and time evolutions of the initial wave defined by Eq. (12) are presented in Fig. 9.

Initial wave parameters are shown in Table 3.

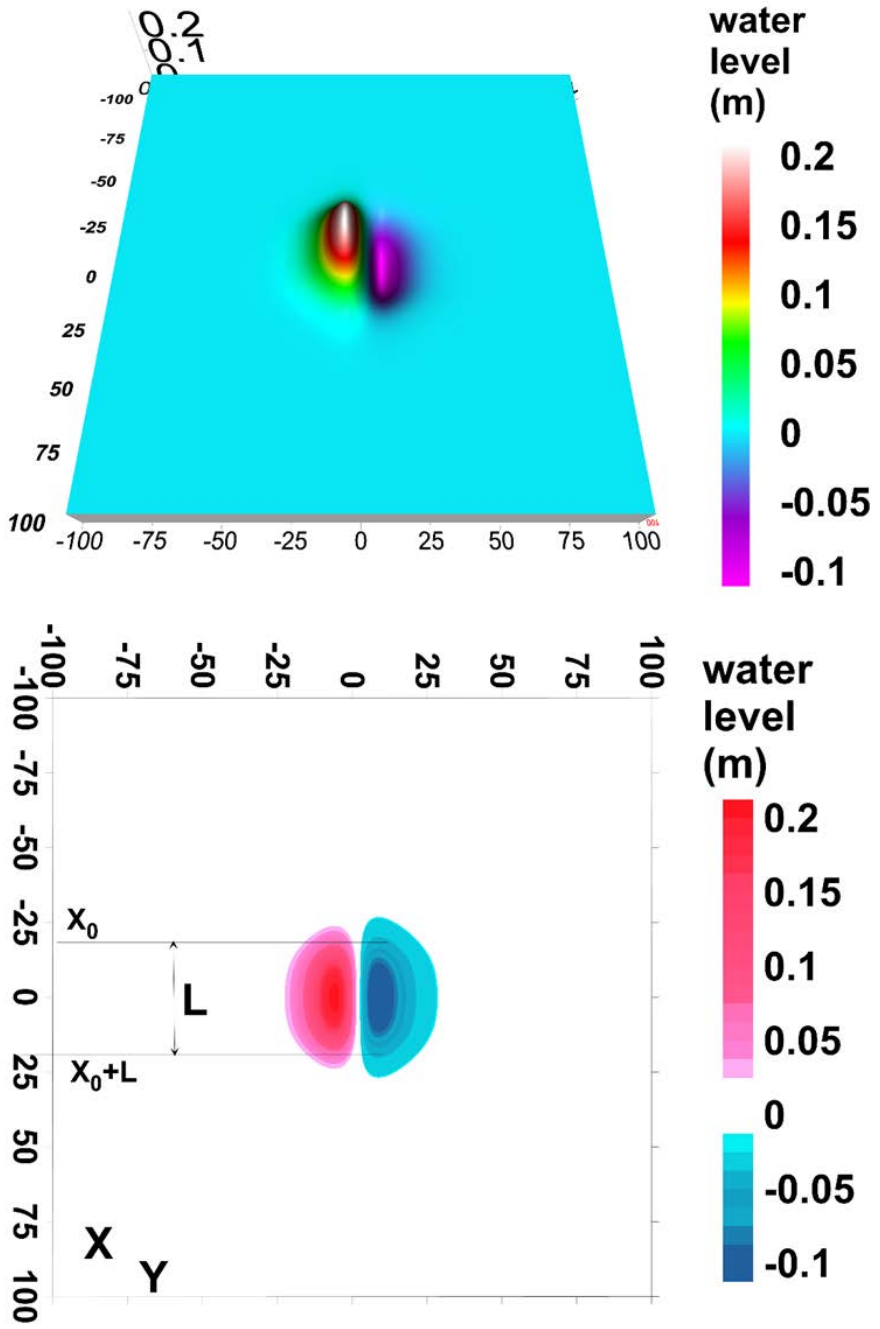

FIG. 8. Initial displacement given in Eq. (12) (top) and the computational domain (bottom).

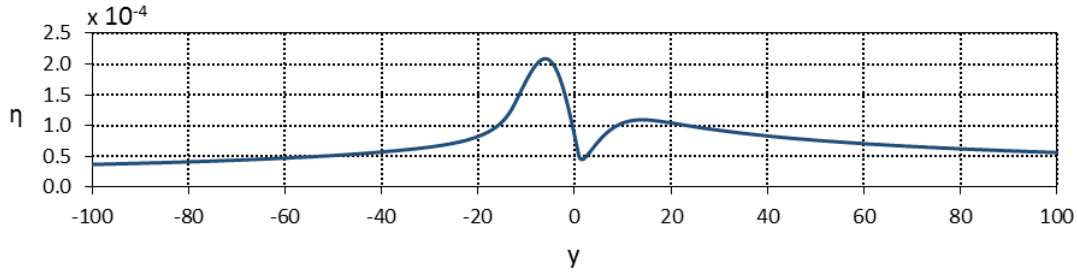

(a) Maximum envelope

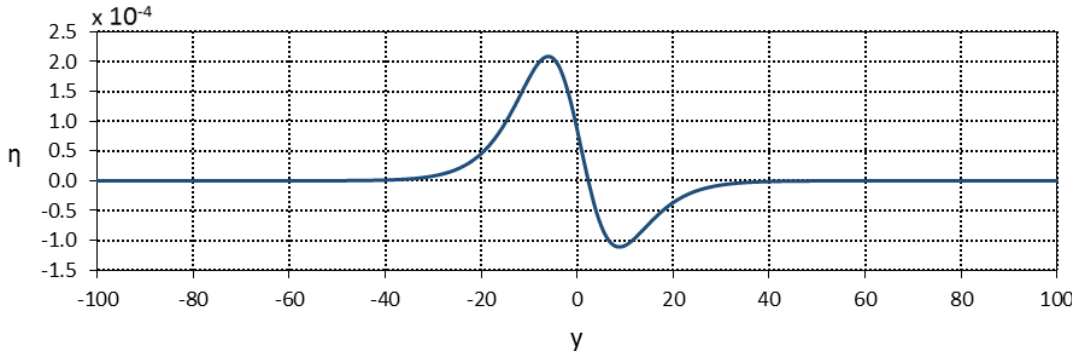

(b) t = 0 s

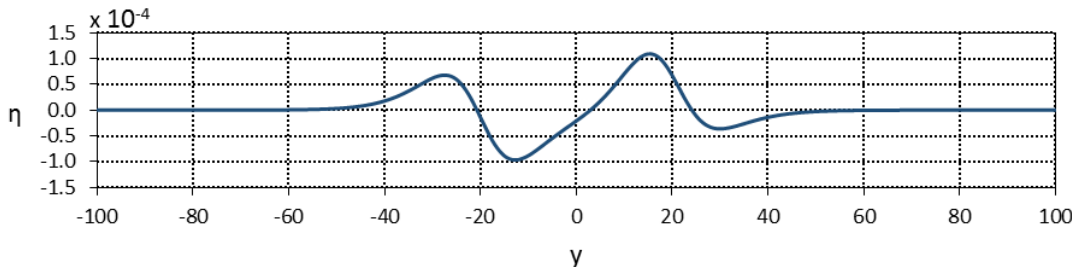

(c) t = 20 s

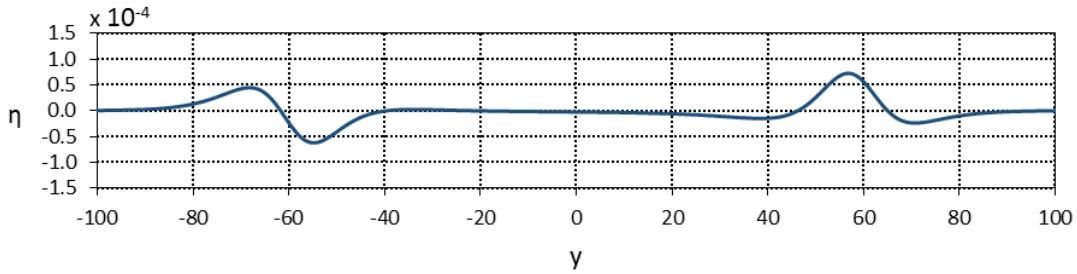

(d) t = 60 s

FIG. 9. (a) Maximum wave envelope along the wave direction, (i.e. maximum water level for the entire time at each spatial location), time evolutions of water surface at (b) t = 0 s, (c) t = 20 s and (d) t = 60 s for the initial wave defined by Eq. (12) are plotted along the x-bisector line (x = 0).

TABLE 3. PARAMETERS OF THE INITIAL WAVE GIVEN IN Eq. (12)

Parameter	Definition	Value (m)
H	Initial water level	0.001
L	Crest length	30
y_1	Elevation location of the *N*-wave	0
y_2	Depression location of the *N*-wave	2.3
x_0	Starting point of the wave on *x*-axis	-15
ε	Scaling parameter	-0.0040
P_0	Steepness parameter	15
γ	$\sqrt{3Hp_0/4}$	0.106
α	$\pi/(2\gamma)$	14.81

3.3.2. Data

The data (the location in the y-axis and water surface elevations at the channel for maximum envelope and for snapshots at the time 0 s, 20 s and 60 s) are given in the excel file "Analytical solution-2.xlsx" enclosed in the link with supplementary material.

4. BENCHMARK PROBLEMS BASED ON LABORATORY EXPERIMENTS

4.1. BACKGROUND

Experimental data using the irregular shaped bathymetry and topography are useful for validation and testing of the performance of the numerical models. It is difficult to conduct experiments to study the tsunami behaviour since a large-scale tank is necessary to establish proper model scale for minimizing scale effects and experimental errors.

One of the useful experimental benchmarks is the model tests applied to the 1993 Okushiri tsunami run-up performed in a large-scale tank at the Central Research Institute for Electric Power Industry in Abiko, Japan [8]. The tests were performed to investigate the extreme run-up of 32 m that was measured near the village of Monai in Okushiri Island Japan in the 1993 Okushiri event.

4.2. LABORATORY BENCHMARK PROBLEM (RUN-UP OF OKUSHIRI TSUNAMI ON MONAI)

4.2.1. Problem definition

The 1993 Hokkaido Nansei-oki earthquake caused many unexpected phenomena in Okushiri Island Japan and at coastal areas of the Sea of Japan. One of them was the extreme run-up of 32 m that was the run-up mark discovered at the tip of a very narrow gulley within a small cove. This benchmark problem is modelled in 1/400 scale in the laboratory experiments named as Monai run-up experiments [8]. A large wave flume of the tank 205 m long, 6 m deep and 3.4 m wide is used in these experiments. The time history of the tsunami wave based on the data of the tsunami caused by the 1993 Hokkaido Nansei-oki earthquake was inputted to the experimental basin from the border and the time histories of the water level were measured at the wave gauges located at the shallow zone.

The offshore profile of the experimental area, experimental setup, gauge locations, time history of wave inputted from the left border and the time histories of water level at different gauges are shown in Figs 10–16.

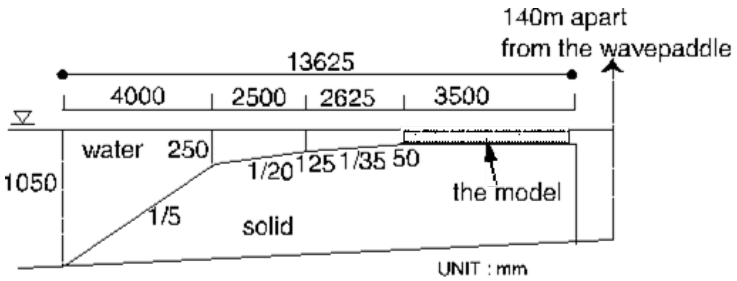

FIG. 10. Offshore profile of the experiment area (reproduced with the permission of World Scientific Publishing Co., Singapore [20]).

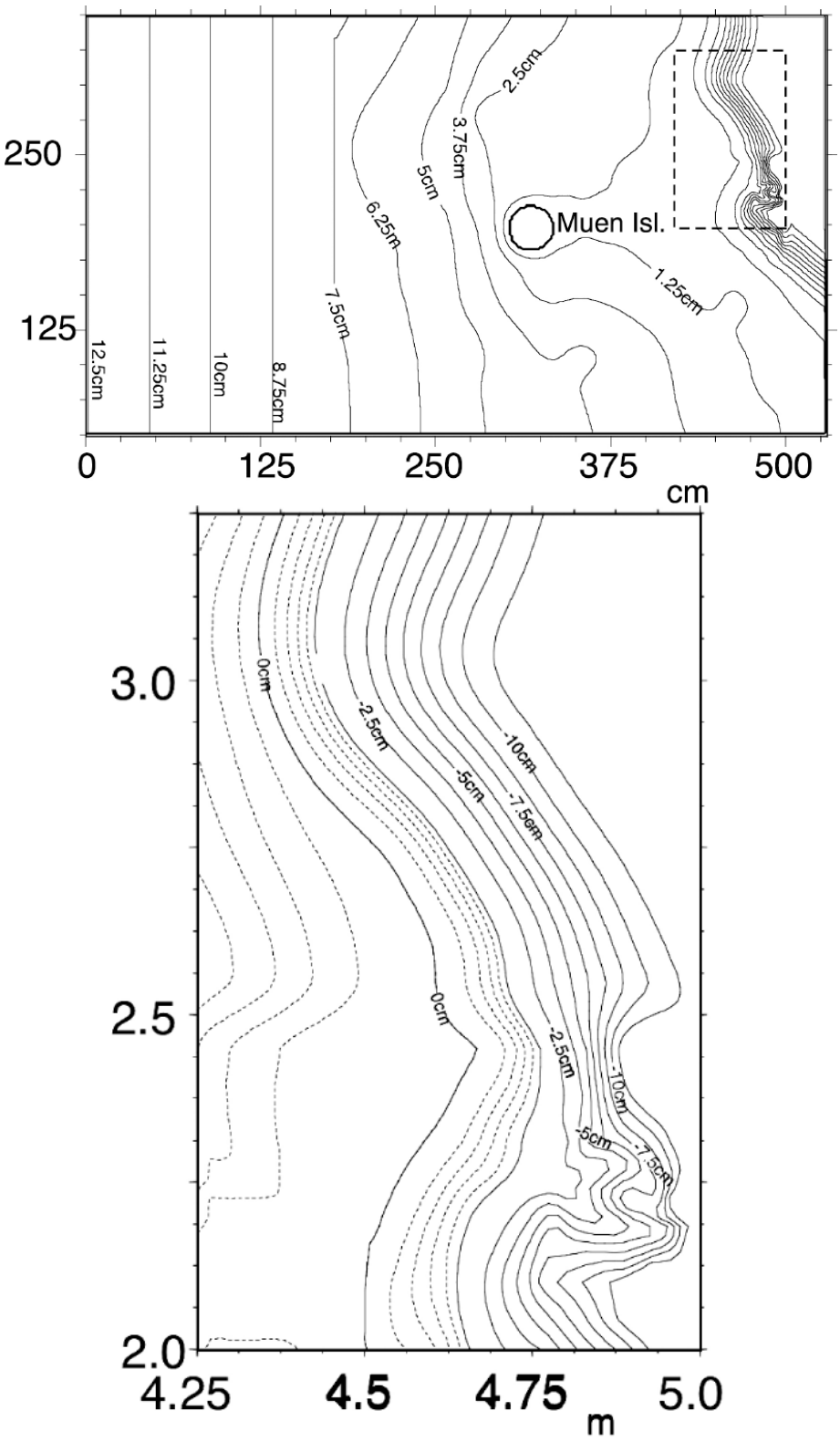

FIG. 11. Bathymetry and topography near the run-up area (reproduced with the permission of World Scientific Publishing Co., Singapore [20]).

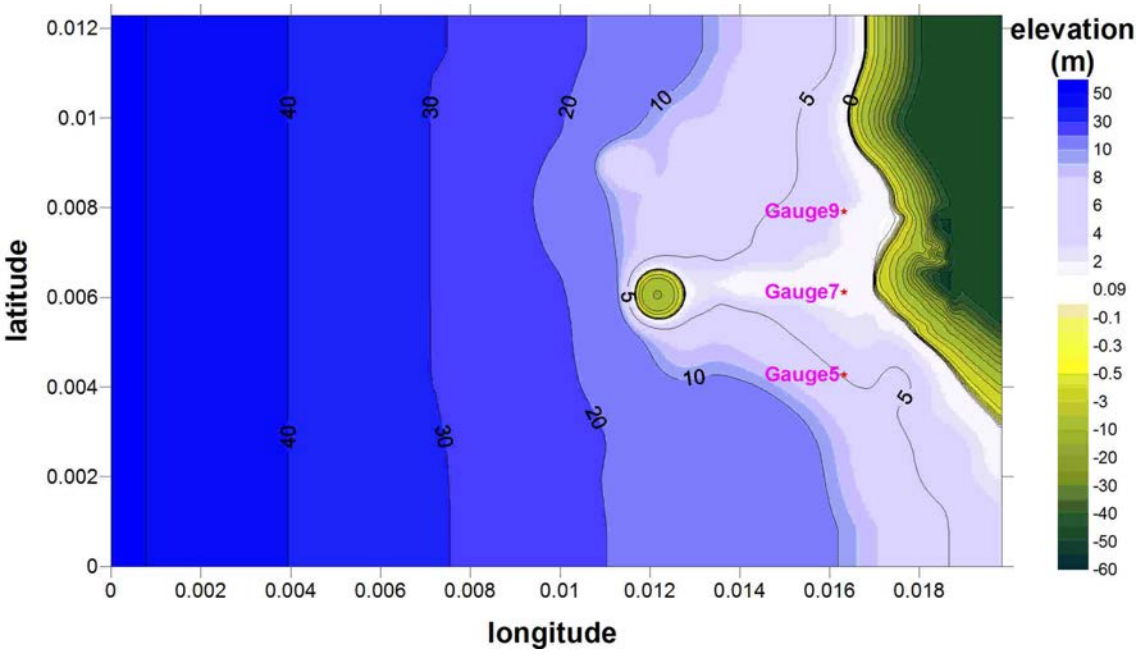

FIG. 12. Experimental basin and gauge locations.

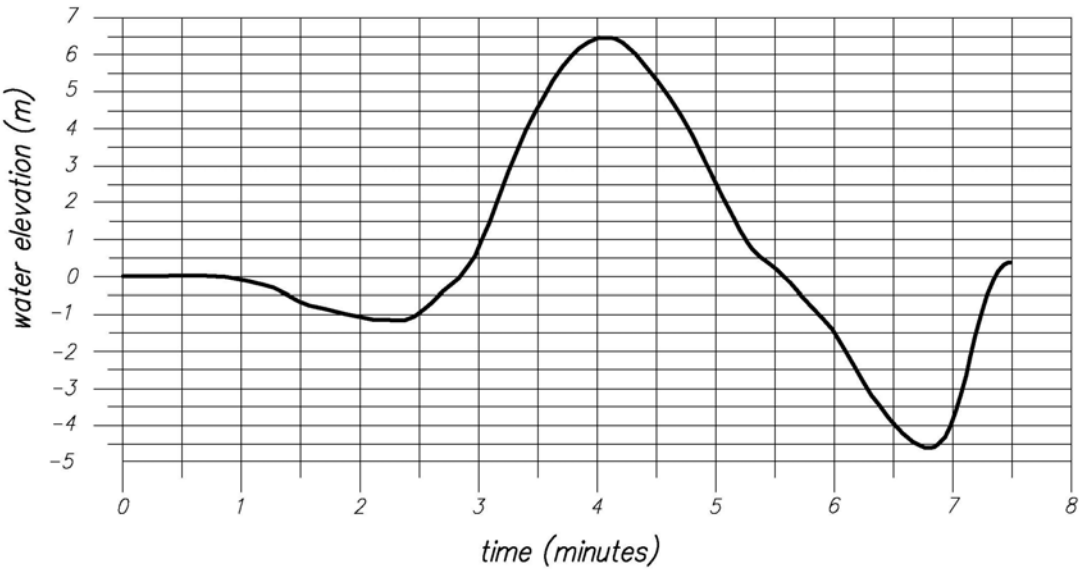

FIG. 13. Profile of the input wave from the left border.

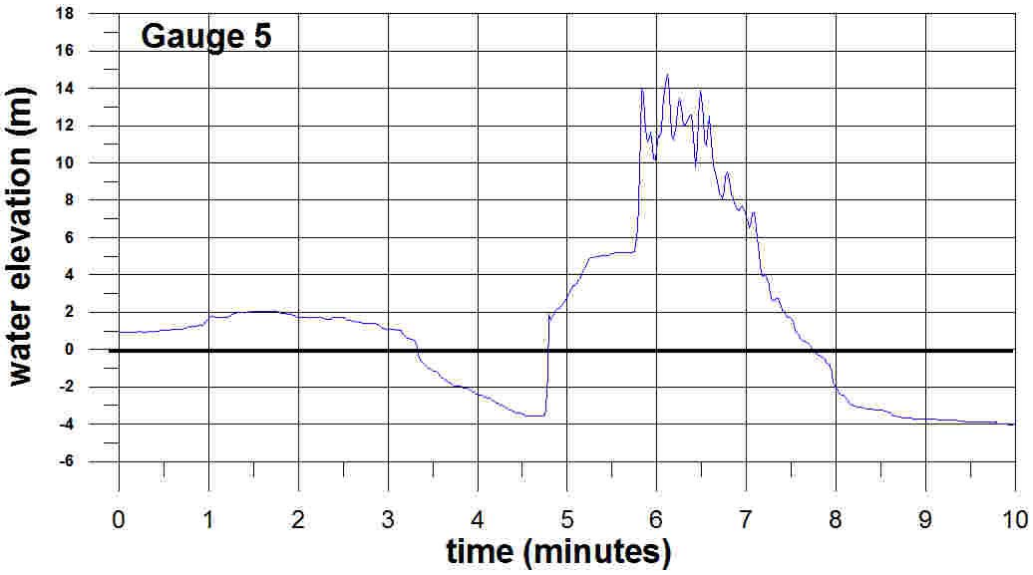

FIG. 14. Time history of water level at Gauge 5.

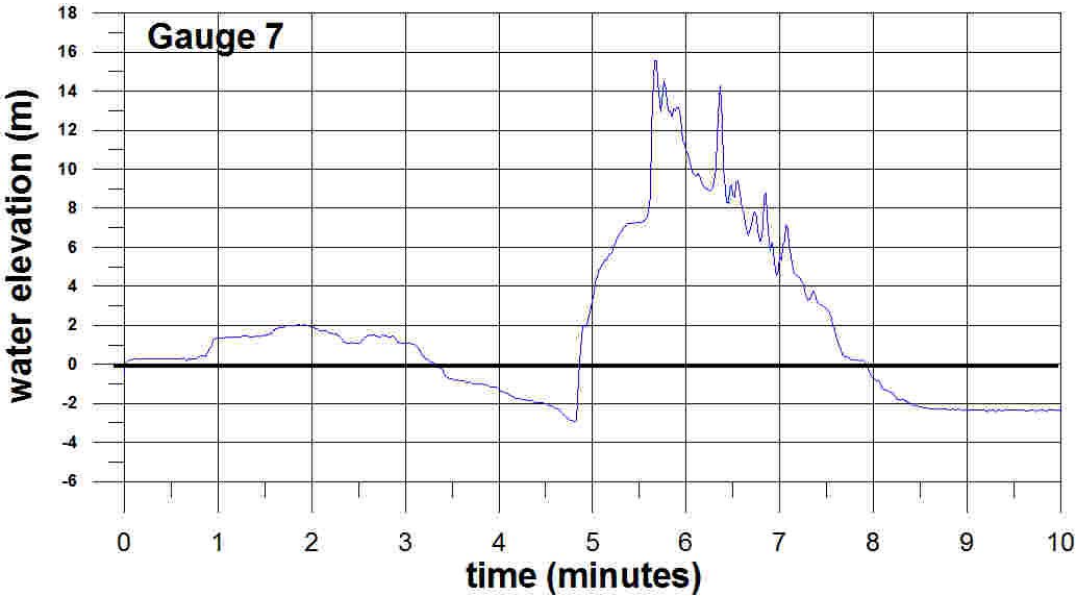

FIG. 15. Time history of water level at Gauge 7.

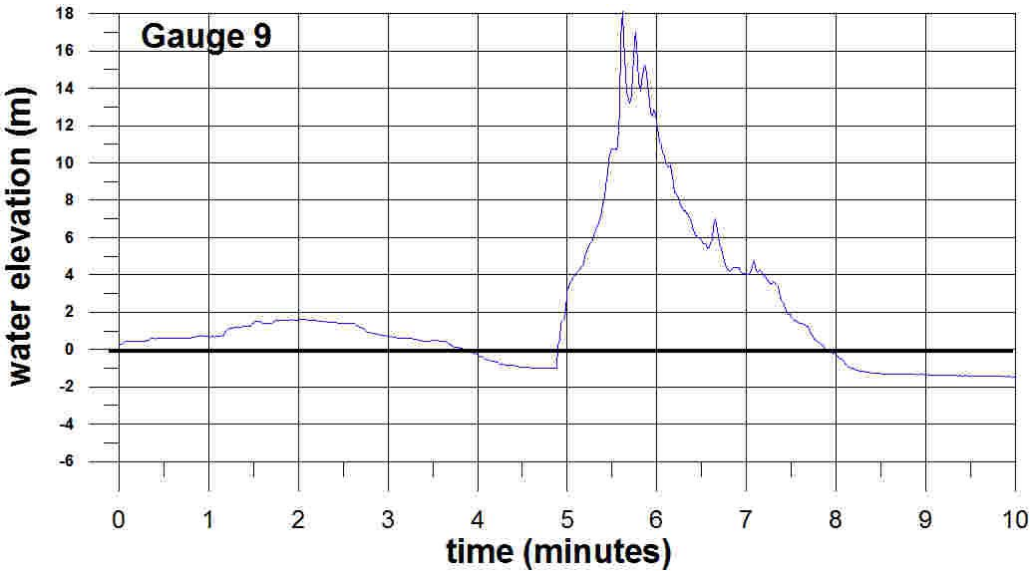

FIG. 16. Time history of water level at Gauge 9.

It is noted here that the data are in prototype coordinates in metres spatially but if the model uses global coordinates, then conversion is necessary.

4.2.2. Data

The bathymetry file, gauge locations, input wave data and measured time histories of the water level at Gauges number 5, 7 and 9 are given in the file "output_ch5-7-9-original-prototype-min-meter-total-10min-record.dat" to be found under the link with supplementary material (Annex IV).

5. BENCHMARK PROBLEM BASED ON FIELD MEASUREMENTS

5.1. BACKGROUND

The benchmark problems of tsunamigenic events with observed records provide an opportunity to the user for validation of numerical models for tsunamis in real world scale. The validation could cover initiation, propagation and run-up phase of tsunamis and the exercise calls for availability of methodically recorded data. Collection of the well recorded data of tsunami events both in terms of source model and propagation is a difficult task due to infrequent occurrence of large tsunamis and inadequate coverage of instrumentation.

The tsunamis of 2004 and 2011 caused widespread destruction along the coasts of the Indian Ocean and the Pacific Ocean, respectively. Of these, the event of 2011 occurred in a region which was well covered with instruments and the records provide researchers a golden opportunity to evaluate the performance of the numerical models for tsunami propagation and run-up against the simulations. This benchmark is expected to provide a real world well constrained tsunami propagation problem along with the observed data to the Member States for validation of the numerical models.

5.2. PROBLEM DEFINITION

This section brings out details of real world benchmark problems for tsunami propagation using the data from the 2011 Great East Japan tsunami. The tsunami impact from the GEJE event could be divided into two cases: (i) local (near field) tsunami and (ii) distant (far field) tsunami. These benchmark problems address coastal tsunami heights, near shore and offshore along the Japanese coast, offshore tsunami waveforms in the Pacific Ocean and tide gauge records in Hawaii.

The inputs needed for the benchmark problem are presented in the following manner:

(a) Tsunami source model (see Section 5.3.1).

(b) Local tsunami (see Section 5.3.2):

  (i) Bathymetric and topographic data;

  (ii) Time history of water level at tide gauge;

  (iii) Maximum water level at tide gauge and inundation.

(c) Distant tsunami (see Section 5.3.3):

  (i) Bathymetric and topographic data;

  (ii) Linear propagation phase;

  (iii) Maximum observed water level, time of arrival and time history of water level in deep ocean;

  (iv) Deep ocean bathymetric data.

(d) Linear propagation and non-linear shoaling (see Section 5.3.3.2):

  (i) Time history of water level at tide gauge;

  (ii) Deep ocean and shallow water bathymetric data.

With the above inputs and observed data, as part of benchmarking, the user has to simulate the propagation of tsunami waves as local and distant tsunamis and compare the results with the run-ups and water levels on the observation points.

5.3. DATA

Apart from the numerical scheme, key inputs are needed with respect to modelling of source, modelling of deep ocean bathymetry and shallow water bathymetry, including topography for effectively capturing the run-up characteristics. The benchmark problem includes the measurements available in deep ocean, run-ups along the coast as well as tide gauge measurements along the coast. Each of these is discussed in detail in the subsequent subsections. Additional information for the generation of numerical models is provided in Annex III.

5.3.1. Source models

On 11 March 2011, a M9.0 earthquake occurred off the Pacific coast of Tohoku, Japan and generated a huge tsunami. The epicentre of the 2011 GEJE was 38.103°N, 142.860°E and the origin time was 14:46:18 Japan Standard Time (JST), Universal Time Coordinated (UTC) +9 h, according to the Japan Meteorological Agency. The earthquake focal mechanism solution shows a thrust-type fault movement on a shallowly dipping plane, indicating that it occurred on the boundary between the Pacific plate and the overlying North American plate [21].

The slip distribution of the GEJE main shock was estimated from various geophysical datasets such as seismic waves [22], global navigation satellite system (GNSS) [9], marine geodetic measurements [10] and tsunami waveforms [21]. The slip caused significant sea floor displacement, which became the source of the tsunami when translated to the water column (Fig. 17).

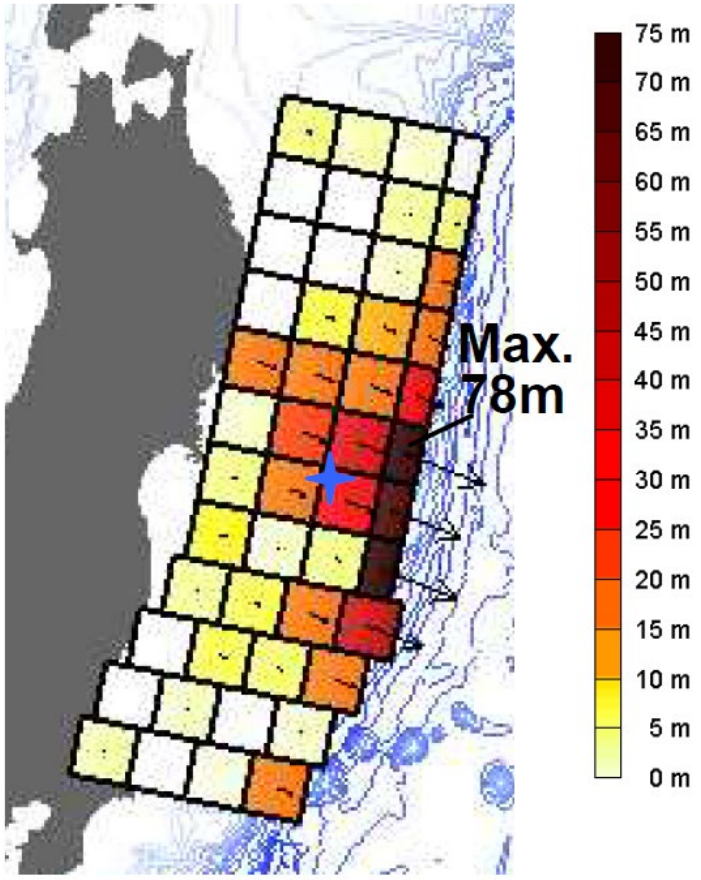

FIG. 17. Estimates of deformation during the 2011 earthquake (reproduced with permission of Japan Association for Earthquake Engineering [23]).

The 2011 tsunami was instrumentally recorded on various types of gauges. These included coastal tide and wave gauges, offshore GPS buoys, cabled ocean bottom pressure gauges and deep-ocean assessment and reporting of tsunami (DART) buoys.

The tsunami source model determines the initial condition for the sea surface in the tsunami simulation; the initial velocity is zero at time $t = 0$ s. These two are the initial conditions for the tsunami simulation. The source models are defined by parameters such as forward or inversion analysis of observed tsunami waveforms and GNSS data. Forward

modelling of a tsunami uses the given tsunami source, mostly based on the seismological analyses. Then, the model computes tsunami propagation in the ocean and calculates times of arrival of the tsunami and/or water level on target areas. Inverse modelling estimates the tsunami source more directly by solving the inverse problem. The modelling starts from the observed tsunami data, such as times of arrival of the tsunami, heights or waveforms recorded on instruments. The propagation phase is numerically computed as in the forward modelling.

There could be differences in parameters for tsunami sources and this depends on the methodology of the modelling. For example, since the earthquake rupture process is generally shorter than the time needed for a tsunami to propagate from the source region to the coast, the tsunami generation can be often assumed to be instantaneous. However, some other available source models take into account the duration of the seismic rupture due to the large fault size of GEJE (e.g. [23, 24]). The amount of the vertical displacement of the sea floor induced by an earthquake event is generally computed via the elastic dislocation theory proposed by Mansinha and Smylie [25] and Okada [26]. This sea floor displacement causes an initial sea surface deformation that creates the initial tsunami waveform.

Several tsunami source models have been proposed by scientific researchers for GEJE [21, 23]. For details of other tsunami sources, the reader may refer to the publication by MacInnes et al. [27], which compared 10 tsunami sources proposed by different research groups. Appropriate selection of the tsunami source model is necessary to properly simulate tsunami propagation and inundation.

In Annex III, the Fujii and Satake model [21] and the Japan Nuclear Energy Safety Organization (JNES) model [22] are used for distant and local tsunami analysis, respectively. In Ref. [21] the tsunami waveform inversion is computed using 40 sub faults of 50 km × 50 km located within the aftershock area. The Japan Nuclear Energy Safety Organization model aimed to reproduce not only the tsunami waveforms but also the tsunami traces at the nuclear power plant sites on the Pacific coast. Sugino et al. [23] set up the tsunami source area based on the Fujii and Satake model [21]. Table 4 presents an overview of these source models.

TABLE 4. TSUNAMI SOURCE MODELS OF THE GEJE TSUNAMI EVENT

Source model	Fujii et al. [21]	Satake et al. [24]	JNES [23]
Modelling methodology	Inversion analysis (Tsunami waveform)	Inversion analysis (Tsunami waveform)	Inversion analysis (Tsunami waveform and crustal movement)
Number of sub faults	40	33 and 22	40 and 8
Sub fault size (length × width, km)	50 × 50	50 × 50 and 50 × 25	50 × 50 and 50 × 30
Total fault size (length x width, km)	about 500 × 200	about 550 × 200	about 600 × 200
Duration of rupture (s)	Instantaneous	300	300
Tsunami propagation model	Shallow-water wave equations	Shallow-water wave equations	Shallow-water wave equations
Equation for relation of sea surface deformation to slip	Okada [26] and Tanioka and Satake [28]	Okada [26] and Tanioka and Satake [28]	Manshinha and Smylie [25]

5.3.1.1.Data for crustal movement

Data of crustal movement is indispensable to measure run-up accurately. These data are also important for the inversion analysis of the tsunami source by the inversion of the ground displacement. The observed coseismic displacements of the GEJE show eastward movements of up to 5.3 m and subsidence by up to 1.2 m along the coastal line of the Tohoku region (Fig. 18).

The coseismic and post-seismic deformations were detected by the GNSS Earth Observation Network operated by the Geospatial Information Authority of Japan. The control stations cover the Japanese archipelago with over 1200 stations at an average interval of about 20 km.

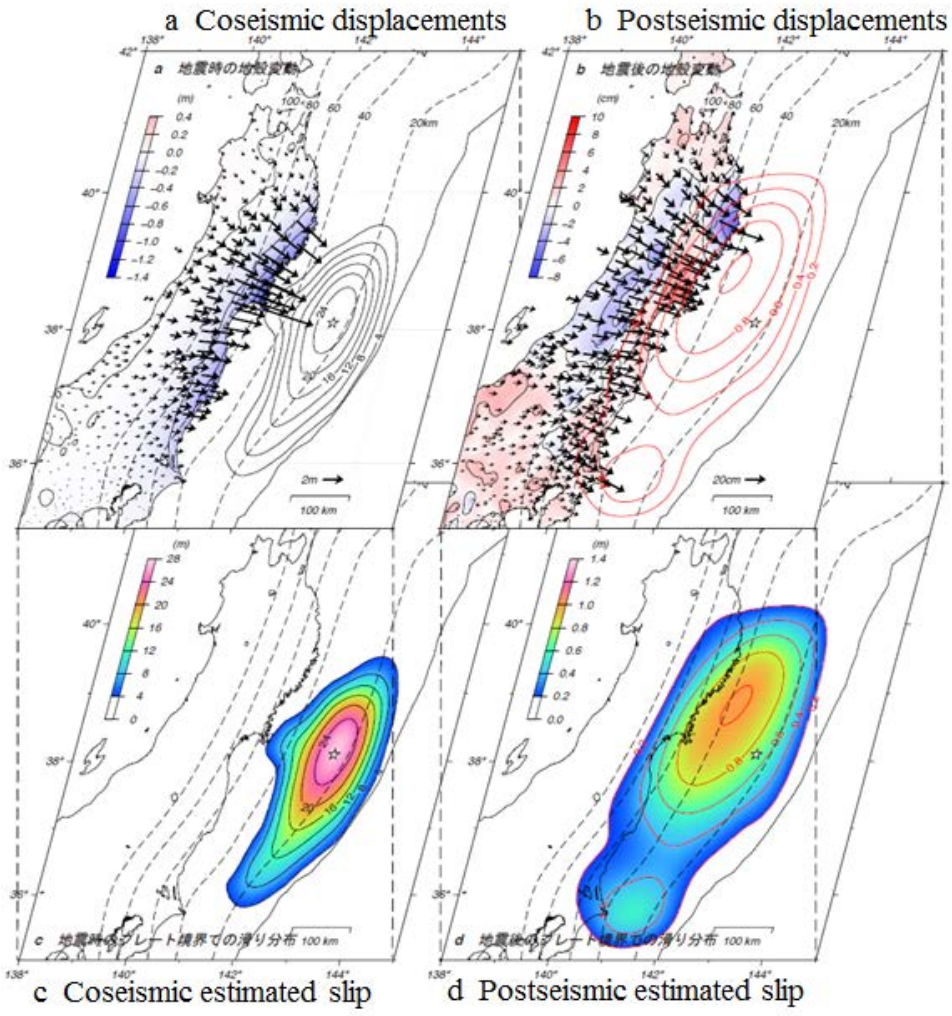

FIG. 18. Coseismic (10–11 March 2011) and post seismic (12–25 March 2011) displacements (a, b) and estimated slip (c, d). The black arrows indicate the horizontal coseismic movements of the GNSS sites. The colour shading indicates vertical displacement. The star on figure c shows the location of the earthquake epicentre. The dotted lines indicate the isodepth contours of the plate boundary at 20 km intervals. The red contours show the after slip distribution in metres (reproduced with the permission of Geospatial Information Authority of Japan:[29]).

5.3.2. Simulation of local tsunami

Analysis of a local tsunami or a tsunami from a nearby source demands accurate bathymetric data along the tsunami propagation path. After the tsunami propagation and

inundation analysis, observed tide gauge and run-up data are also needed to validate the results. Regarding the local tsunami analysis for the GEJE event, both bathymetric data and observed records around Japan are available. The following subsections describe the typical data source for general use.

5.3.2.1.Data for propagation phase

Bathymetry

Dense and accurate bathymetric data are essential to simulate tsunamis accurately, because tsunami propagation and run-up depend on the topography of the ocean floor as well as on nearby coastal topography to compute inundation correctly. Bathymetric data around Japan constitute valuable input data for local tsunami simulation for GEJE. Two data types are commonly used as bathymetric data. The first type is grid data, for which each cell in the grid illustrates the elevation at a certain point. These data are commonly referred to as 'digital elevation models'. The data in the second category are referred to as 'digital bathymetric map data' that represent the contour lines.

The following grid data and depth contour data around Japan can be referred for simulation of near field tsunami:

(a) J-EGG500 [29] Marine Information Research Center, News Letter No. 4, February 1999 (Japan Oceanographic Data Centre-Expert Grid data for Geographic -500 m), 500 m gridded bathymetric dataset (Japan Oceanographic Data Center).

(b) M-7000 [30] Journal of Earthquake and Tsunami, Vol. 11, No. 5(2017) doi: 10.1142/S179343111750018X, the depth Contour Data (Japan Hydrographic Association).

(c) Topographic data of The Central Disaster Prevention Council (2006) [31] (The expert examination committee in relation to subduction zone earthquake around Japan Trench and Kuril trench).

The Japan Oceanographic Data Centre manages and provides several kinds of bathymetric data. J-EGG500, a 500 m gridded bathymetric dataset around Japan, is one of its publicly available datasets. A large amount of the depth-sounding data has been combined and gridded by 500 m intervals for general use. The M-7000 series provides depth contour data based on some bathymetric information around Japan. High-resolution grid data can be constructed from depth contour data by using the Triangulated Irregular Network modelling. An example of combined J-EGG500 and M-7000 data by using the Triangulated Irregular Network is shown in the report of Japan's Central Disaster Prevention Council. However, the accuracy of the final form of data are same as in the original one.

Records

Wave and tide gauges can record time series of sea levels or tsunami waveforms at specified time intervals. The Ports and Harbours Bureau, Ministry of Land, Infrastructure, Transport and Tourism, Japan and the Port and Airport Research Institute, have been conducting wave and tide observations around Japan through the Nationwide Ocean Wave Information Network for Ports and Harbours (NOWPHAS). The gauges of NOWPHAS were successful to acquire the 2011 Tsunami waveforms. Locations of NOWPHAS GPS and wave gauges available on 11 March 2011 are shown in Fig. 19.

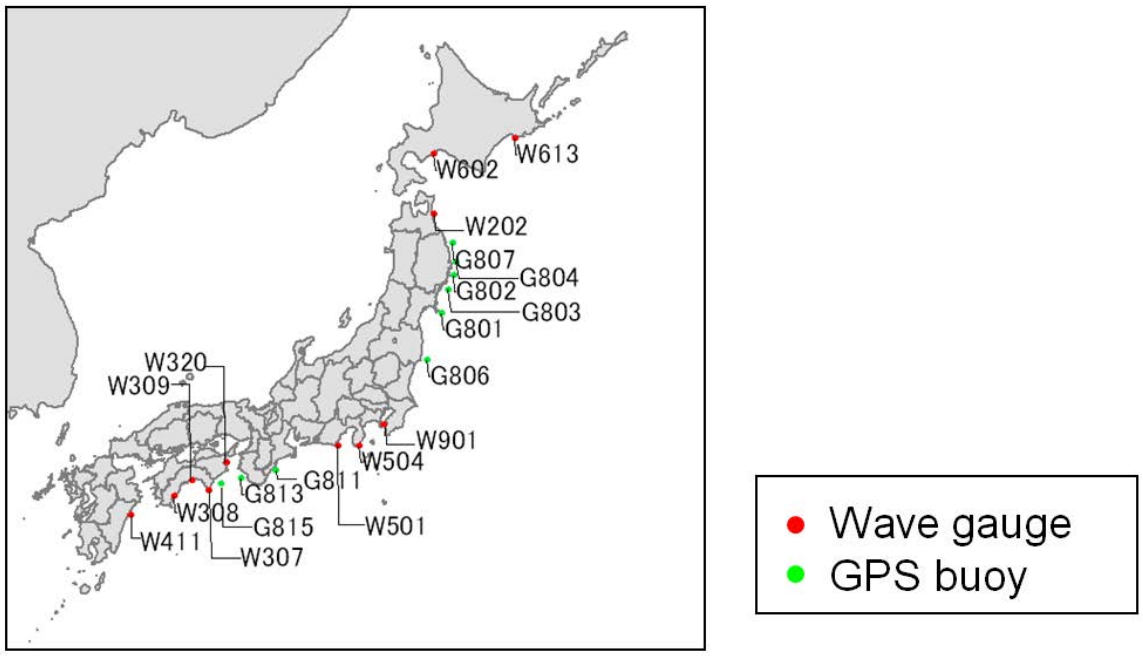

FIG. 19. Locations of NOWPHAS GPS and wave gauges available on 11 March 2011 (reproduced with permission of Japan Association for Earthquake Engineering [23]).

NOWPHAS has three types of equipment: GPS-mounted buoys, seabed-installed type and coastal tide gauges [11]. GPS-mounted buoys acquire sea level data every second using Real Time Kinematic (RTK) GPS. The GPS buoys are moored in 100–400 m water depth and at 10–20 km away from the shore. Pressure gauges and ultra-sonic wave gauges are seabed-installed type gauges within a few kilometres of the shore. Pressure gauges obtain the variation of water pressure on the seabed and convert it into the water surface profile. Ultrasonic wave gauges measure the distance from the sea bottom to the surface. Coastal tide gauges measure the water level using acoustic wave radars located all over the Japanese coasts.

A typical plot of NOWPHAS GPS record on 11 March 2011 is given in Fig. 20. The GPS buoys can record the sea level at a sampling interval of 1 second.

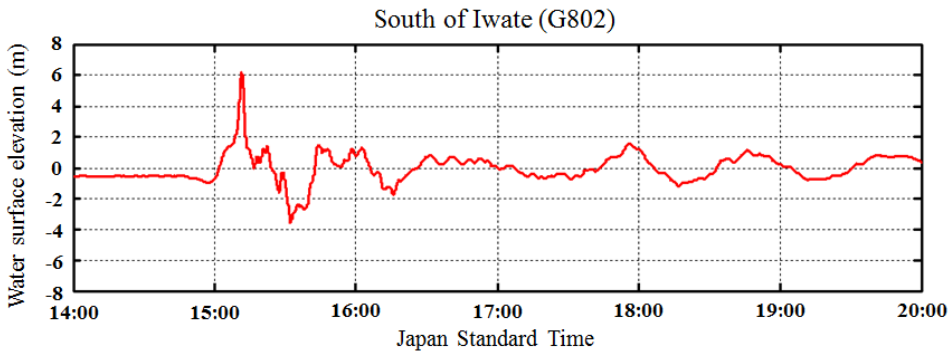

FIG. 20. Typical recording made by NOWPHAS GPS buoy during the 2011 GEJE event (reproduced with permission of Japan Association for Earthquake Engineering [23]).

5.3.2.2.Data for shoaling inundation and run-up

Bathymetry

The accuracy and density of topographic data are important for precise calculations of tsunami inundation. Airborne laser scanners (LiDAR, Light Detection and Ranging) that measure the distance by illuminating a target with a laser and analysing the reflected light have made it possible to scale elevation in an extensive area with high precision and to produce detailed topographic data. As for the topography of Japan, reliable digital elevation data have been published by the Geospatial Information Authority of Japan (GSI). Figure 21 shows the contours of 1:25 000 topographical maps. GSI's Digital Map's 50 m grid data are also available, which are measured and calculated from the contours of 1:25 000 topographical maps. These provide the elevation data of the centre of the grid. Coastal data are provided by linear interpolation from the coastline where the elevation is 0 m, while 5 m and 10 m grid data are available on the GSI's website.

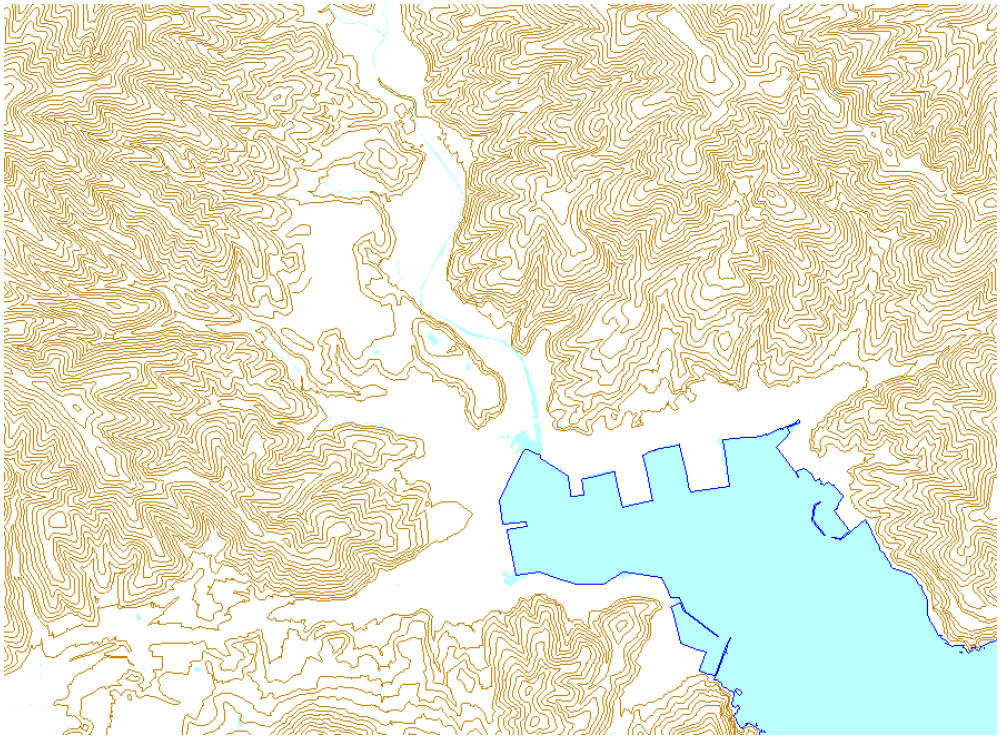

FIG. 21. Example of topography contour map (reproduced with the permission of the Fundamental Geospatial Data published by Geospatial Information Authority of Japan).

Records

The coastal plains in the Tohoku area were extensively inundated by the Great East Japan tsunami (see Fig. 22).

With the participation of 297 tsunami, coastal, seismology and geology researchers from throughout Japan, joint research groups conducted a tsunami survey along a 2000 km stretch of the Japanese coast. Inundation heights and run-ups (see Fig. 23) have been surveyed at more than 5900 points in total, which make this the largest tsunami survey dataset in the world [32]. The survey began within two days after the earthquake. Inundation height (local tsunami height from sea level at the time when the tsunami comes ashore) and run-up (the height at maximum inundation, where the velocity of a tsunami become zero) were measured along the Japanese coast except for the 30 km zone of the Fukushima Daiichi nuclear power plant.

Joint research groups [33] measured inundation height and run-up from watermarks on buildings, trees and walls by using laser range finders, RTK GNSS transmitter–receivers and total stations within a precision of a few centimetres. Run-up was determined from the debris and seawater marks. Tide effects are corrected by using tide gauge information and astronomical tidal data.

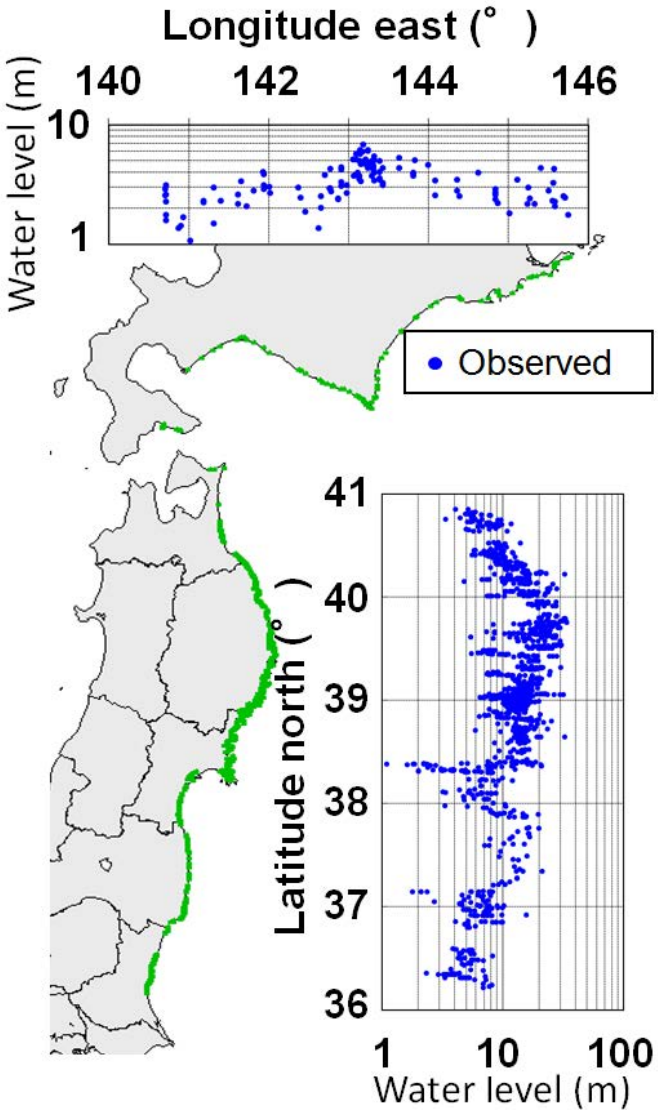

FIG. 22. Measured data around the Pacific coast of Japan. Green plots on the map indicate the observation points along the coast. Blue plots on the graphs indicate inundation height (local tsunami height from sea level at the time when the tsunami comes ashore) and run-up (the height at maximum inundation) (reproduced with the permission of Japan Association for Earthquake Engineering [23]).

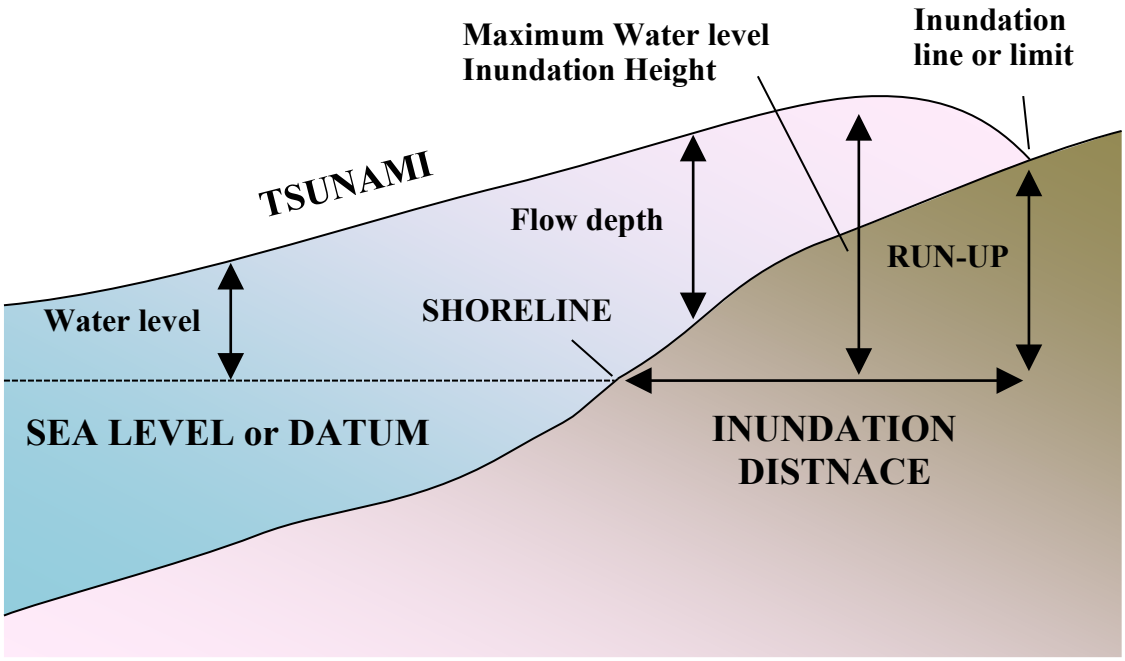

FIG. 23. Definition of tsunami heights.

5.3.3. Simulation of distant tsunami

This section covers the modelling and validation on far field propagation (across the Pacific Ocean) and run-up at distant locations caused by the 2011 GEJE event. The countries located along the rim of the Pacific Ocean have installed a variety of instrumentation capable of detecting and recording the tsunami waveforms. These include bottom pressure recorders and/or tsunami meters in the deep ocean and tide gauges located in harbours. In addition, run-ups (observed and/or measured) during the 2011 event along the coasts (e.g. United States of America, Chile, Hawaii) located far away from the tsunami source are also available.

The measurements in deep ocean and the measurements in shallow water contribute in a complementary way in the process of validation of tsunami simulations. The recordings made in deep ocean by various instruments, such as bottom pressure recorders, essentially capture the propagation of the tsunami when the linear approximations of the shallow water equations for tsunami propagation are still valid. The tide gauge data and run-ups measured along the coast capture shoaling and non-linear phenomena associated with tsunami propagation and evolution in the shallow water region.

Tsunami forerunners in the far field with a reversed polarity were also reported in publications [34, 35]. The travel time delays and the initial negative depressions are attributed to the effects of the elastic loading of the sea floor, the compressible seawater and the geopotential variation due to the moving water mass [35]. A few methods to account for elastic loading during tsunami propagation or to correct the computed waveforms have been proposed [34–36].

In the simulation of distant tsunamis, due to the long distances travelled by tsunami waves, additional phenomena such as wave dispersion or Coriolis force, could become the predominant contributors to characterization of propagating waves. These are sometimes ignored during the formulation of linear shallow water equations.

The following sections describe a set of typical input and observed data as well as corresponding data sources for 2011 GEJE event that can be used for validation of numerical models for tsunami propagation. The data are presented in two sub sections. The first subsection concerns the bathymetric and the observed data corresponding to propagation in deep ocean region. The data that captures near shore amplification subsequent to far field propagation, at a location in Hawaiian Islands, is described in the second subsection.

5.3.3.1.Data for propagation phase

NOAA is a federal agency of the United States of America that focuses on the study of the conditions of the oceans and the atmosphere. As part of the activities in areas relating to tsunami hazard and risk evaluation, NOAA has deployed a set of bottom pressure recorders, DARTs, in regions that are vulnerable to tsunamis, with the majority of them being in the Pacific Ocean.

Among the deployed DART buoys by NOAA, DART buoy #21418 was the first bottom pressure recorder to pick up the tsunami waveform of the tsunami caused by the GEJE event. The tsunami took 25 minutes to reach the location of recorder. Subsequent to their generation, the tsunami waves fanned out in the Pacific Ocean and reached the coast of Chile, located on the opposite coast, after about 22 hours. The arrival as well as the progression of the tsunami waves through the Pacific Ocean was well recorded by a number of DART buoys.

The sources of bathymetric and water level data (i.e. DART records) needed for verification of numerical models with respect to deep ocean propagation is given in the following sections.

Bathymetry

One of the most important inputs needed for modelling of tsunami propagation is the information about the sea floor. The numerical modelling of tsunami propagation demands high resolution maps of the ocean floor. However, unlike dry land where regions can be easily mapped using satellite, LiDAR, mapping of sea floor poses challenges owing to absorption of visible light and radar frequencies by water. The data recorded by ships, possibly with large gaps in between, formed one of the initial data resources for bathymetry.

Subsequent advances such as the usage of marine gravity anomalies resulted in a boom in the development of bathymetric datasets and the data derived from gravity anomalies were used to estimate the sea floor depth between ship tracks with better accuracies. Though these data could be sufficient for modelling of deep ocean propagation of tsunamis, for accurate prediction of wave amplification near the shore in shallow waters, accurately measured data at finer resolutions would be necessary.

The sources of bathymetric and topographic data include the following:

(a) ETOPO: released by the National Geophysical Data Center of NOAA, United States of America, currently available at a grid resolution of 1 minute.

(b) General Bathymetric Chart of the Oceans: available at a grid resolution of 30 seconds.

A detailed discussion on publicly available bathymetric data sources and their evaluation is provided in Marks and Smith [37].

A typical plot of bathymetry of the Pacific Ocean is given in Fig. 24. For further information on bathymetric data sources for analysis of distant tsunamis, Annex III may be referred.

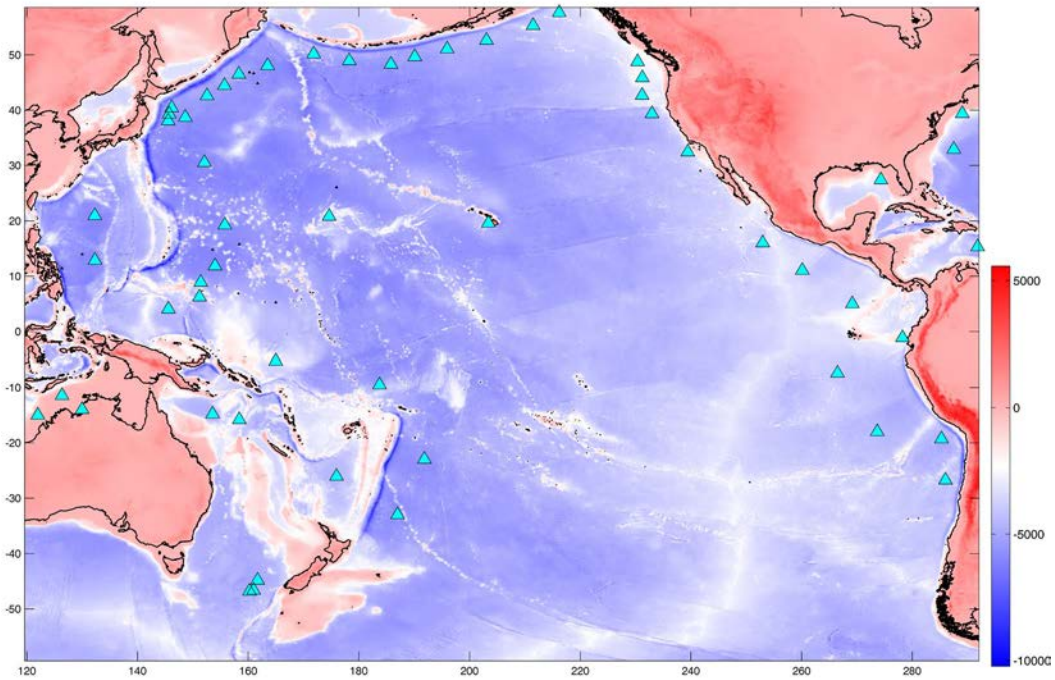

FIG. 24. False colour map of bathymetry of Pacific Ocean also depicting DART buoy locations in Pacific [38].

Records

NOAA has deployed a set of bottom pressure recorders, DARTs, in regions that are vulnerable to tsunamis. Each DART is capable of detecting and reporting tsunamis without any external instructions. DART could be triggered by a passing tsunami as well from a distance or remotely by the land station. DART works on the principle of water pressure detection at the location of deployment. The DART system consists of an anchored sea floor bottom pressure recorder and a companion moored surface buoy for real time communications Fig. 25 [38]. The data from the bottom pressure recorder on the sea floor to the surface buoy is transmitted through an acoustic link.

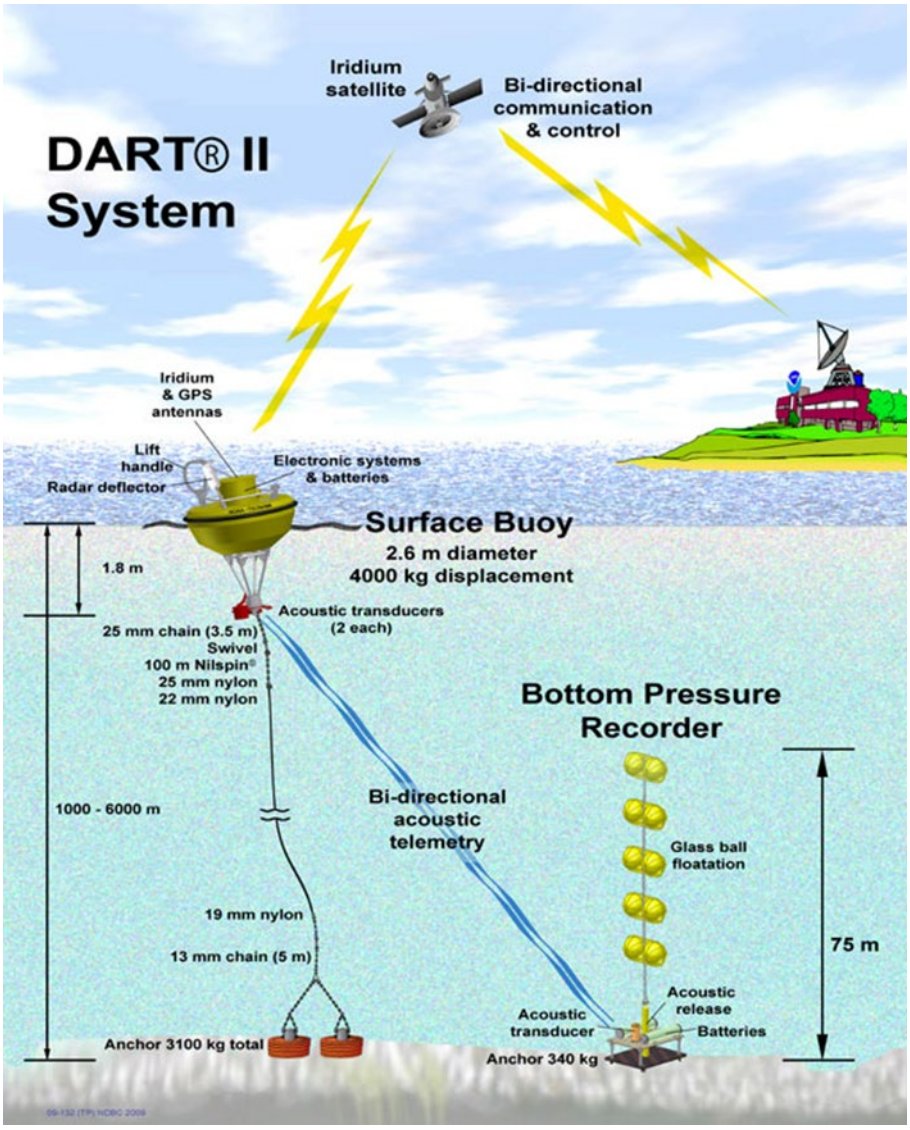

FIG. 25. DART system and its components (reproduced from Ref. [38] with permission).

Based on the location of the tsunami generation, these recorders, which are located in deep ocean, pick up the tsunami signals. Using the recorded wave forms and the time gap between wave arrivals at different recorder locations, the data could be inverted to arrive at the preliminary estimate of the possible slip distribution. This could be also used to obtain a realistic estimate of expected run-ups at various regions.

The recording by DART is generally made at a sampling interval of 15 minutes. However, provisions exist for sampling at higher resolutions for adequately capturing wave travel during the tsunami propagation phase (e.g. 1 minute, 15 s). A typical plot of a DART record captured during the propagation phase of the 2011 tsunami is given in Fig. 26. The figure also shows various sampling intervals followed by DART during collection of tsunami wave form data.

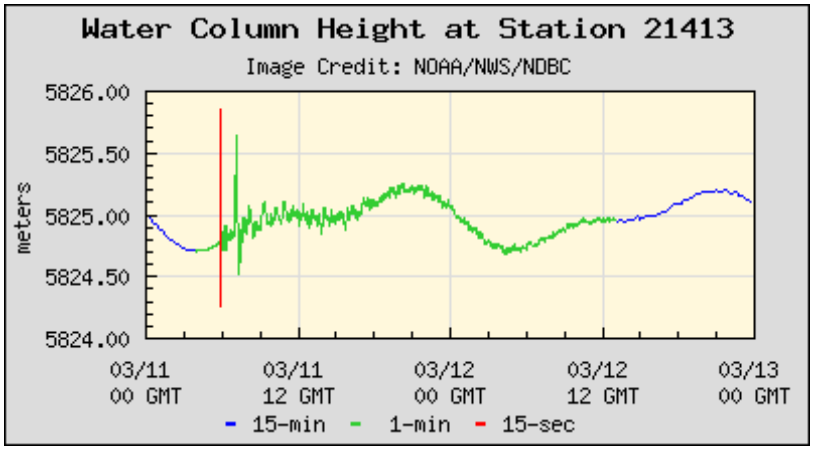

FIG. 26. Record of DART Station 21413 in the 2011 GEJE event, the line colours indicating the frequency of data (data taken from DART system).

To compare the data from different DART stations, the tide level in each station has to be considered. NOAA also provides data after the tidal effect has been removed. The plots of de-tided DART data from different DART stations are given in Fig. 27. The user may refer to Annex III for detailed information on DART data sources for far field analysis.

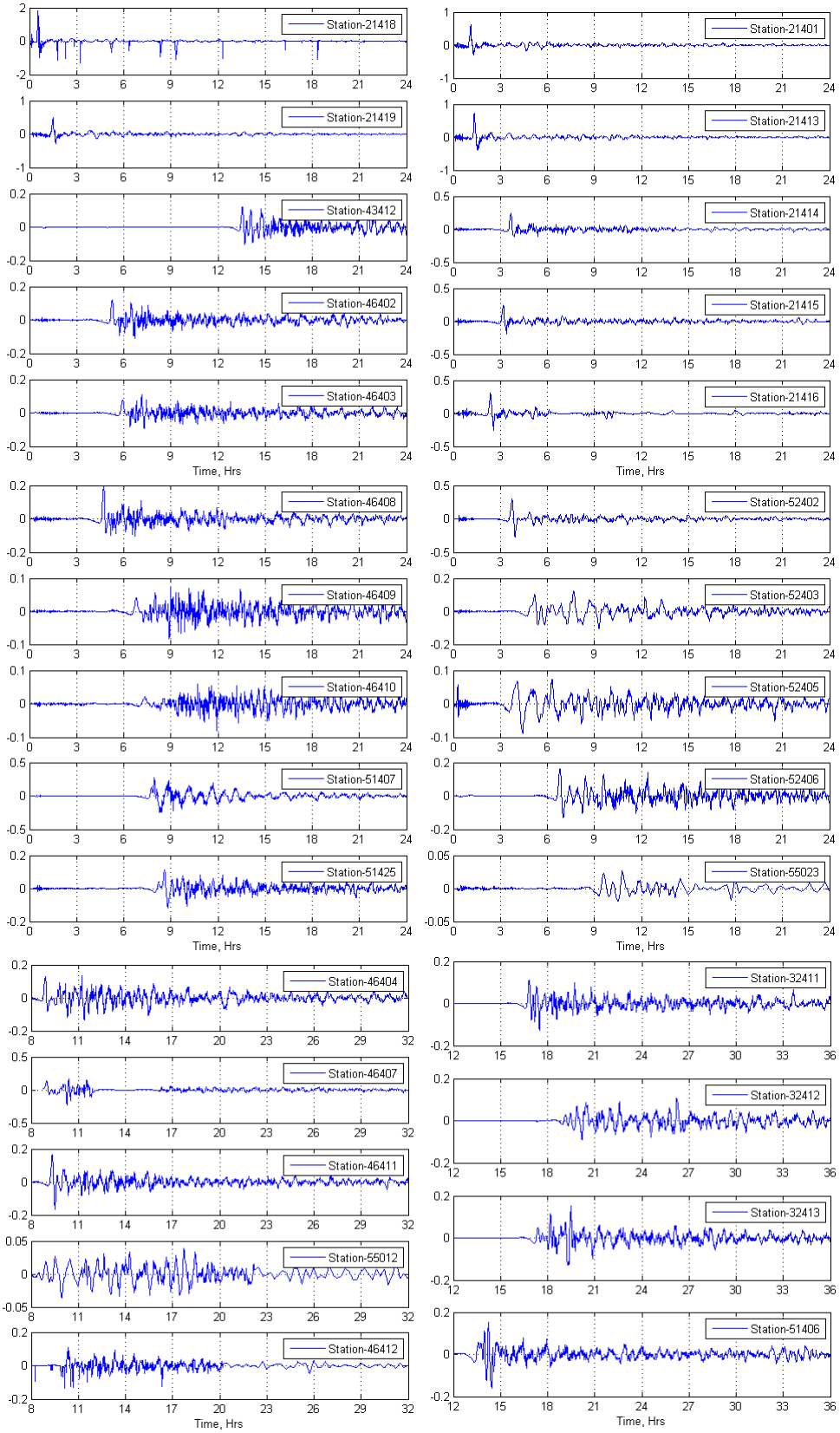

FIG. 27. Plots of water level (in metre) recorded by various DART stations (de-tided), X axis indicate elapsed time since GEJE (05:46 UTC).

5.3.3.2. Data for shoaling and run-up

Bathymetry

As part of the benchmark exercise on the evaluation of far field propagation and run-up, the data recorded by the tide gauge station located at Kahului harbour in Maui island in Mid Pacific is proposed to be used. Maui island is part of the Islands of Hawaii, United States of America. A general view of the Islands of Hawaii is given in Fig. 28. The figure also depicts the observed run-ups along their coast. It can be seen that the data recorded by the tide gauge at Kahului were among the highest recorded in the archipelago.

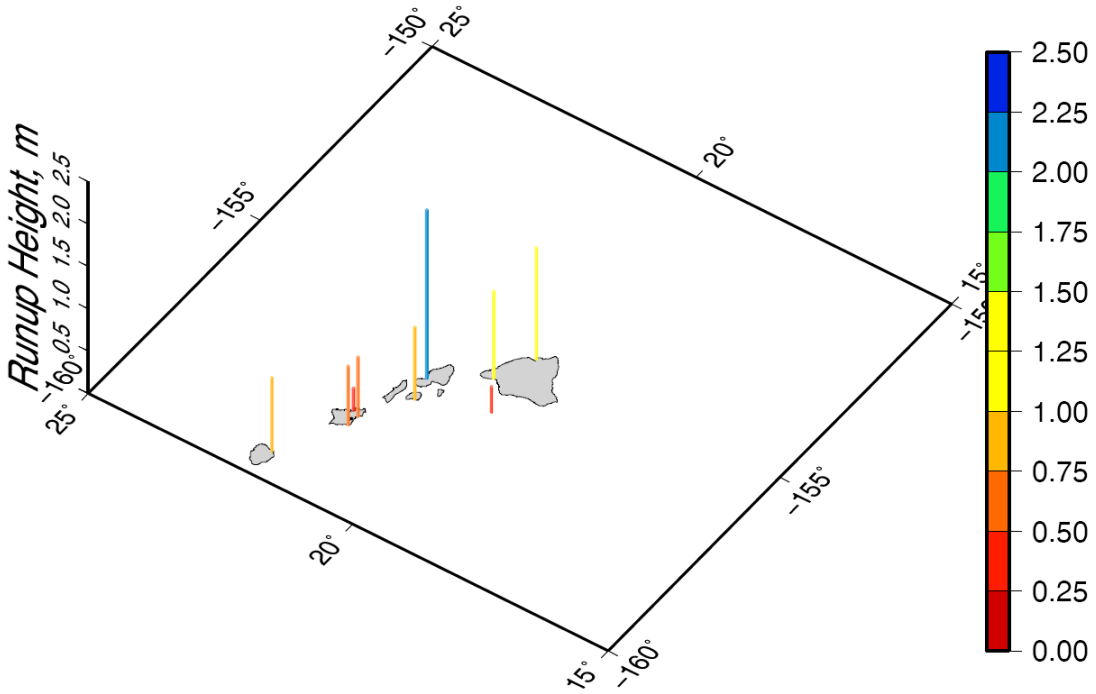

FIG. 28. Distribution of maximum water level along Hawaiian Islands (blue coloured vertical bar indicates maximum water level measured at Kahului tide gauge) (data from [39]).

The harbour of Kahului is confronted by a steeply sloping continental shelf about 35 km wide, beyond which bathymetry suddenly increases to 4000–5000 m. A number of islands confront the tsunami waves originating from the coast of Japan and could also possibly influence the approaching wave behaviour at Kahului.

The point of interest with respect to the application of tsunami codes for the evaluation of far field propagation and run-up is the tide gauge station at Kahului harbour, shown in Fig. 29. The tide gauge station is located inside the harbour (Longitude: 156° 28.6' W, Latitude: 20° 53.7' N).

FIG. 29. Kahului harbour and location of tide gauge (data from National Oceanic and Atmospheric Administration Center for Operational Oceanographic Products and Services) [39].

Kahului harbour has two breakwaters that protrude into the sea and tsunami waves enter into the harbour through a relatively small opening between the two breakwaters. It has to be noted that the bathymetric data and the grid resolution need to be sufficiently detailed as to capture these features in the numerical model. A typical plot of bathymetry and topography of the area surrounding the harbour is given in Fig. 30. The figure also includes the location of the tide gauge station.

There exist several sources of bathymetric and/or topographic data including details in the shallow water region. The data include those provided by commercial vendors and those available in the public domain which are free. The publicly available databases include: (i) multi-beam bathymetry synthesis for the main Hawaiian Islands available at a grid spacing of 50 m, (ii) the National Elevation Data set by the U.S. Geological Survey, whose resolution varies from 30 m to 3 m depending on the regions.

Depending on the techniques used for measurements and collection of data, the accuracy and quality of data in these databases could vary. While synthesizing various datasets, the user also needs to be aware of the horizontal and vertical data adopted by each of the datasets and to carry out data transformations, if necessary. Non-adherence to these principles could result in artificial jump or drop in merged topographic and bathymetric data.

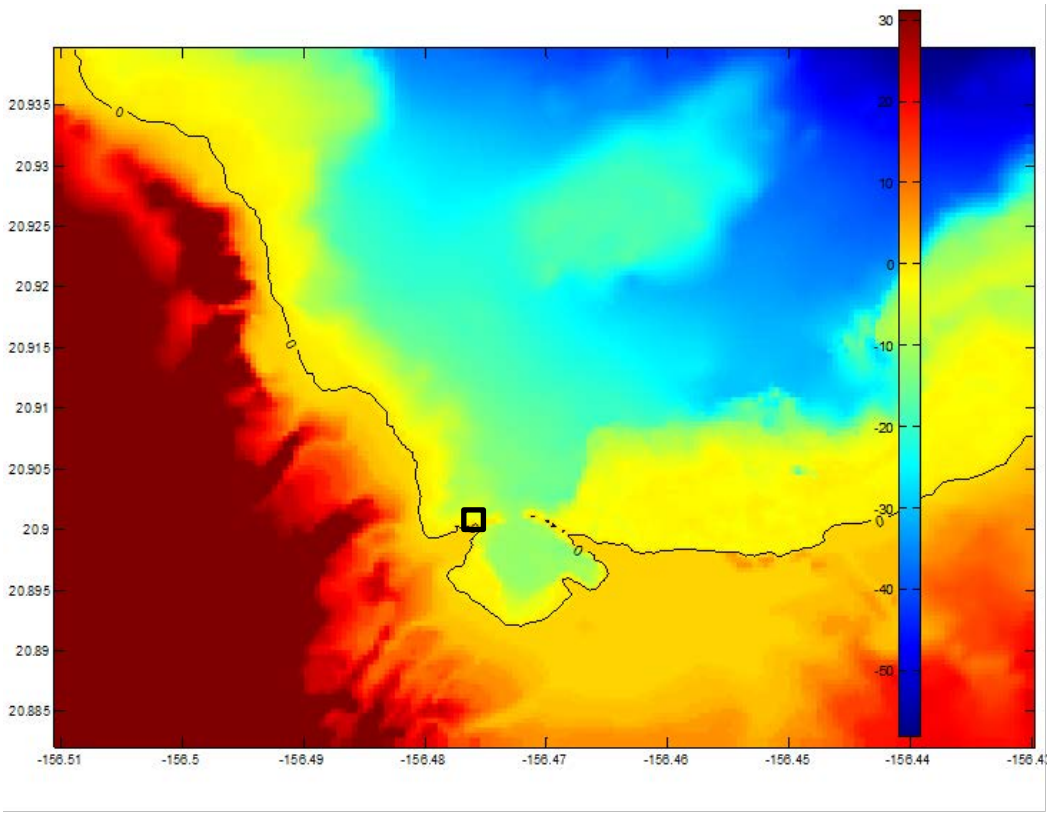

FIG. 30. Typical plot of bathymetry and topography of the area surrounding the Kahului harbour. The mark shows the place of the tide gauge station [39].

Records

The tidal variations in Kahului harbour are in the sub-meter scale with a difference between mean higher high water and mean lower low water of about 0.7 m. Annex III includes additional information, such as details of tidal variations in the Kahului harbour.

The tsunami waves took more than 7 hours to reach Kahului and the first wave was recorded at about 7.9 hours after the earthquake event. The maximum water level was about 2 m and four trains of waves with almost similar values were recorded in a time span of 1.5 hours. (This data was taken from National Oceanic and Atmosphere Administration Center for Operational Oceanographic Products and Services.)

Further information on the collection of the related tide gauge data is given in Annex III.

6. CONCLUSION

Tsunami hazard assessment has a possibility to practically simulate near shore tsunami parameters including current velocities, which govern the momentum, force and impact of tsunamis at near shore and in the inundation zone. To put this into practice, some tsunami numerical models are proposed, and analysis codes incorporating these models have been verified with laboratory and measured data.

The benchmarks proposed in this publication are useful for testing the performance of numerical models to conduct tsunami hazard assessments for nuclear installations.

This publication provides analytical, experimental and field benchmark problems including bathymetric data, coastal data, and data of water level and water velocity for all the proposed benchmark problems.

Three computer codes were used to model all three sets of data (analytical, experimental and recorded data); results are compared in terms of error in the annexes.

In general, the comparison shows a very good match between reference data and calculated values, for all three computer codes. The highest contribution to the error arises from data quality and uncertainties in the source definition; these are particularly evident in the case of benchmarking with physical data.

The wide range of benchmark problems given in the main text together with the validation procedures given in Annex I, II and III fulfil the objectives of this publication.

REFERENCES

[1] INTERNATIONAL ATOMIC ENERGY AGENCY, Meteorological and Hydrological Hazards in Site Evaluation for Nuclear Installations, IAEA Safety Standards Series No. SSG-18, IAEA, Vienna (2011).

[2] SYNOLAKIS, C.E., BERNARD, E.N., TITOV, V., KANOĞLU, U., GONZÁLEZ, F.I., Validation and verification of tsunami numerical models, Pure Appl. Geophys. **165** (2008) 2197–2228.

[3] SYNOLAKIS C.E., BERNARD E.N., Tsunami science before and beyond Boxing Day 2004, Philosophical Transactions of The Royal Society A, Mathematical, Physical and Engineering Sciences **364** (2006) 2231–2265.

[4] SYNOLAKIS, C., BERNARD, E., TITOV, V, KANOĞLU U, GONZÁLEZ F., Standards, criteria and procedures for NOAA evaluation of tsunami numerical models, NOAA Tech. Memo, OAR PMEL-135 special report, NOAA/Pacific Marine Environmental Laboratory, Seattle and Washington (2007) 55 pp.

[5] KANOĞLU, U., et al., Focusing of long waves with finite crest over constant depth, Proc. R. Soc. Lond. A **469** (2013) 20130015.

[6] NATIONAL OCEANIC AND ATMOSPHERIC ADMINISTRATION, Proc. and Results of the 2011 NTHMP Model Benchmarking Workshop, National Tsunami Hazard Mitigation Program, NOAA Special Report, U.S. Dept. of Commerce/NOAA/NTHMP, Boulder, July 2012, 436 pp.

[7] KANOĞLU, U., Nonlinear evolution and runup-rundown of long waves over a sloping beach, Journal of Fluid Mechanics **513** (2004) 363–372.

[8] MATSUYAMA, M., TANAKA, H., An experimental study of the highest run-up height in the 1993 Hokkaido Nansei-oki earthquake tsunami, U.S. National Tsunami Hazard Mitigation Program Review and International Tsunami Symposium (ITS), Seattle, Washington, 7-10 August 2001, (2001) 879–889.

[9] OZAWA, S., et al., Coseismic and postseismic slip of the 2011 magnitude-9 Tohoku-oki earthquake. Nat. **474** (2011) 373–376.

[10] SATO, M., et al., Displacement above the hypocenter of the 2011 Tohoku-oki earthquake, Sci. **332** 6036 (2011) 1395, 1207401.

[11] KAWAI, H., Various aspects of the 2011 Tohoku earthquake tsunami profiles acquired through NOWPHAS (<Special Review> Hydrodynamics of Tsunamis), Nagare 31 (2013) 21–26 (in Japanese).

[12] AIDA, I., Reliability of a tsunami source model derived from fault parameters, J. Phys. Earth **26** (1978) 57–73.

[13] JAPAN SOCIETY OF CIVIL ENGINEERS, Tsunami Assessment Method for Nuclear Power Plants in Japan, Technical Document, 2002 (2006).

[14] SYNOLAKIS C.E., The runup of solitary waves, Journal of Fluid Mechanics **185** (1987) 523–545.

[15] KANOĞLU, U., SYNOLAKIS, C., Initial Value Problem Solution of Nonlinear Shallow Water-Wave Equations, Physical Review Letters 97 (2006) 148501.

[16] TADEPALLI, S., SYNOLAKIS, C.E., The run-up of N-waves on sloping beaches, Proc. R. Soc. Lond. A **445** (1994) 99–112.

[17] CARRIER, G.F., WU, T.T., YEH, H., Tsunami run-up and draw-down on a plane beach, Journal of Fluid Mechanics **475** (2003) 79–99.

[18] KANOĞLU, U., "Theoretical solution of the wave run-up on 1/10 sloping beach", Joint Workshop of Benchmark Problems, Numerical Models, Inundation Maps and Test Sites in EC funded TRANSFER Project, Fethiye (2007).

[19] HORRILLO, J. J., et al., Report of The Third International Workshop on Long-Wave Runup Models, Wrigley Marine Science Center, Catalina Island, CA, 17018 (2004).

[20] LIU, P.L.-F., YEH, H., SYNOLAKIS, C., Advanced Numerical Models for Simulating Tsunami Waves and Run-up in Advances in Coastal and Ocean Engineering, Vol.10, Chapter 6, World Scientific Publishing Co., Singapore (2008) 223–230.

[21] FUJII, Y., SATAKE, K., SAKAI, S., SHINOHARA, M., KANAZAWA, T., Tsunami source of the 2011 off the Pacific coast of Tohoku Japan earthquake, Earth Planets Sp. **63** 7 (2011) 815–820.

[22] IDE, S., BALTAY, A., BEROZA, G.C., Shallow dynamic overshoot and energetic deep rupture in the 2011 Mw 9.0 Tohoku-oki earthquake, Sci. **332** 6036 (2011) 1426–1429.

[23] SUGINO, H., et al., Analysis and verification of the 2011 Tohoku earthquake tsunami at nuclear power plant sites, The Journal of JAEE **13** 2 (2013) 2–21 (in Japanese).

[24] SATAKE, K., FUJII, Y., HARADA, T., NAMEGAYA, Y., Time and space distribution of coseismic slip of the 2011 Tohoku earthquake as inferred from tsunami waveform data, Bull. Seismol. Soc. Am. **103** 2B (2013) 1473–1492.

[25] MANSINHA, L., SMYLIE, D.E., The displacement fields of inclined faults, Bull. Seismol. Soc. Am. **61** 5 (1971) 1433–1440.

[26] OKADA, Y., Surface deformation due to shear and tensile faults in a half-space. Bull. Seismol. Soc. Am. **75** 4 (1985) 1135–1154.

[27] MACINNES, B.T., GUSMAN, A.R., LEVEQUE, R.J., TANIOKA, Y., Comparison of earthquake source models for the 2011 Tohoku event using tsunami simulations and near-field observations, Bulletin of the Seismological Society of America **103** 2B (2013) 1256-1274.

[28] TANIOKA, Y., SATAKE, K., Tsunami generation by horizontal displacement of ocean bottom, Geophys. Res. Lett. **23** (1996) 861–864.

[29] MARINE INFORMATION RESEARCH CENTER, News Letter No. 4 (1999).

[30] JAPAN HYDROGRAPHIC ASSOCIATION, The Depth Contour Data, Journal of Earthquake and Tsunami, **11** 5 (2017).

[31] DIRECTOR GENERAL FOR DISASTER MANAGEMENT, Japan's Natural Disaster Early Warning Systems and International Cooperative Efforts, The Central Disaster Prevention Council Japan, Prime Minister's Cabinet (2006).

[32] MORI N., TAKAHASHI, T., The 2011 Tohoku Earthquake Tsunami Joint Survey Group, Nationwide post event survey and analysis of the 2011 Tohoku earthquake tsunami, Coastal Engineering Journal, **54** 4 (2012), 1250001, 27p.

[33] MORI, N., TAKAHASHI, T., YASUDA, T., YANAGISAWA, H., Survey of 2011 Tohoku earthquake tsunami inundation and run-up, Geophys. Res. Lett. **38** 7 (2011) L00G14.

[34] ALLGEYER, S., CUMMINS, P., Numerical tsunami simulation including elastic loading and seawater density stratification, Geophysical Research Letters **41** 7 (2014) 2368-2375.

[35] WATADA, S., KUSUMOTO, S., SATAKE, K., Traveltime delay and initial phase reversal of distant tsunamis coupled with the self-gravitating elastic Earth, Journal of Geophysical Research **119** (2014) 4287–4310.

[36] INAZU, D., SAITO, T., Simulation of distant tsunami propagation with a radial loading deformation effect, Earth Planets Space **65** (2013) 835–842.

[37] MARKS, K.M., SMITH, W.H.F., An evaluation of publicly available global bathymetry grids, Marine Geophysical Researches **27** 1 (2006) 19–34.

[38] GONZALEZ, F.I., MILBURN, H.M., BERNARD, E.N., NEWMAN, J.C., Deep-ocean assessment and reporting of tsunamis (DART®): Brief overview and status report, Proceedings of the International Workshop on Tsunami Disaster Mitigation, Tokyo, Japan (1998).

[39] NATIONAL OCEANIC AND ATMOSPHERIC AUTHORITY, The NCEI/WDS Global Historical Tsunami Database.

ANNEX I: BENCHMARK PROBLEMS BASED ON ANALYTICAL SOLUTIONS

Two different analytical benchmark problems were presented in Section 3 and are selected as analytical benchmark problems for testing the tsunami numerical models. Those problems are: (i) run-up of long waves on the sloping beach and (ii) focusing of long waves. The data of these benchmark problems and the comparison between analytical and numerical results using specific software are given in the Annex IV (Analytical solution-1.xlsx).

I–1. DATA OF ANALYTICAL BENCHMARK PROBLEM 1 (RUN-UP OF LONG WAVES)

The data (bathymetry, input wave, water surface elevations and velocities along the channel at 160 s, 170 s and 220 s) and the time history of shoreline coordinates and shoreline velocity are given in the link to the supplementary material. The file is in MS Excel format and the content of each column in the MS Excel file is given in Table I–1.

TABLE I–1. CONTENT OF EACH COLUMN IN MS EXCEL FILE

Column	Parameter	Remark
A, D, G, J, N	X coordinate (m)	
B	Water surface elevation (m) of the input wave	at time t=0
C	Water particle velocities (m/s) under the input wave	at time t=0
E	Water surface elevation (m)	at time t=160 s
F	Water particle velocity (m/s)	at time t=160 s
H	Water surface elevation (m)	at time t=175 s
I	Water particle velocity (m/s)	at time t=175 s
K	Water surface elevation (m)	at time t=220 s
L	Water particle velocity (m/s)	at time t=220 s
M	Time (s)	
O	Elevation of shoreline(m)	
P	Velocity of shoreline (m/s)	

Further information is available in [I–1], [I–3] and [I–4]. It is suggested that the reliable model outputs of inundation can be obtained if the number of grid cells are more than 10 along the inundation distance.

I–2. DATA OF ANALYTICAL BENCHMARK PROBLEM 2 (FOCUSING OF LONG WAVES)

Kanoğlu et al. [I–2] introduced an exact solution to the problem. The solution focuses on a finite strip source over constant depth using linear shallow-water wave theory. This problem is about the evolution and focusing of long waves with finite crest over constant depth.

The data (the location in y-axis and water surface elevations at the channel for maximum envelope and for snapshots at 0 s, 20 s and 60 s) are given in Annex IV (Analytical solution-2.xlsx). The file is in MS Excel format and the content of each column in the MS Excel file is given in Table I–2.

TABLE I–2. DATA EXPLANATIONS FOR EXCEL FILE

Column	Parameter	Remark
A, E, I, M	Time (s)	
B, F, J, N	Location in y-axis	
C	Water surface elevation (m)	For maximum wave envelope
G	Water surface elevation(m)	at time t=0 s
K	Water surface elevation (m)	at time t=20 s
O	Water surface elevation (m)	at time t=60 s

I–3. APPLICATION USING SPECIFIC SOFTWARE

Non-linear shallow water equations with a friction term are the main set of equations in the majority of all tsunami software. These equations are based on using the constant velocity profile throughout the water depth and hydrostatic pressure.

Two different tsunami numerical models are used to make the comparisons of numerical and analytical results. These codes are NAMI DANCE and Tsunami Code, briefly described in the following subsections.

I–3.1. NAMI DANCE

Tsunami numerical modelling by NAMI DANCE is based on the solution of the non-linear form of the long wave equations with respect to related initial and boundary conditions. There are several numerical solutions of long wave equations for tsunamis. In general, the explicit numerical solution of the non-linear shallow water equations is preferable for use since it consumes reasonable computer time and memory and provides the results within an acceptable error limit [I-5].

The most important development in tsunami modelling has been achieved by Shuto and Imamura, who developed the model TUNAMI N2 and made it available to be used by tsunami scientists under the umbrella of UNESCO [I–6] to [I–8] in Tsunami Inundation Modelling Exchange (TIME). TUNAMI N2 determines the tsunami source characteristics from earthquake rupture characteristics. It computes all necessary parameters of tsunami behaviour in shallow water and in the inundation zone, allowing for a better understanding of the effect of tsunamis according to the bathymetric and topographical conditions.

NAMI DANCE has been developed in C++ language with user interface using the similar computational procedures of TUNAMI N2. NAMI DANCE has additional input and output modules as well as different numerical procedures. Both codes are cross-tested and verified in international workshops specifically organized for testing and verification of tsunami numerical models [I–9, I–10]. These models have been applied to different tsunami events all over the world (i.e. Refs [I–5], [I–10] to [I–17]). As well as tsunami parameters, NAMI DANCE computes all the necessary tsunami parameters such as the distributions of current velocities and their directions, flow depths, discharge and momentum fluxes, water levels at selected time intervals and the distributions of the maximum values of these parameters and time histories of these parameters at selected numerical gauge locations [I–5].

I–3.2. Tsunami code

I–3.2.1. Description of software

The Tsunami Code was developed by the Japan Nuclear Energy Safety Organization. The Tsunami Code was produced considering the latest knowledge of the tsunami simulation technology in reference to a Tsunami Code open in the TIME project of Tsunami Engineering Laboratory in Tohoku University, Japan. It is written in Fortran language. The Japan Nuclear Energy Safety Organization provided the Tsunami Code to the IAEA. This code is made available to all institutions participating in the tsunami research programmes initiated by the IAEA [I–18].

The Tsunami Code [I–19, I–20] consists of two separate programs: (i) the Tsunami Mesh and (ii) the Tsunami Analysis Program. The Tsunami Mesh is a pre-processor that allows the user to prepare the input files needed for distant (far-field) and local (near-field) tsunami analysis models with the help of a graphical user interface. The Tsunami Mesh works in a geographical coordinate system (latitude and longitude as axes), therefore simulations of laboratory and/or closed form solutions that may need non-geographical coordinates cannot be processed with the Tsunami Mesh.

The bathymetric and/or topographic data built-in with the Tsunami Mesh are in a 2-minute grid. In addition, the user can specify several other data formats like contour lines and random points as input to the program.

The front end of the local tsunami analysis program is also responsible for generation of boundary data between nested grids. A small post processor with which the tide gauges and/or mareographs at pre-defined output locations could be viewed, is available with the same program.

The Tsunami Code consists of two programs, namely the distant tsunami analysis program and the local tsunami analysis program. The distant tsunami simulation is conducted using a spherical coordinate system. The governing equations of near field problems are described in the Cartesian coordinate system. Both codes compute the tsunami sources and the deformation as the initial conditions. The local tsunami analysis module has some additional functionalities that include modelling of propagation of waves as input from the boundary of domain (i.e. from the distant tsunami analysis code), nesting of grids and estimation of wave inundation into dry land. The distant tsunami analysis code generates input waves to boundaries of only one near field domain at a time.

The Tsunami Code can predict data such as maximum water level, range of run-up areas and first-wave times of arrival in coastal areas. The code calculates water level and discharge flux at a time interval Δt by using the equation of fluid motion and the equation of continuum for given parameters such as bathymetric data, still water depth and source conditions. As an example, governing equations for local tsunami analysis and its coordinate system are expressed as follows (see Fig. I–1).

Equation of Motion:

$$\frac{\partial M}{\partial t} = -g(h+\xi)\frac{\partial \xi}{\partial x} - \frac{\partial}{\partial x}\left(\frac{M^2}{h+\xi}\right) - \frac{\partial}{\partial y}\left(\frac{MN}{h+\xi}\right)$$

$$+\nu_H\left(\frac{\partial^2 M}{\partial x^2} + \frac{\partial^2 M}{\partial y^2}\right) - \gamma_b^2 \frac{M\sqrt{M^2+N^2}}{h+\xi} \quad \text{(I–1)}$$

$$\frac{\partial N}{\partial t} = -g(h+\xi)\frac{\partial \xi}{\partial y} - \frac{\partial}{\partial x}\left(\frac{MN}{h+\xi}\right) - \frac{\partial}{\partial y}\left(\frac{N^2}{h+\xi}\right)$$

$$+\nu_H\left(\frac{\partial^2 N}{\partial x^2} + \frac{\partial^2 N}{\partial y^2}\right) - \gamma_b^2 \frac{N\sqrt{M^2+N^2}}{h+\xi} \quad \text{(I–2)}$$

Where: M is the discharge flux in the x-direction (m^2/sec), N is the discharge flux in the y-direction (m^2/sec), t is time (sec), g is the gravitational acceleration (m/sec^2), h is the still water depth (m), ξ is the water level (m), ν_H is the horizontal eddy viscosity and γ_b^2 is bottom friction.

Equation of continuum:

$$\frac{\partial \xi}{\partial t} = -\frac{\partial M}{\partial x} - \frac{\partial N}{\partial y} + \frac{\partial \eta}{\partial t} \quad \text{(I–3)}$$

Where: η is bottom deformation (m).

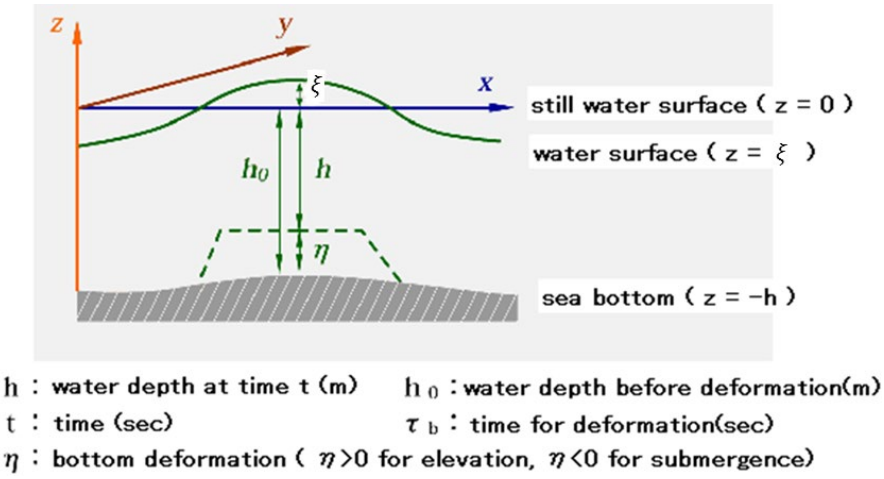

FIG. I–1. Coordinate system of local tsunami analysis (reproduced with permission of Nuclear Regulation Authority Japan [I–20]).

The details on the validation of the Tsunami Code as well as a comparison of its performance with other codes are covered also in the following publications [I–21, I–22]. The appendices to these publications also cover information on the performance of the Tsunami Code with respect to benchmark problems.

I–3.2.2. Analysis procedure (how to)

The flowchart of the calculation process is shown in Fig. I–2. Firstly, the code reads analysis conditions, bathymetric data and water surface displacement. The analyst can choose whether to provide the value of water surface displacement directly or to compute the ocean bottom deformation from fault parameters. Then, the code calculates the water level and the discharge flux at selected time intervals on the basis of the equation of motion and the equation of continuum. Water level and fluid velocity at selected time intervals are given as output data.

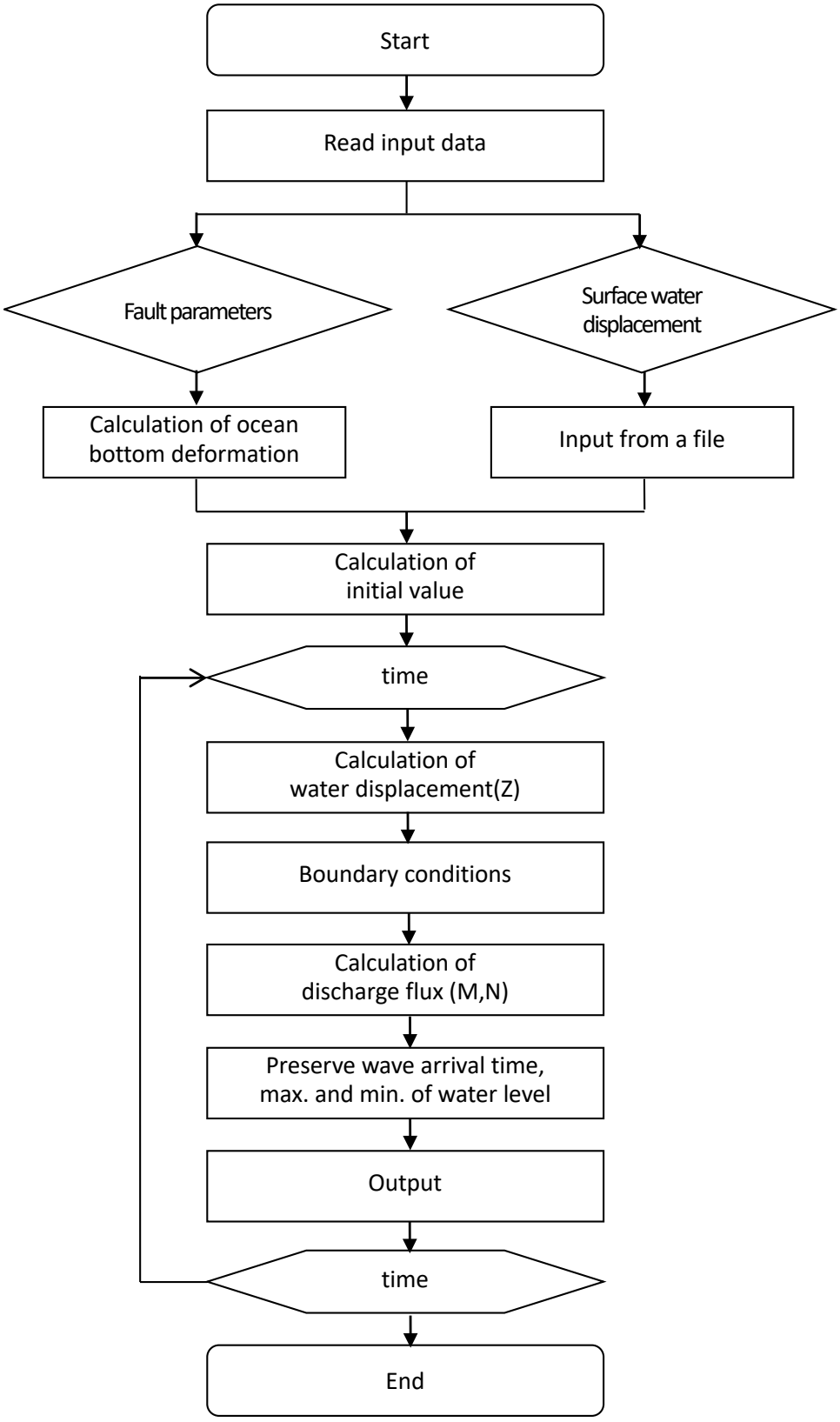

FIG. I–2. Flow chart of program. (Reproduced with the permission of Regulatory Standard and Research Department Secretariat of Nuclear Regulation Authority [I–20]).

I–3.2.3. Input data

The Tsunami Code uses three types of data as input files of simulation;

(a) FT07: conditions for analysis (e.g. time duration, region data, output interval);

(b) FT08: bathymetric data;

(c) FT10: tsunami source parameters (ocean bottom deformation data or water surface displacement data).

The Tsunami Code can compute the following:

(a) The tsunami source from either rupture characteristics or a pre-determined wave form;

(b) Propagation;

(c) Time of arrival;

(d) Coastal amplification;

(e) Inundation (according to the accuracy of the grid size);

(f) Distribution of discharge fluxes at selected time intervals;

(g) Distribution of water surface elevations (sea state) at selected time intervals;

(h) Time histories of water surface fluctuations at selected gauge locations;

(i) Animation of tsunami propagation between the source and the target regions.

Note that the Tsunami Code is not aimed to simulate the velocity of the tsunami. Users have to calculate it manually based on the data of discharge fluxes and water levels at the same point.

I–4. THE SIMULATIONS AND COMPARISONS WITH ANALYTICAL DATA

The results of the application of NAMI DANCE and Tsunami Code to analytical benchmark problems 1 and 2 are given in this subsection.

I–4.1. Testing of analytical benchmark 1 by using NAMI DANCE

Table I–3 presents the simulation condition of analytical benchmark 1 by using NAMI DANCE. X-direction is chosen as the long side of the model. The model is gridded to 10 m-mesh with closed boundary condition. The water surface elevations and current velocity distribution along the channel axis at different time steps ($t = 0$ s, $t = 160$ s, $t = 175$ s and $t = 220$ s) are plotted for comparison of the numerical and analytical results. Figure I–3 shows the inputted wave and Figs I–4 and I–5 show the numerical and analytical results for analytical benchmark 1. Based on special variations in water level, RMS Error and MAX are obtained at each selected time as shown in Table I–4. The time of arrival of the simulated wave and the water level at 175 s and 225 s correspond well to the analytical ones, satisfying the acceptance criteria for RMS error (≤ 10%, see Section 2.3.2). Table I–4 also shows the RMS error.

TABLE I–3. SIMULATION CONDITION OF ANALYTICAL BENCHMARK 1 BY USING NAMI DANCE

Mesh number in X-direction	Mesh number in Y-direction	Mesh size (m)	Boundary condition of Channel sides
2401	401	10	Open boundary

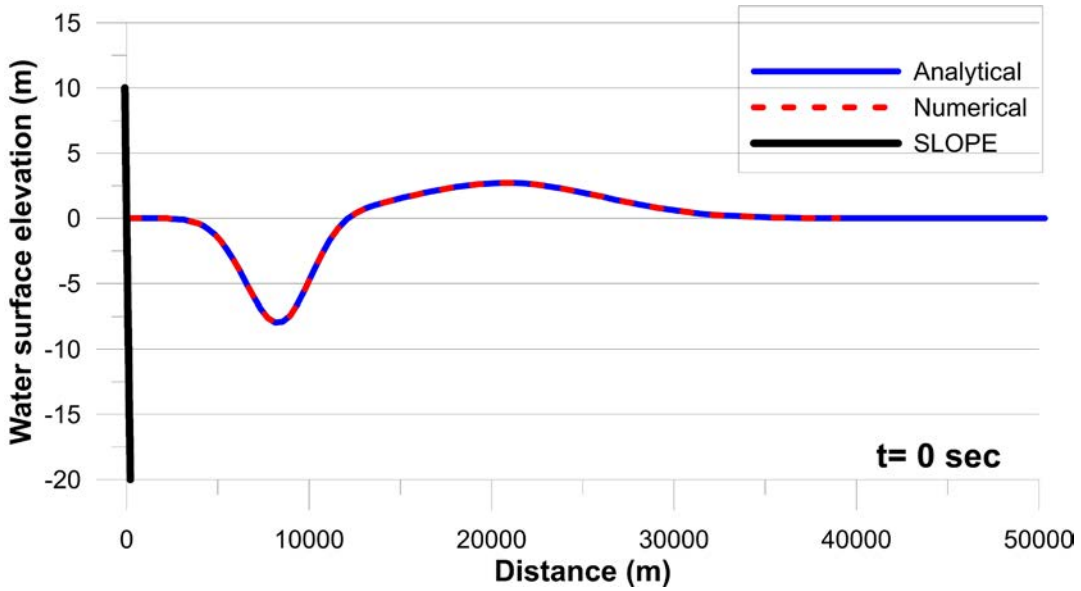

FIG. I–3. Initial water surface elevation along the axis perpendicular to shoreline for numerical and analytical results (Units are in metre).

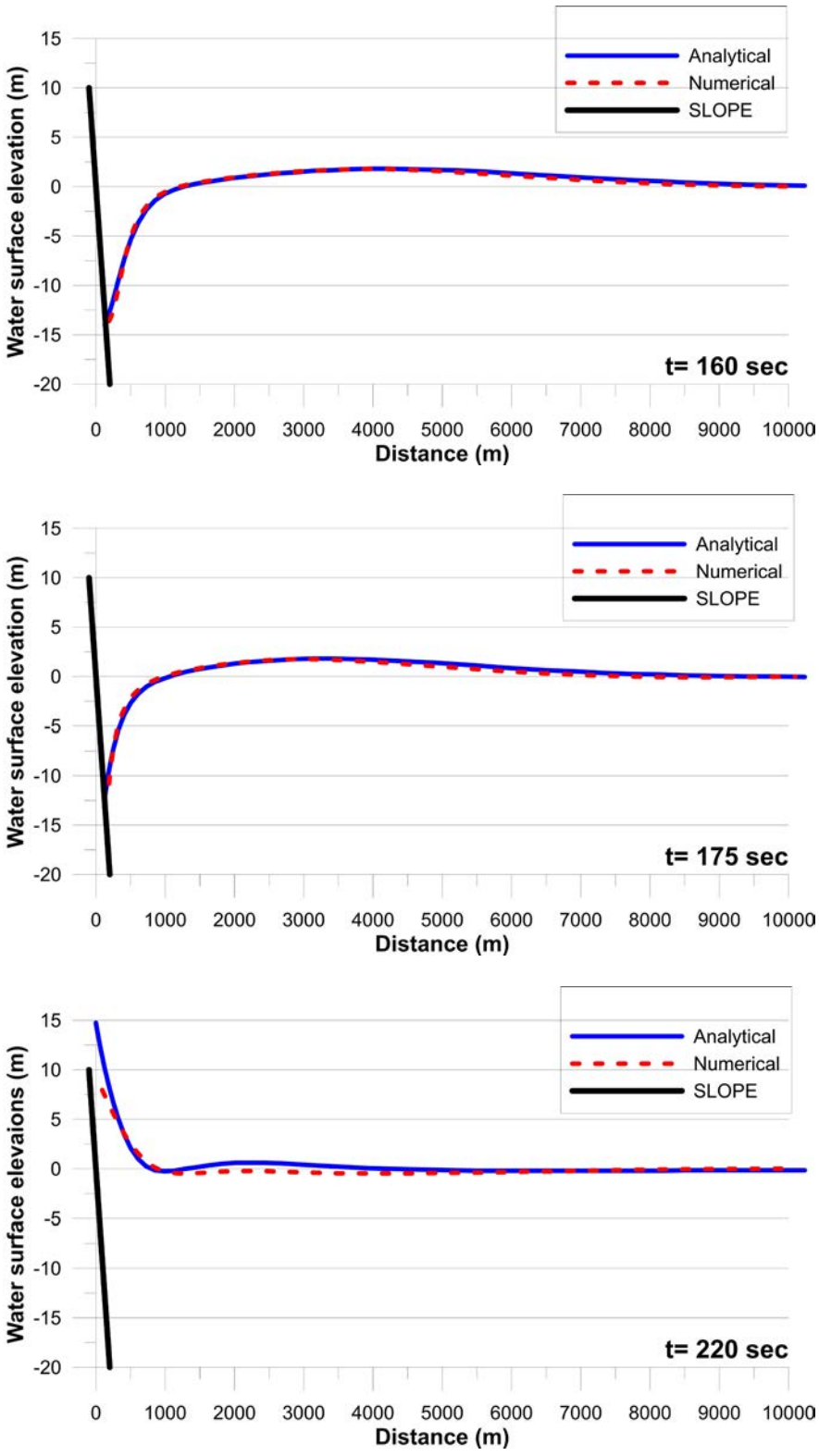

FIG. I–4. Water surface elevations along the axis perpendicular to shoreline at t=160 s, t=175 s and t=220 s for numerical and analytical results.

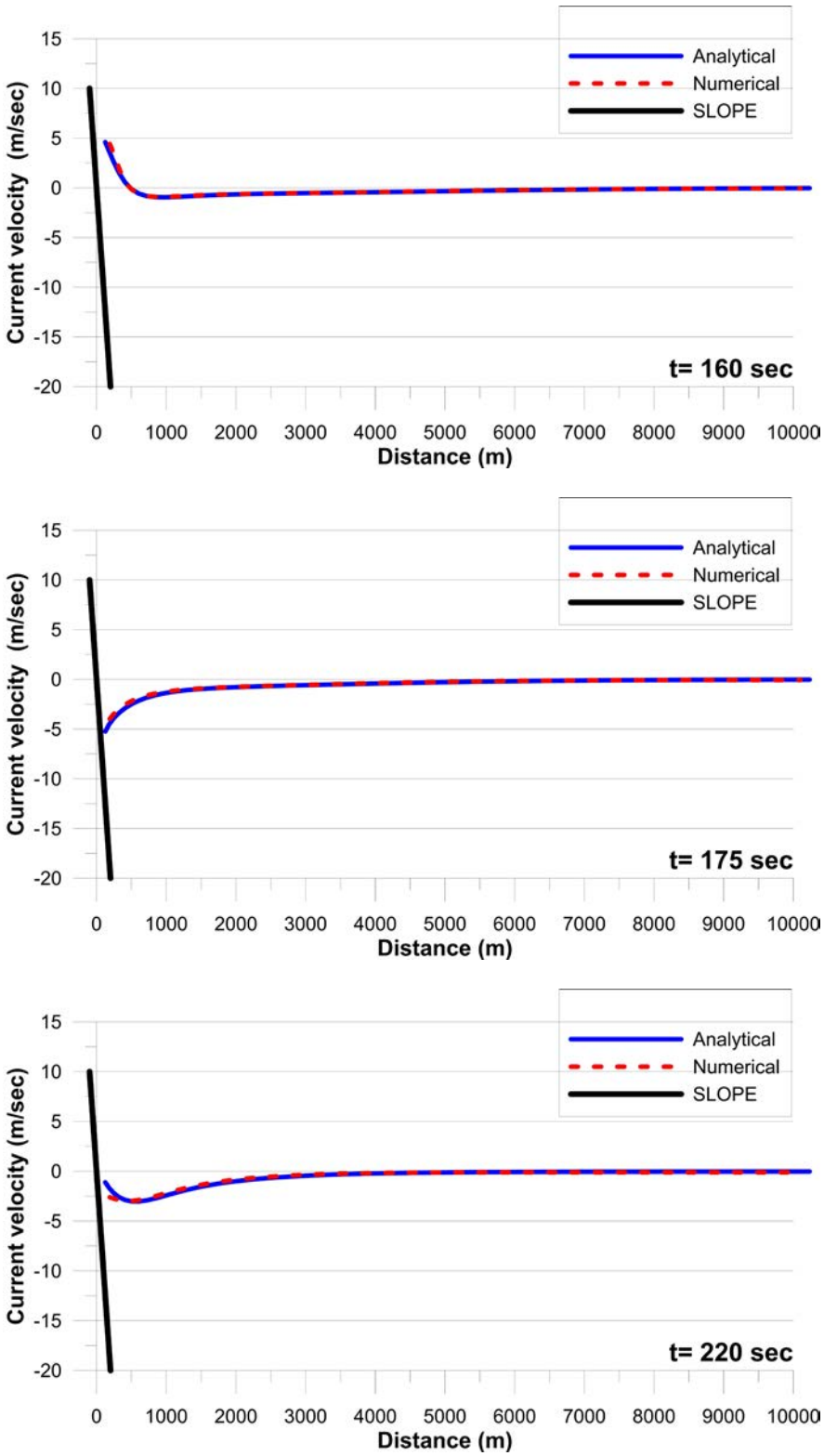

FIG. I–5. Current velocity distribution along the axis perpendicular to shoreline at t=160 s, t=175 s and t=220 s for numerical and analytical results (vertical axis is m/s, horizontal axis is m).

TABLE I–4. RMS ERROR OF NAMI DANCE COMPUTED FOR 50 m DATA SPACING FOR ANALYTICAL BENCHMARK PROBLEM 1 AT SPECIFIED TIME (*In the Interval from Shoreline to X=10 000 m*)

Time (s)	Parameter	RMS error (%)
0	Water elevation	0
160	Water elevation	1
175	Water elevation	2
220	Water elevation	10
0	Velocity	0
160	Velocity	1
175	Velocity	2
220	Velocity	6

I–4.2. Testing of analytical benchmark 1 by using the Tsunami Code

Table I–5 presents the simulation condition of analytical benchmark 1 by using the Tsunami Code. X-direction is chosen as the long side of the model. The model is gridded to 25 m -mesh with closed boundary condition. Figure I–6 shows the numerical and analytical results for analytical benchmark 1. The water surface elevations plotted along the channel axis at t = 0 s, t = 160 s, t = 175 s and t = 220 s from the front edge to x = 10 000 m. Based on special variations in the water level, RMS error is obtained at each time as shown in Table I–6. The time of arrival of the simulated wave and the water level correspond well to the analytical ones, satisfying the acceptance criteria for the RMS error (≤ 10% for RMS. see Section 2.3.2). However, RMS errors for velocity at t = 220 s do not satisfy the acceptance criteria. This may be attributed to inaccuracy in the velocity simulation at a shallow part of the wave.

TABLE I–5. SIMULATION CONDITION OF ANALYTICAL BENCHMARK1 BY USING TSUNAMI CODE

Mesh number in X-direction	Mesh number in Y-direction	Mesh size (m)	Boundary condition
1612	400	25	Closed boundary

FIG. I–6. Water surface elevations along the axis perpendicular to shoreline at t=0sec, t=160 s, t=175 s and t=220 s for numerical and analytical results (in the interval between the front edge and x=10 000 m).

TABLE I–6. RMS ERROR OF TSUNAMI CODE COMPUTED FOR 25 M DATA SPACING FOR ANALYTICAL BENCHMARK 1 (IN THE INTERVAL BETWEEN THE FRONT EDGE AND X=10 000 M)

Time (s)	Parameter	RMS error (%)
0	Water elevation	0
160	Water elevation	0
175	Water elevation	0
220	Water elevation	2
0	Velocity	0
160	Velocity	10
175	Velocity	1
220	Velocity	14

I–4.3. Testing of analytical benchmark 2 by using NAMI DANCE

The plan view of the initial wave and the section used to plot water surface at different time steps are given in Fig. I–7. Table I–7 presents the simulation condition of analytical benchmark 2 by using NAMI DANCE. The cross-sectional view of the water surface elevation at different time steps (0, 20 and 60 s) and the maximum water levels for analytical and numerical results are given in Figs I–8 and I–9. Table I–8 shows RMS error and MAX at t = 0 s, t = 20 s and t = 60 s based on special variations in the water level. The time of arrival of the simulated wave and the water level are in good agreement with the analytical ones.

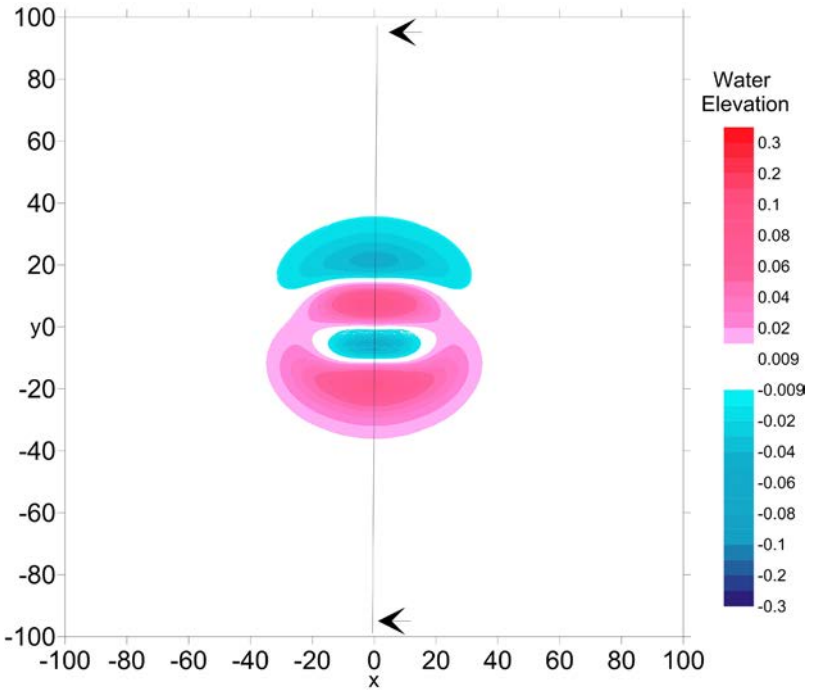

FIG. I–7. Plan view of initial water level distribution in dimensionless form.

TABLE I–7. SIMULATION CONDITION OF ANALYTICAL BENCHMARK 2 BY USING NAMI DANCE

Mesh number in X-direction	Mesh number in Y-direction	Mesh size (m)	Boundary condition
2222	2222	100	Open boundary

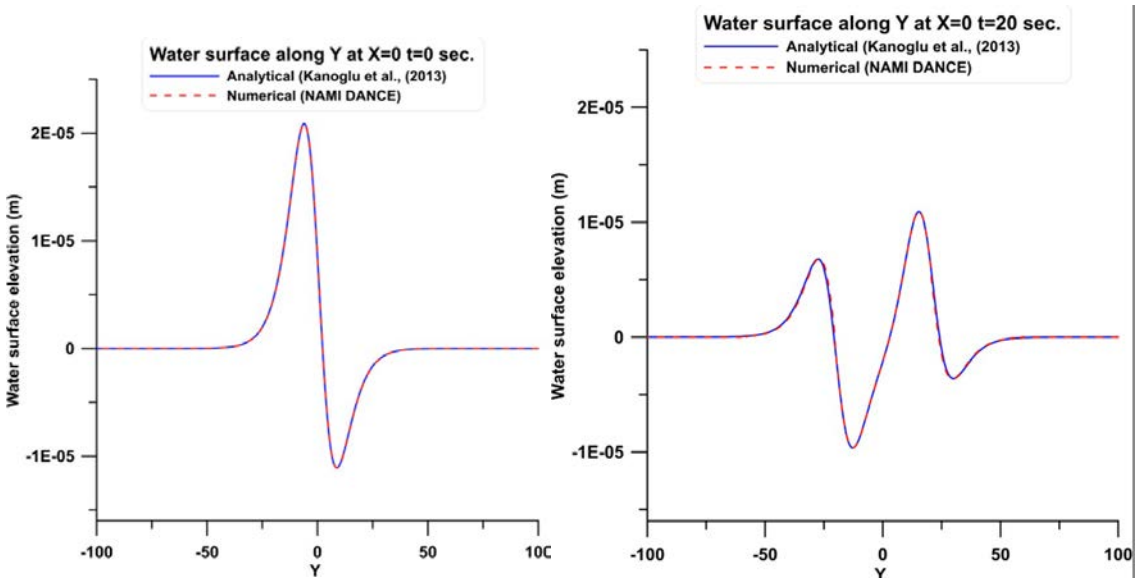

x=0 and t=0 s x=0 and t=20 s

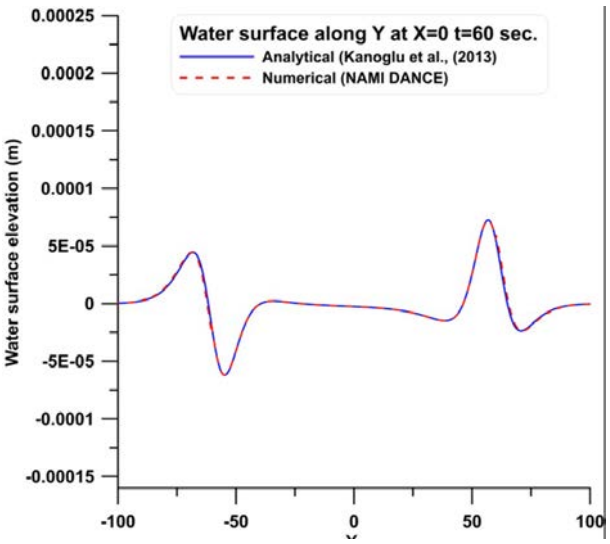

x=0 and t=60 s

FIG. I–8. Cross-section of water surface elevation of analytical and numerical results.

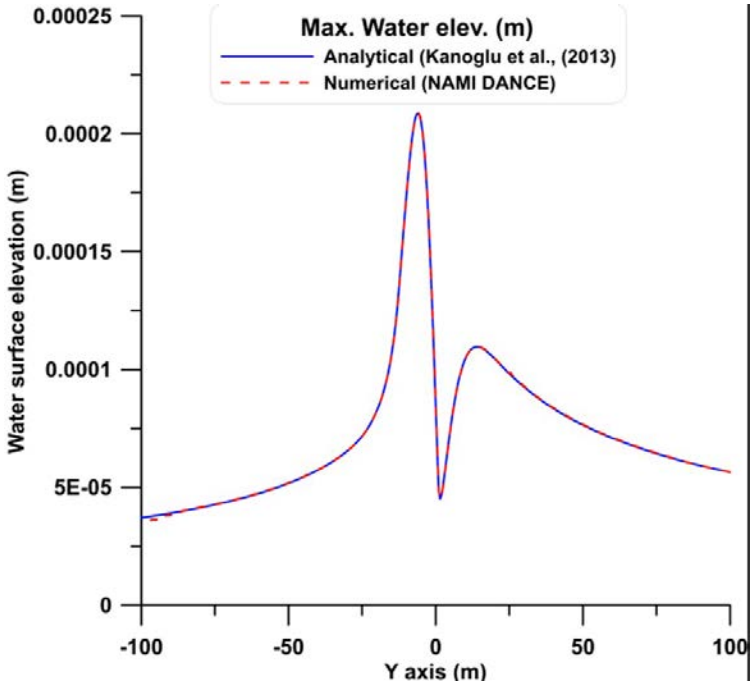

FIG. I–9. Comparison of maximum water elevations of analytical and numerical results.

TABLE I–8. RMS ERROR AND MAX OF NAMI DANCE FOR ANALYTICAL BENCHMARK PROBLEM 2

Time (s)	Parameter	RMS error (%)	MAX (%)
0	Water elevation	0	0
20	Water elevation	1	0
60	Water elevation	1	1

I–4.4. Testing of analytical benchmark 2 by using tsunami code

Table I–9 presents the simulation condition of analytical benchmark 2 by using the Tsunami Code. Note that the spatial variables and the temporal variables were multiplied by 10 000 and by 100 as a scale factor, respectively. The cross-sections of water surface elevation at 0, 20 and 60 s for analytical and numerical results are shown in Fig. I–10. The cross-section of the maximum water level and its contour for numerical results are given in Figs I–11 and I–12. Table I–10 shows RMS Error and MAX at t = 0 s, t = 20 s and t = 60 s based on special variations in the water level. The time of arrival of the simulated wave and the water level are in good agreement with the analytical ones. Though RMS and MAX slightly increase with the elapse of time, the results satisfy the acceptance criteria within the simulation time (≤ 10% for RMS and ≤ 5% for MAX, see Section 2.3.2).

TABLE I–9. SIMULATION CONDITION OF ANALYTICAL BENCHMARK 2 BY USING TSUNAMI CODE

Mesh number in X-direction	Mesh number in Y-direction	Mesh size (m)	Boundary condition
405	405	5 000	Open boundary

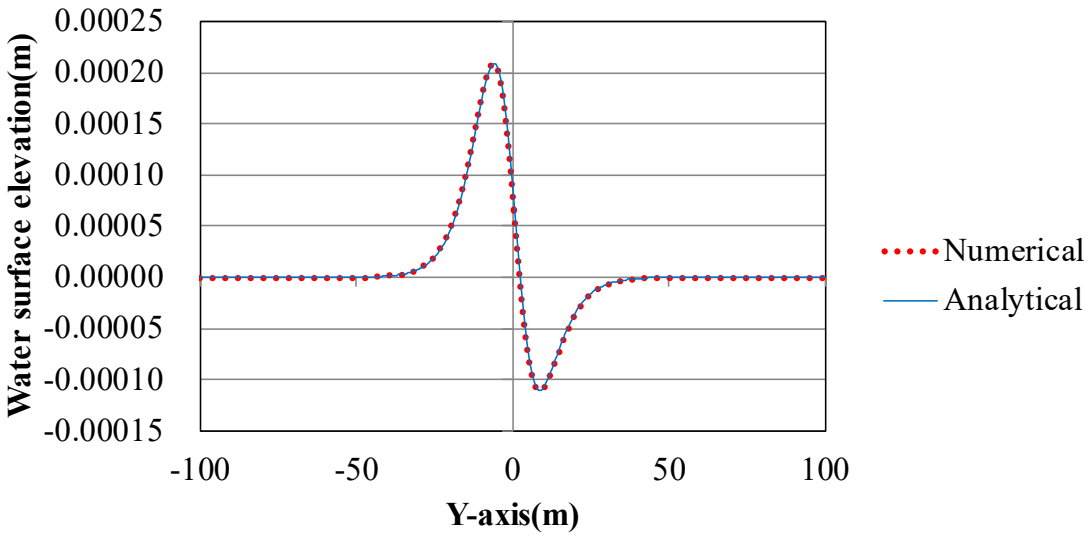

x =0 and t=0 s

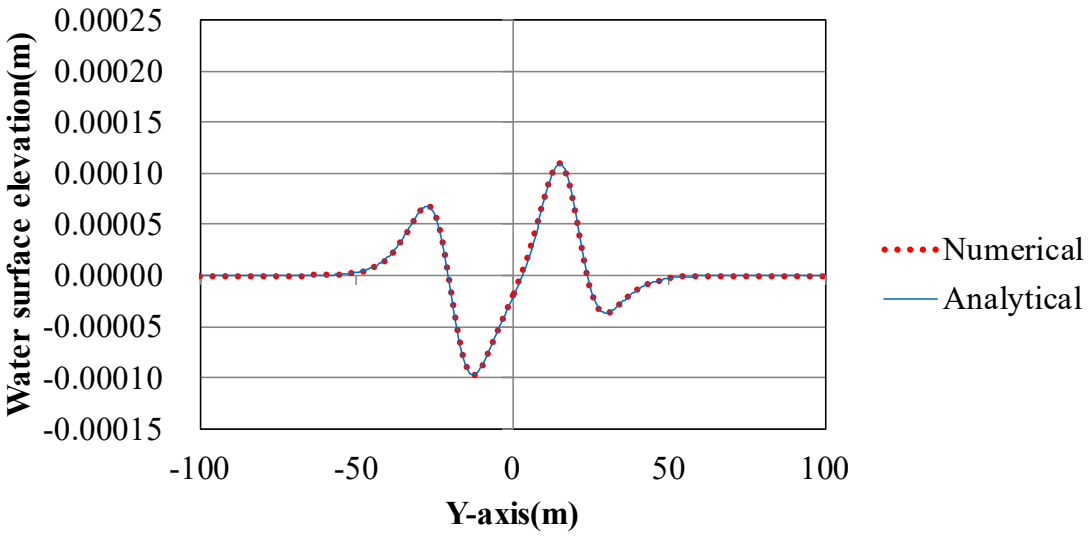

x = 0 and t = 20 s

FIG. I–10. Cross-section of water surface elevation for analytical and numerical results.

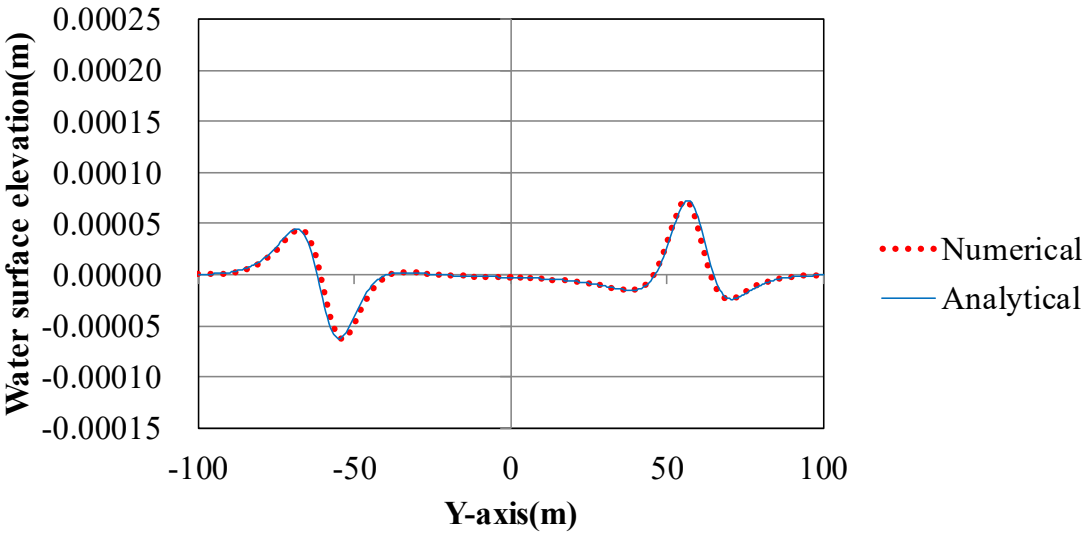

x = 0 and t = 60 s

FIG. I–10. Cross-section of water surface elevation for analytical and numerical results. (cont.)

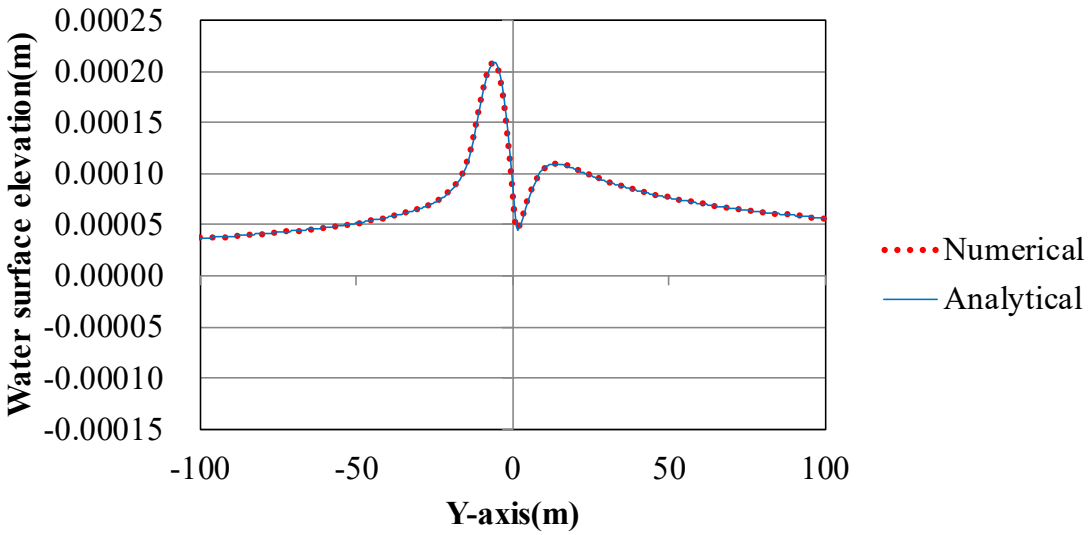

FIG. I–11. Cross-section of maximum water level (x=0).

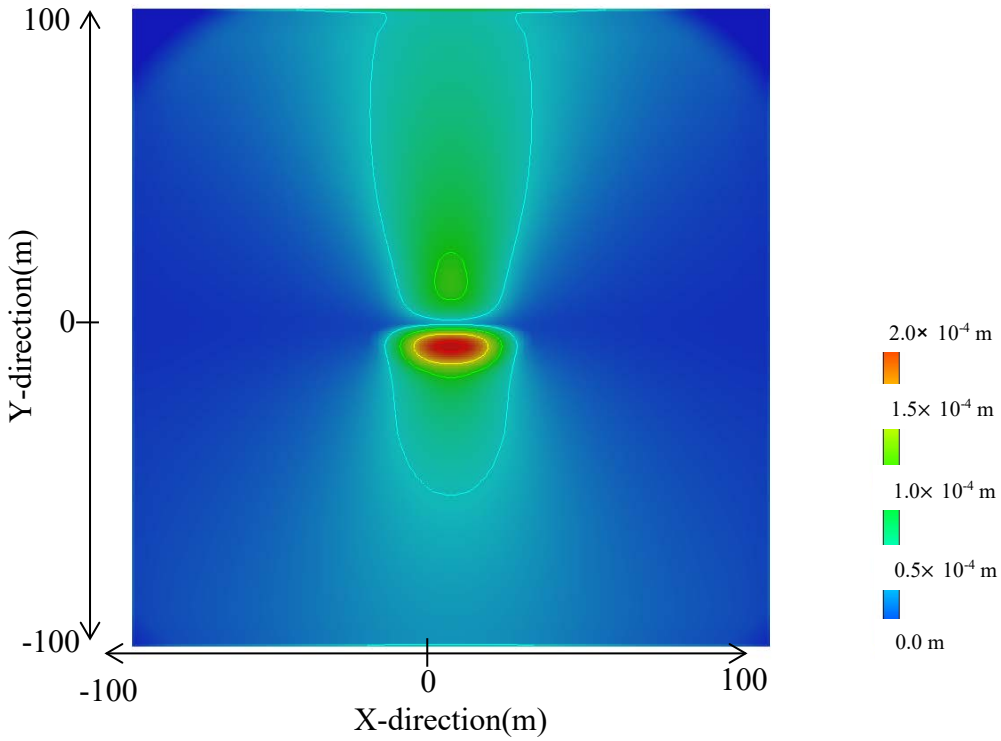

FIG. I–12. Contour for maximum water level.

TABLE I–10. RMS ERROR AND MAX OF TSUNAMI CODE FOR ANALYTICAL BENCHMARK PROBLEM 2

Time (s)	Parameter	RMS error (%)	MAX (%)
0	Water elevation	0	0
20	Water elevation	1	0
60	Water elevation	2	1

REFERENCES TO ANNEX I

[I-1] KANOĞLU, U., Nonlinear evolution and runup-rundown of long waves over a sloping beach, Journal of Fluid Mechanics **513** (2004) 363–372.

[I-2] KANOĞLU, U., et al., Focusing of long waves with finite crest over constant depth, Proc. R. Soc. Lond. A **469** (2013) 20130015.

[I-3] KANOĞLU, U., SYNOLAKIS, C., Initial value problem solution of nonlinear shallow water-wave equations, Physical Review Letters **97** (2006) 148501.

[I-4] KANOĞLU, U., Theoretical Solution of the Wave Run-up on 1/10 Sloping Beach, Joint Workshop of Benchmark Problems, Numerical Models, Inundation Maps and Test Sites in EC funded TRANSFER Project, Fethiye (2007).

[I-5] YALCINER, A.C., PELINOVSKY, E., ZAYTSEV, A., KURKIN, A., OZER, C., KARAKUS, H., NAMI DANCE Manual, Middle East Technical University, Civ. Eng. Dep., Ocean Eng. Res. Cent., Ankara (2006).

[I-6] IMAMURA F., Tsunami Numerical Simulation with the staggered leap-frog scheme (Numerical code of TUNAMI-N1), School of Civil Engineering, Asian Inst. Tech. and Disaster Control Research Center, Tohoku University (1989).

[I-7] SHUTO, N., GOTO, C., IMAMURA, F., Numerical simulation as a means of warning for near-field tsunamis, Coastal Engineering in Japan **33** 2 (1990) 173–193.

[I-8] GOTO, C., OGAWA, Y., "Numerical Method of Tsunami Simulation With the Leap ‐Frog Scheme", Translated for the Time Project by Prof. Shuto, N., Disaster Control Res. Cent., Faculty of Eng., Tohoku University (1991).

[I-9] SYNOLAKIS, C.E, LIU, P.L.F., YEH, H., Third International Workshop on Long-Wave Run-up Models, Organized by National Science Foundation, Catalina Island, California, USA (2004).

[I-10] YALCINER, A.C., SYNOLAKIS, C.E, GONZALES, M., KANOĞLU, U., Inundation Map and Test Sites of EU TRANSFER Project, Joint Workshop of Benchmark Problems, Numerical Models, Inundation Maps and Test Sites in EC funded TRANSFER Project, Fethiye (2007).

[I-11] YALCINER, A.C., KURAN, U., AKYARLI, A., IMAMURA, F., "An Investigation on the Propagation of Tsunamis in the Aegean Sea by Mathematical Modeling", Tsunami: Progress in Prediction, Disaster Prevention and Warning (TSUCHIYA, Y., SHUTO, N., Eds), Advances in Natural and Technological Hazards Research, Volume 4, Springer Netherlands, Houten (1995) 55–70.

[I-12] YALCINER, A.C., ALPAR, B., ALTINOK, Y., OZBAY, I., IMAMURA, F., Tsunamis in the sea of Marmara: Historical documents for the past, models for the future, Mar. Geol., Special Issue **190** (2002) 445–463.

[I-13] YALCINER, A.C., PELINOVSKY, E.N., TALIPOVA, T.G., KURKIN, A.A., KOZELKOV, A.C., ZAITSEV, A.I., Tsunamis in the Black Sea: Comparison of the historical, instrumental and numerical data, Journal of Geophysical Research **109** (2004) C12023.

[I-14] YALCINER, A.C., IMAMURA, F., SYNOLAKIS, EC, Simulation of Tsunami Related to Caldera Collapse and a Case Study of Thera Volcano in Aegean Sea, Session NH8, EGS XXVII General Assembly, Nice (2002) (abstract #5450).

[I-15] YALCINER, A.C., PELINOVSKY, E., ZAYTSEV, A., KURKIN, A., OZER, C., KARAKUS, H., Modeling and visualization of tsunamis: Mediterranean examples, Tsunami and Nonlinear Waves (KUNDU, A., Eds), Springer Berlin Heidelberg, Heidelberg (2007) 273-263.

[I-16] ZAHIBO, N., PELINOVSKY, E., YALCINER, A.C., KURKIN, A., KOZELKOV A., ZAITSEV, A., The 1867 Virgin Island tsunami: observations and modelling, Oceanologica Acta **26** 5-6 (2003) 609–621.

[I-17] ZAHIBO, N., PELINOVSKY, E., KURKIN, A., KOZELKOV, A., Estimation of far-field tsunami potential for the Caribbean coast based on numerical simulation, Science of Tsunami Hazards **21** 4 (2003) 202–222.

[I-18] INTERNATIONAL ATOMIC ENERGY AGENCY, IAEA Extra Budgetary Project (EBP) on Protection of Nuclear Power Plants against Tsunamis and Post Earthquake Considerations in The External Zone (TiPEEZ), Final Report, IAEA-EBP-TS-004, IAEA, Vienna (2010).

[I-19] JAPAN NUCLEAR ENERGY SAFETY ORGANIZATION, Tsunami Code Manual, JNES, Tokyo (2014).

[I-20] JAPAN NUCLEAR ENERGY SAFETY ORGANIZATION, Tsunami Simulation Code, Tsunami Manual, JNES, Tokyo (2012).

[I-21] ROSHAN, A.D., Benchmark analysis of JNES software: Experience feedback from AERB, Kick-off Meeting of Tsunami Hazards Work Area, Vienna (2011).

[I-22] ROSHAN, A.D., BASU, P.C, JANGID, R.S., Performance evaluation of some tsunami numerical models for far field propagation of 2011 tsunami, International Tsunami Symposium (ITS), Göcek and Rodos (2013).

ANNEX II: BENCHMARK PROBLEMS BASED ON LABORATORY EXPERIMENTS

The laboratory experiment, run-up of the Okushiri tsunami at Monai [II-1], as given in Section 4 is selected as experimental benchmark problem for testing the tsunami numerical models. The data of the benchmark problem are given in this annex.

II–1. DATA OF EXPERIMENTAL BENCHMARK PROBLEM (RUN-UP OF OKUSHIRI TSUNAMI AT MONAI)

The offshore profile of the experimental area, experimental setup, gauge locations, time history of the wave inputted from the left border and the time histories of water levels at different gauges are shown in Section 4. The bathymetry file, gauge locations, input wave data and measured time histories of the water levels at Gauges number 5, 7 and 9 are given in Annex IV (Laboratory Experiments). The content of each file is given in Table II–1.

TABLE II–1. SHORT DESCRIPTION OF THE FILES IN THE SUPPLEMENT

File Name	Description
domain-b-spherical-prototype-wall.dat	The bathymetry of the benchmark area in prototype-geophysical scale (Monai region). The data are in XYZ ASCII format with X: longitude, Y: latitude and Z: water depth. X and Y are in degree, decimal format and Z is in metre (sea is positive, and land is negative).
gauges-locations-5-7-9-b-spherical-x-400.dat	The coordinates of each gauge (Channel 5, 7, 9). The data are 3 columns. First column represents name of the Channel and second and third columns show the coordinates (longitude and latitude, respectively) of each Channel in degree, decimal format.
input-wave-from-left-border-prototype-400-dt-point-0125sec.dat	Input wave record is two-column file. First column is time, and second column is the respective water elevation. The file is 0.0125 s intervals.
output_ch5-7-9-original-prototype-min-meter-total-10min-record.dat	The record of measured water elevations during the experiments. The file is 4 columns. First column is time in seconds, the other columns are the water elevations measured at Channel 5, 7 and 9, respectively.
domain-b-cartesian-prototype.dat	The bathymetry of the benchmark area in model scale (in Cartesian coordinates). If any user wishes to simulate this benchmark in model scale, then this file can be used as bathymetry file. The data are in XYZ ASCII format with X: in wave direction, Y in the direction perpendicular to wave direction in horizontal plane and Z: water depth. X, Y and Z are in metre. X is positive in the direction of the wave. Z is positive in the sea and negative at land.

II–3. APPLICATION USING SPECIFIC SOFTWARE

Two different tsunami numerical models are used to make the comparisons between experimental and analytical results. The models are NAMI DANCE and Tsunami Code and they are briefly described in Section I–3 of Annex I.

II–4. SIMULATIONS AND COMPARISONS WITH EXPERIMENTAL DATA

The results of the application of NAMI DANCE and Tsunami Code to the experimental benchmark problem are given in the following subsections.

II–4.1. Testing of experimental benchmark by using NAMI DANCE

The experiment benchmark is simulated by NAMI DANCE according to the simulation conditions given in Table II–2. Although the observation data were acquired in laboratory scale, a full scale model ($\Delta x = \Delta y = 5$ m) was constructed for the simulation. The side boundaries are selected as wall type to prevent energy loss in lateral direction.

The comparison of experimental and numerical results of time histories of water levels at channels 5, 7 and 9 are given in Figs II–1, II–2 and II–3. The numerical results given in the figures are computed by solving the non-linear shallow water equations in spherical coordinates (in prototype dimensions).

Table II–3 shows RMS error and MAX of temporal variations in water level from $t = 0$ s to $t = 450$ s. Regarding RMS and MAX, the results satisfy the criteria for the laboratory experimental benchmark (≤ 15% for RMS and ≤ 10% for MAX. see Section 2.3.2).

TABLE II–2. SIMULATION CONDITION OF EXPERIMENTAL BENCHMARK BY USING NAMI DANCE

Nested Domains	Mesh number in X-direction	Mesh number in Y-direction	Mesh size (m)	Total simulation duration (s)	Boundary condition
Largest Domain	190	306	7.2	600	Closed boundary

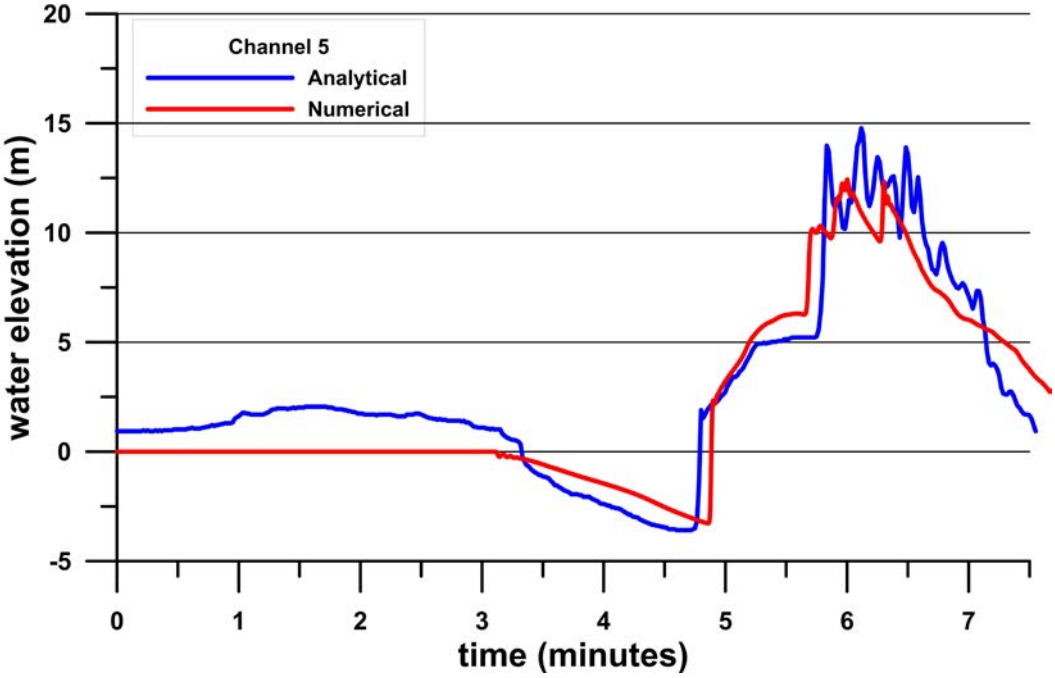

FIG. II–1. Comparison of the measured and computed water elevations at channel 5.

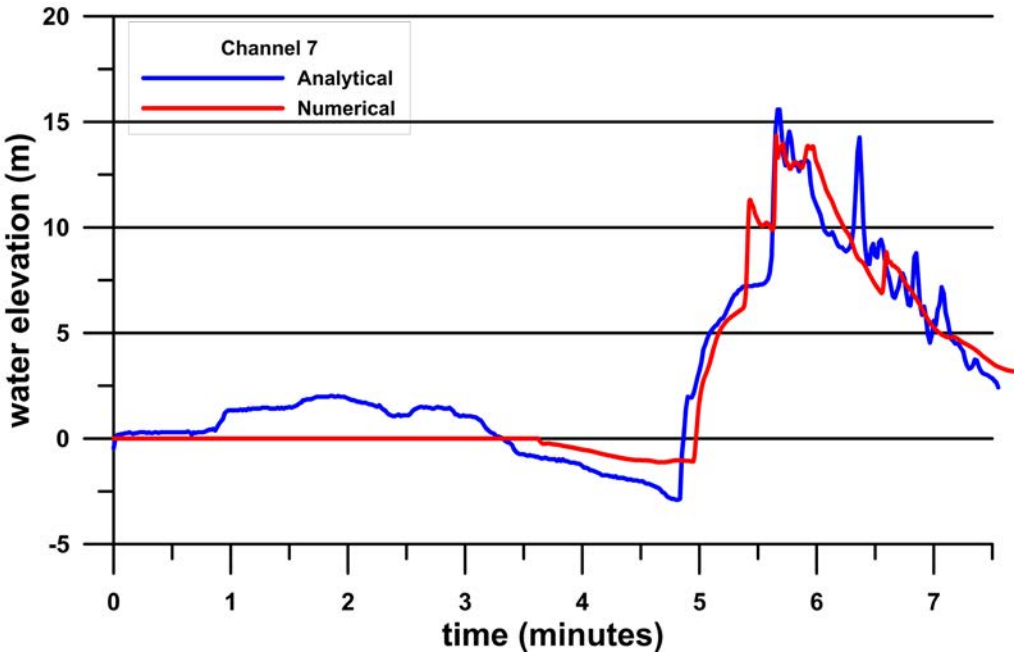

FIG. II–2. Comparison of the measured and computed water elevations at channel 7.

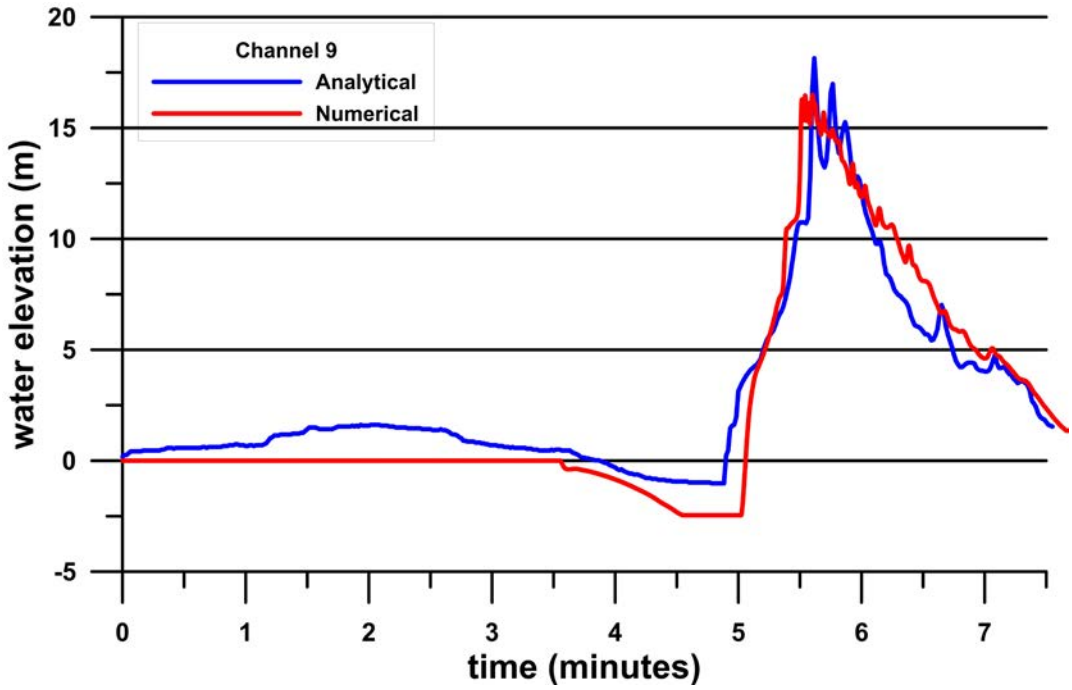

FIG. II–3. Comparison of the measured and computed water elevations at channel 9.

TABLE II–3. RMS ERROR AND MAX OF NAMI DANCE FOR EXPERIMENTAL BENCHMARK PROBLEM IN TIME SPAN BETWEEN WAVE RISE UP TO 450 s

Channel	Parameter	RMS error (%)	MAX (%)
5	Water elevation	10	15
7	Water elevation	12	8
9	Water elevation	10	9

II–4.2. Testing of experimental benchmark 1 by using tsunami code

Tsunami Code is used to simulate experimental benchmark 1. The simulation condition is shown in Table II–4. Although the observation data were acquired in laboratory scale, a full scale model ($\Delta x = \Delta y = 5.6$ m) was constructed for the simulation. The boundary condition at all the boundaries is the reflecting condition. On the whole, Figs II–4, II–5 and II–6 show good agreement of the simulated waveform with the laboratory observation at channels 5, 7 and 9. Table II–5 shows RMS error and MAX for temporal variations in water level from $t = 0$ s to $t = 450$ s. Regarding RMS and MAX, the results satisfy the criteria for the laboratory experimental benchmark ($\leq 15\%$ for RMS and $\leq 10\%$ for MAX, see Section 2.3.2).

TABLE II–4. SIMULATION CONDITION OF EXPERIMENTAL BENCHMARK BY USING TSUNAMI CODE

Mesh number in X-direction	Mesh number in Y-direction	Mesh size (m)	Total simulation time (s)	Boundary condition
399	250	5.6	450	Closed boundary

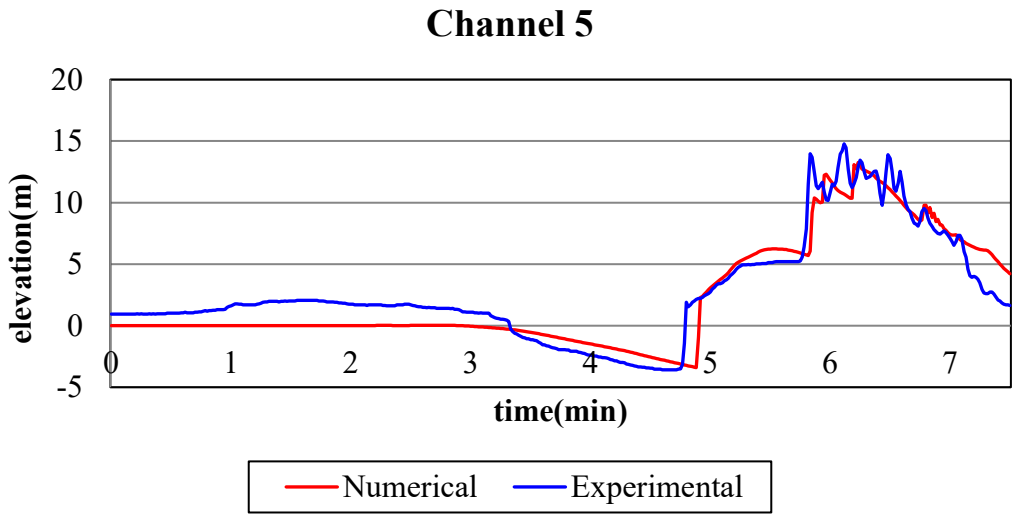

FIG. II–4. Comparison of the measured and computed water elevations at channel #5.

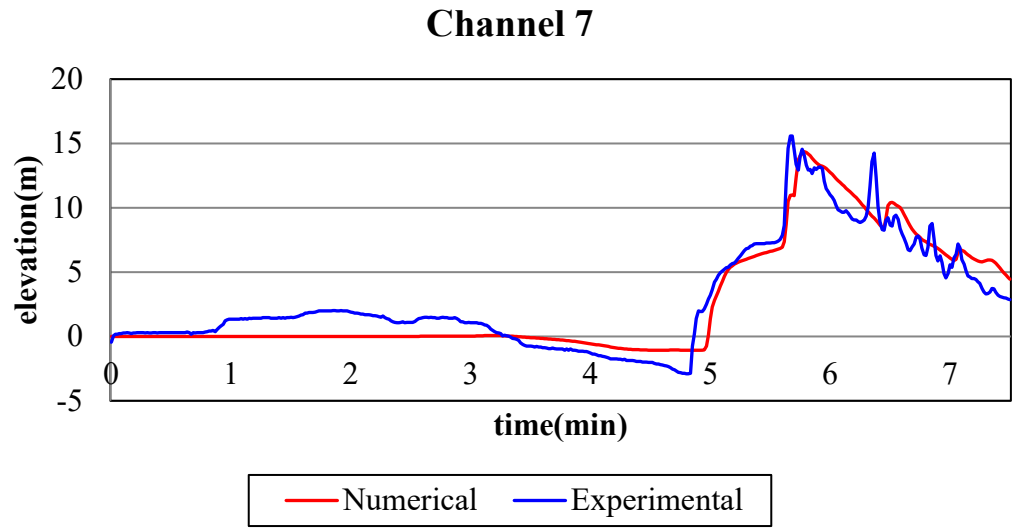

FIG. II–5. Comparison of the measured and computed water elevations at channel #7.

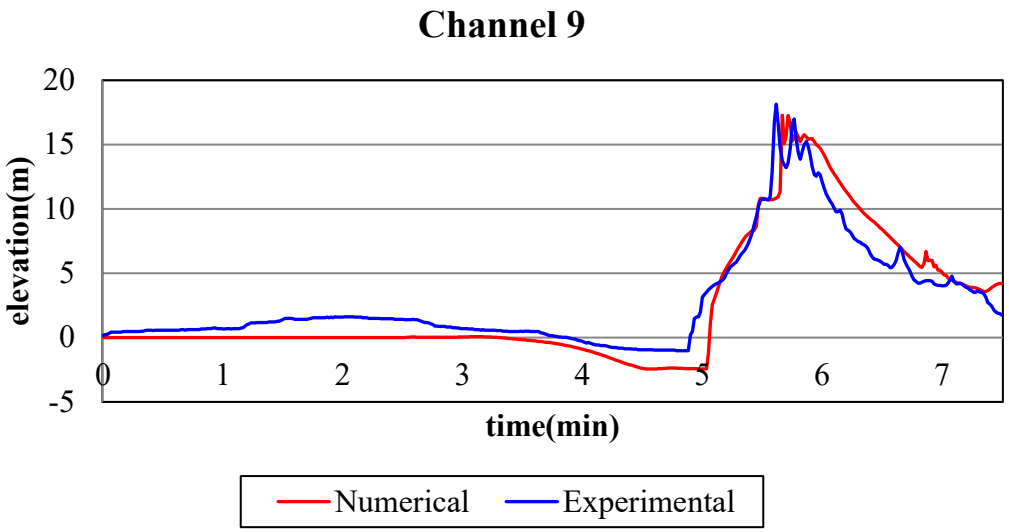

FIG. II–6. Comparison of the measured and computed water elevations at channel #9.

TABLE II–5. RMS ERROR AND MAX OF TSUNAMI CODE FOR EXPERIMENTAL BENCHMARK PROBLEM IN TIME SPAN BETWEEN WAVE RISE UP TO 450 S

Channel	Parameter	RMS error (%)	MAX (%)
5	Water elevation	9	10
7	Water elevation	7	8
9	Water elevation	8	5

REFERENCES TO ANNEX II

[II-1] MATSUYAMA, M., TANAKA, H., An experimental study of the highest runup height in the 1993 Hokkaido Nansei-oki earthquake tsunami, U.S. National Tsunami Hazard Mitigation Program Review and International Tsunami Symposium (ITS), Seattle, WA (2001) 879–889.

ANNEX III: BENCHMARK PROBLEMS BASED ON FIELD MEASUREMENTS

The objective of this annex is to demonstrate the details of the validation process for the benchmark problems based on field measurements. The benchmark problems are defined, and the source model, bathymetric data and tsunami records are described in main text. This annex describes practical details of the above conditions and data, as well as tsunami simulation codes. Information on relevant inputs needed for numerically simulating the local (near-field) and distant (far-field) tsunami propagation and run-up from the 2011 Great East Japan tsunami are also brought out along with examples of application using some numerical models.

III–1. LOCAL TSUNAMI DATA

This section covers the datasets that could be used to evaluate local tsunami propagation and run-up caused by the 2011 GEJE event.

III–1.1. Source model

This benchmark problem uses the Japan Nuclear Energy Safety Organization model as the source model for the Great East Japan tsunami [III–1]. The Japan Nuclear Energy Safety Organization model is aimed at reproducing not only the tsunami waveforms but also the tsunami traces at the nuclear power plant sites on the Pacific coast. The Japan Nuclear Energy Safety model is specified in the tsunami source area with reference to the Fujii and Satake model [III–2] from the Tohoku University and divided into 40 sub-faults (50 km × 50 km) and 8 sub faults (50 km × 30 km) as shown in Fig. III–1. The fault parameters are shown in Table III–1. The vertical displacement of the ocean floor was modelled using the elastic dislocation theory [III–3]. Tsunami waveforms are calculated assuming a dynamic rupture of the subfaults where the duration was 300 s. Further information on this model can be found in the following references [III–1, III–4].

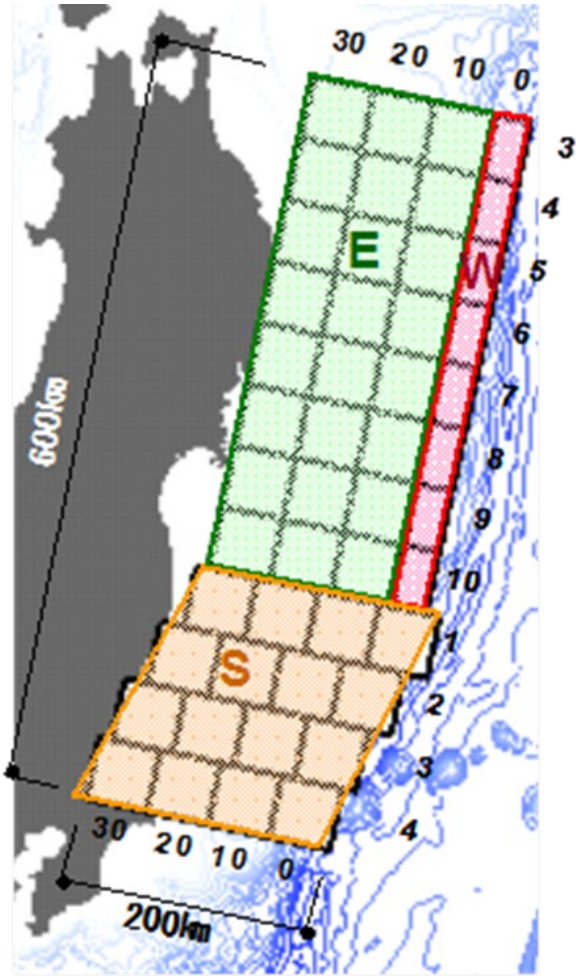

FIG. III–1. Sub-fault location of Japan Nuclear Energy Safety Organization model [III–1].

TABLE III–1. FAULT PARAMETERS OF JAPAN NUCLEAR ENERGY SAFETY MODEL

Fault number	Lat (°)	Lon (°)	Depth (km)	Strike (°)	Dip Angle (°)	Slip Angle (°)	Length (km)	Width (km)	Slippage(m)					Total slippage (m)
									30 s	90 s	150 s	210 s	270 s	
W03	40.68070	144.41018	0.00	192	20	81	50	30	0.00	0.00	0.00	0.00	0.00	0.00
W04	40.24438	144.26598	0.00	192	20	81	50	30	0.00	1.23	0.00	1.53	1.79	4.56
W05	39.80778	144.12379	0.00	192	20	81	50	30	0.00	0.00	0.00	0.00	15.16	15.16
W06	39.37091	143.98356	0.00	192	20	81	50	30	0.00	0.00	2.10	0.00	17.64	19.73
W07	38.93378	143.84523	0.00	192	20	81	50	30	0.00	3.91	4.15	1.32	16.54	25.92
W08	38.49639	143.70875	0.00	192	20	81	50	30	16.88	14.67	21.15	8.14	17.06	77.90
W09	38.05876	143.57406	0.00	192	20	81	50	30	16.00	9.12	17.21	14.51	10.06	66.91
W10	37.62089	143.44111	0.00	192	20	81	50	30	16.30	9.14	17.38	21.65	9.94	74.42
E13	40.74260	144.08682	10.26	192	9	81	50	50	0.00	0.00	1.41	0.00	0.00	1.41
E14	40.30581	143.94452	10.26	192	9	81	50	50	0.00	0.00	1.45	0.39	1.86	3.70
E15	39.86875	143.80421	10.26	192	9	81	50	50	0.00	1.98	0.00	0.00	0.00	1.98
E16	39.43143	143.66582	10.26	192	9	81	50	50	0.00	0.74	0.00	3.99	6.33	11.06
E17	38.99386	143.52930	10.26	192	9	81	50	50	4.61	3.34	3.23	1.12	6.28	18.59
E18	38.55605	143.39459	10.26	192	9	81	50	50	17.69	7.73	0.00	11.52	4.57	41.51
E19	38.11801	143.26163	10.26	192	9	81	50	50	10.36	14.12	1.04	0.14	0.00	25.66
E20	37.67973	143.13038	10.26	192	9	81	50	50	4.76	0.00	0.00	0.00	0.00	4.76
E23	40.84889	143.51879	18.08	192	9	81	50	50	0.00	0.00	0.00	2.81	0.09	2.90
E24	40.41130	143.37989	18.08	192	9	81	50	50	0.00	0.00	0.00	0.00	0.00	0.00
E25	39.97347	143.24290	18.08	192	9	81	50	50	0.00	0.00	0.00	0.00	0.00	0.00
E26	39.53539	143.10778	18.08	192	9	81	50	50	0.00	0.00	0.00	0.00	7.90	7.90
E27	39.09709	142.97446	18.08	192	9	81	50	50	2.37	1.57	5.01	7.99	1.18	18.13
E28	38.65856	142.84289	18.08	192	9	81	50	50	4.55	12.36	2.12	2.97	0.21	22.21

TABLE III–1. FAULT PARAMETERS OF JAPAN NUCLEAR ENERGY SAFETY MODEL (cont.)

Fault number	Lat (°)	Lon (°)	Depth (km)	Strike (°)	Dip Angle (°)	Slip Angle (°)	Length (km)	Width (km)	Slippage(m)					Total slippage (m)
									30 s	90 s	150 s	210 s	270 s	
E29	38.21982	142.71302	18.08	192	9	81	50	50	3.44	11.60	0.00	0.00	0.00	15.04
E30	37.78086	142.58479	18.08	192	9	81	50	50	0.00	1.61	0.00	0.00	0.00	1.61
E33	40.95242	142.94883	25.90	192	9	81	50	50	0.00	0.00	0.00	1.04	3.65	4.69
E34	40.51407	142.81338	25.90	192	9	81	50	50	0.00	0.00	0.00	0.00	0.00	0.00
E35	40.07550	142.67978	25.90	192	9	81	50	50	0.00	0.00	0.00	0.00	0.00	0.00
E36	39.63671	142.54797	25.90	192	9	81	50	50	0.00	0.00	0.00	0.00	0.00	0.00
E37	39.19771	142.41791	25.90	192	9	81	50	50	0.00	0.00	8.92	9.60	0.00	18.52
E38	38.75850	142.28954	25.90	192	9	81	50	50	1.73	0.00	0.00	0.00	0.00	1.73
E39	38.31909	142.16280	25.90	192	9	81	50	50	1.83	2.58	0.00	0.00	0.00	4.41
E40	37.87949	142.03765	25.90	192	9	81	50	50	0.00	0.00	0.00	0.00	8.23	8.23
S01	37.15932	143.43259	0.00	192	9	81	50	50	0.00	3.43	8.34	18.70	18.70	49.16
S02	36.75922	143.10247	0.00	192	9	81	50	50	0.00	0.00	0.00	4.98	13.91	18.89
S03	36.35854	142.77338	0.00	192	9	81	50	50	0.00	0.00	0.00	0.00	1.71	1.71
S04	35.94015	142.53753	0.00	192	9	81	50	50	0.00	0.00	0.00	5.77	10.20	15.97
S11	37.26174	142.89121	7.82	192	9	81	50	50	0.00	0.46	6.28	4.85	4.85	16.44
S12	36.86008	142.56340	7.82	192	9	81	50	50	0.00	0.00	0.00	0.00	5.11	5.11
S13	36.45786	142.23660	7.82	192	9	81	50	50	0.00	0.00	0.00	0.00	0.00	0.00
S14	36.03837	142.00325	7.82	192	9	81	50	50	0.00	0.00	0.00	0.00	0.26	0.26
S21	37.36172	142.34828	15.64	192	9	81	50	50	0.00	6.84	0.00	0.00	0.00	6.84
S22	36.95852	142.02284	15.64	192	9	81	50	50	0.00	1.02	0.12	1.11	4.13	6.37
S23	36.55479	141.69840	15.64	192	9	81	50	50	0.00	0.00	0.11	0.92	0.00	1.02
S24	36.13422	141.46761	15.64	192	9	81	50	50	0.00	0.00	0.00	0.00	0.00	0.00
S31	37.45922	141.80385	23.47	192	9	81	50	50	0.00	0.00	0.00	0.04	3.80	3.84
S32	37.05450	141.48085	23.47	192	9	81	50	50	0.00	0.00	0.00	0.00	0.00	0.00
S33	36.64929	141.15882	23.47	192	9	81	50	50	0.00	0.00	0.00	0.00	0.00	0.00
S34	36.22769	140.93065	23.47	192	9	81	50	50	0.00	0.00	0.00	0.00	2.46	2.46

Note: X-Y coordinate was obtained by performing coordination transformation using UTM54 (WGS84, central latitude of 0 degree and central longitude of 141 degree) and by setting the eastern quasi-original point at 500 km

III–1.2. Bathymetry and gauge locations

This benchmark dataset includes bathymetric data off the coast of east Japan and topographic data of the Tohoku region, Japan. The 50 m–meshed topographic data are available in the Onagawa area, a port town located in the Tohoku region. The town was heavily damaged by the Great East Japan tsunami. The post-event tsunami survey data show that the inundation height reached more than 15 metres in some area of the town. In order to simulate the inundation in the Onagawa area under high resolution, the dataset provides several nested computational grids from offshore to onshore. Figures III–2 and III–3 show the computational area and the topographic model from 1350-meter grid to 50-meter grid. The data sources for the grid are described in this section.

III–1.2.1. J-EGG500, 500 m gridded bathymetric dataset

J-EGG500 is a 500 m gridded bathymetric dataset around Japan (RNODC Activity Report No.13, Japan Oceanographic Data Centre). A large amount of the depth-sounding data has been combined and gridded by 500 m intervals for general use. Since the quality difference of the data may generate improper steps at the boundary between them, data smoothing is applied including to the areas where observed data exist. The processed data have been produced as a 500 m meshed dataset. The dataset includes three areas as follows:

1. Latitude: N 34 to 46 (degrees), longitude: E 135 to 148 (degrees);
2. Latitude: N 30 to 38 (degrees), longitude: E 128 to 144 (degrees);
3. Latitude: N 24 to 30 (degrees), longitude: E 122 to 132 (degrees).

Input data have been taken from WGS-84 [29]. Those data files are described by ASCII character with the following format: (0 or 1, Latitude (deg.), Longitude (deg.), Depth (m)). It is noted that '0' is the averaged value of measured depth and '1' is the interpolated depth [29].

III–1.2.2. M-7000, the depth contour data

'Basic Map of the Sea' published by Hydrographic and Oceanographic Department, Japan Coast Guard (JHOD/JCG) is the basic bathymetric map of Japan. These data consist of two separate datasets: (i) a basic map in coastal waters and (ii) a basic map on the continental shelf. 'Basic Map of the Sea in Coastal Waters' is mainly on the scale of 1/50 000. In some locality, 1/10 000 charts are also available. JHOD/JCG compiled the 'Basic Map of the Sea in Coastal Waters' into M-7000 series, which are submarine topographic data around Japan. M-7000 series contain digital bathymetric counters at 100 m intervals around Japan.

Figure III–2 shows gauge locations, where the gauge succeeded to acquire the waveform of the Great East Japan tsunami around Japan. Precise latitude and longitude of computational areas and gauge location are shown in Table III–2 and III–3.

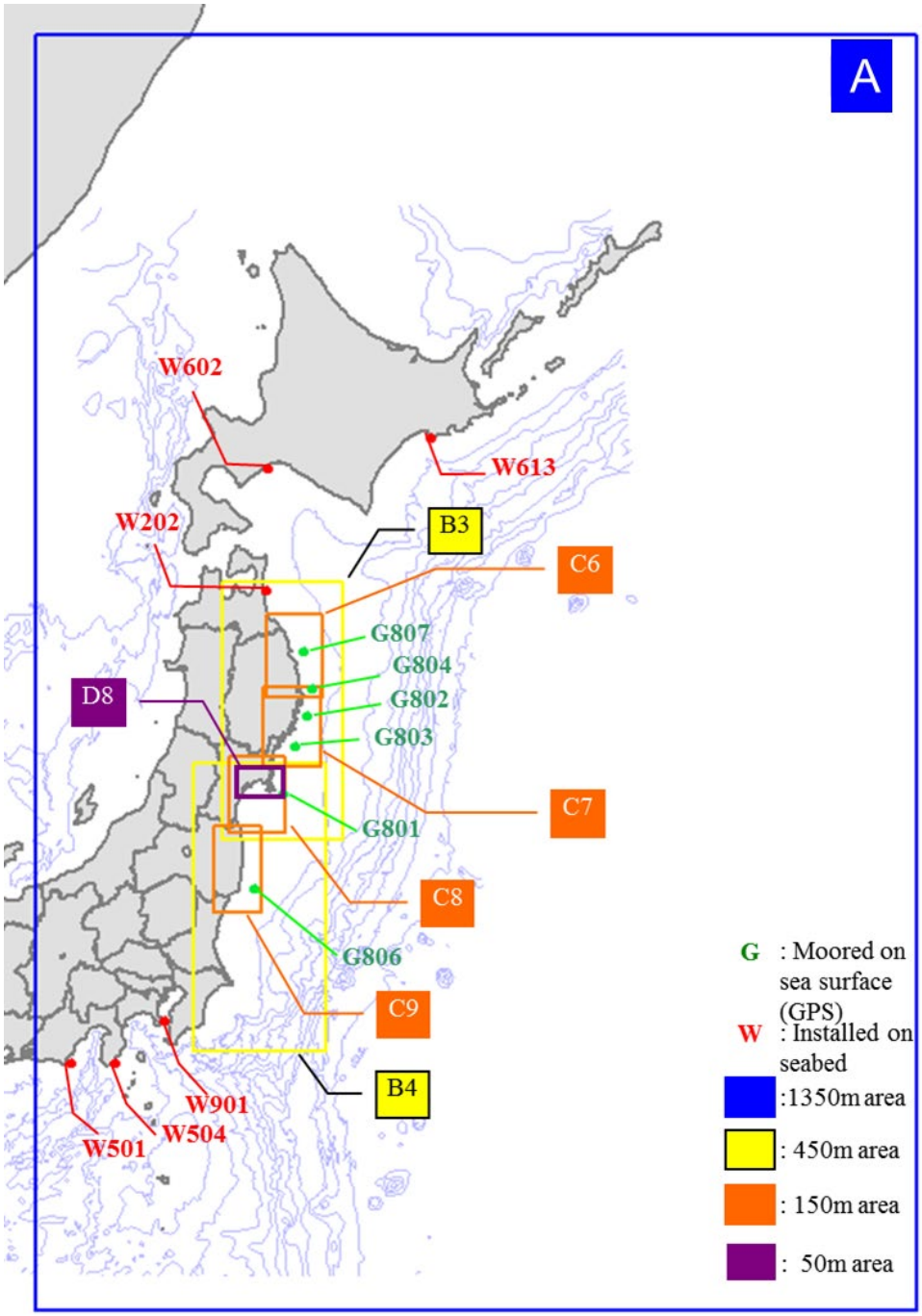

FIG. III–2. Gauge locations and computational areas (each rectangle presents the area covered by grids at the size shown in the legend) [III–1].

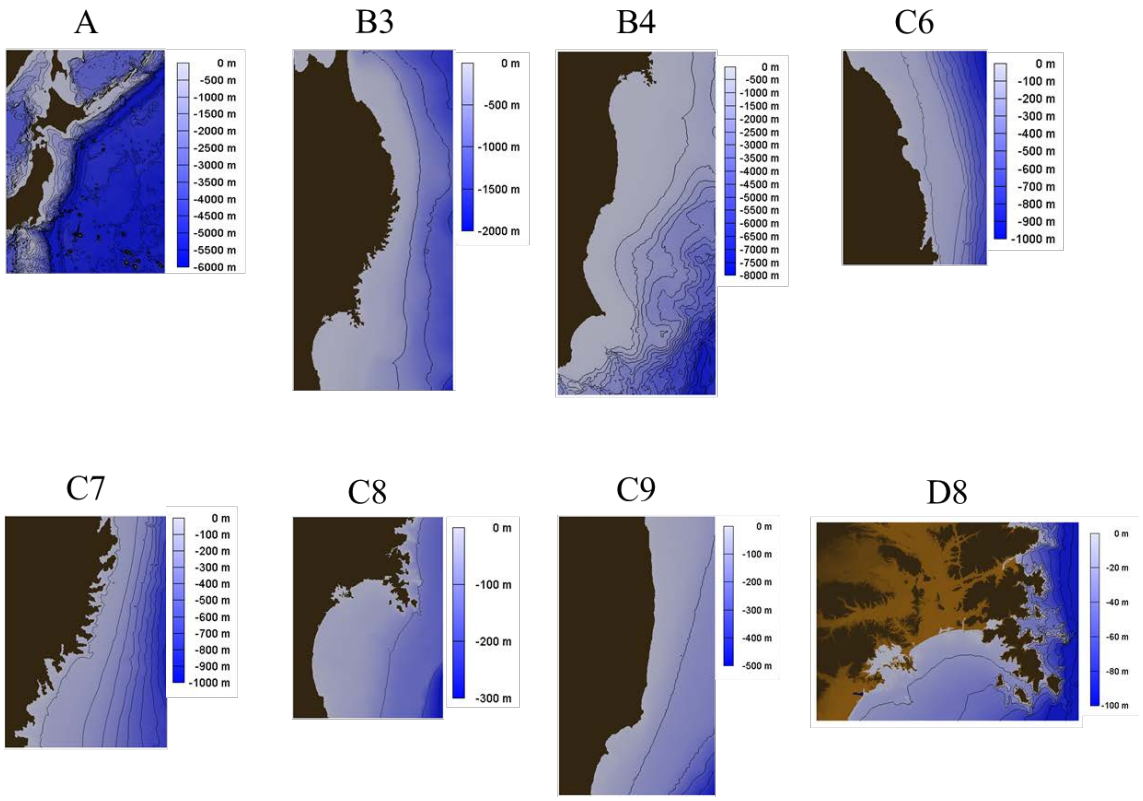

FIG. III–3. Topographic model for Onagawa Area [III–1].

TABLE III–2. COMPUTATIONAL AREAS

Area name	Mesh size (m)	Latitude (degree)	Longitude (degree)	Mesh number in I-direction	Mesh number in J-direction
A	1350	31.298	137.803	964	1396
B3	450	37.618	140.685	400	850
B4	450	34.817	140.224	439	943
C6	150	39.514	141.424	559	826
C7	150	38.594	141.387	559	796
C8	150	37.714	140.796	562	751
C9	150	36.659	140.552	478	850
D8	50	38.209	140.893	1303	988

TABLE III–3. OBSERVED POINT OF TSUNAMI WAVEFORM DATA (from the website of the Hydrographic and Oceanographic Department, Japan Coast Guard (JHOD/JCG) and NOWPHAS GPS)

Tsunami wave file name	Observed point name	Latitude (degree)	Longitude (degree)	Location (I, J) (for simulation using Tsunami Code)	Contained region
G807.csv	G807 North of Iwate	40.117	142.067	364,450	C6
G804.csv	G804 Centre of Iwate	39.627	142.187	437, 89	C6
G802.csv	G802 South of Iwate	39.259	142.097	407,496	C7
G803.csv	G803 North of Miyagi	38.858	141.894	293,198	C7
G801.csv	G801 Centre of Miyagi	38.233	141.684	520,386	C8
G806.csv	G806 Fukushima	36.971	141.186	378,232	C9
W613.csv	W613 Kushiro	42.911	144.397	432,956	A
W602.csv	W602 Tomakomai	42.544	141.446	253,922	A
W202.csv	W202 Mutsu-Ogawara	40.925	141.424	142,817	B3
W901.csv	W901 Ashikajima	35.211	139.734	141,320	A
W504.csv	W504 Shimoda	34.647	138.953	87,274	A
W501.csv	W501 Omaezaki	34.621	138.259	40,273	A

III–1.3. Recorded data (waveform data)

Figure III–4 shows observed the tsunami waveform acquired by the NOWPHAS GPS buoys and the wave gauges of the Tohoku region. The tide effects on tsunami waveforms are adjusted by the Port and Airport Research Institute. The value in unnecessary time range and parameters from the waveform data were cut off. The data was available from 14:00–20:00 on 11 March 2011 (see Table III–4).

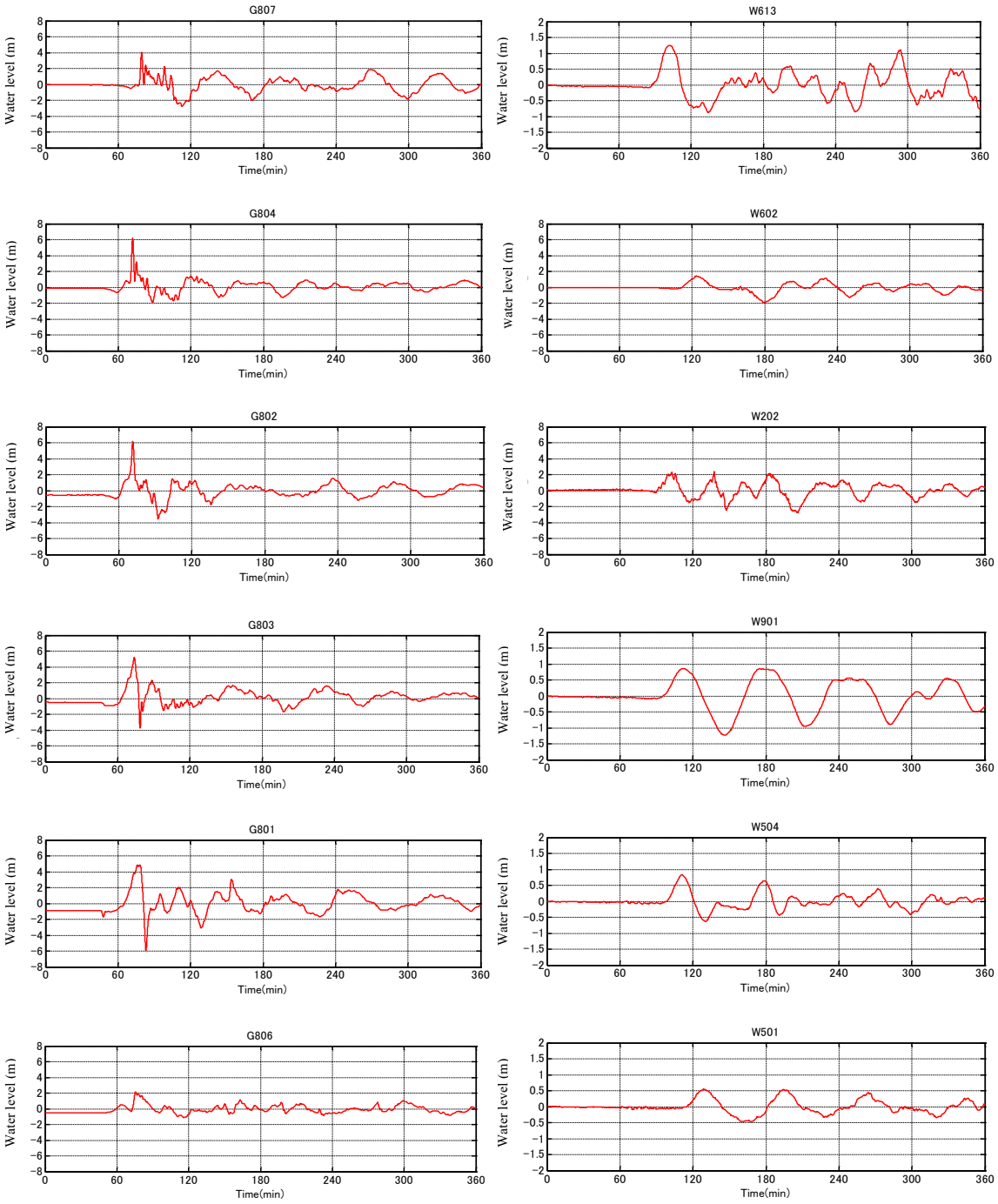

FIG. III–4. Observed tsunami wave form acquired by GPS buoys and the wave gauges (data taken from: The Nationwide Ocean Wave Information Network for Ports and Harbours).

TABLE III–4. TIME INFORMATION OF GAUGE RECORD

Wave gauges type	Start time	End time	Data interval
GPS buoy	14:00:00 11 March 2011	20:00:00 11 March 2011	5 s
Wave gauge	14:00:00 11 March 2011	20:00:00 11 March 2011	20 s

III–1.4. Recorded data (trace data)

The post-event tsunami survey data were collected by scientific volunteers, the '2011 Tohoku Earthquake Tsunami Joint Survey Group'. The data are open for public use on the condition that users cite: a) The '2011 Tohoku Earthquake Tsunami Joint Survey Group'; b) the web site address; and c) the release date, at a minimum. Data are in comma delimited txt files including observation points, measured heights and data reliability. This benchmark problem uses this dataset consisting of tsunami trace data collected in the Onagawa area. For more details, please refer to following websites:

— Results of Tsunami Surveys [31];

— Data format [III-5] .

III–1.5. Application using specific software

III–1.5.1. Tsunami code

Regarding 'Description of software', 'Analysis procedure (how to)' and 'Input data', please refer to Section I.3.2 of Annex I.

III–1.6. Source modelling

Simulations use the source model proposed by Sugino et.al [III–1]. The files of tsunami source parameters are named ‘FT10’. The first line is a comment line and the rest of the lines are ocean bottom deformation data written in Fortran (Format (2 000F8.2)). Positive values and negative values indicate uplifting and subsidence in metres, respectively. ‘FT10’ for the Japan Nuclear Energy Safety Organization [III-15] model contains ocean bottom deformation data which are applied in five sub stages, i.e. 30 s, 90 s, 150 s, 210 s and 270 s. Figure III–5 shows the images of the ocean bottom deformations of the Japan Nuclear Energy Safety model. Further information about fault parameters, subfault location and water displacements are provided in Section III – 1.1.

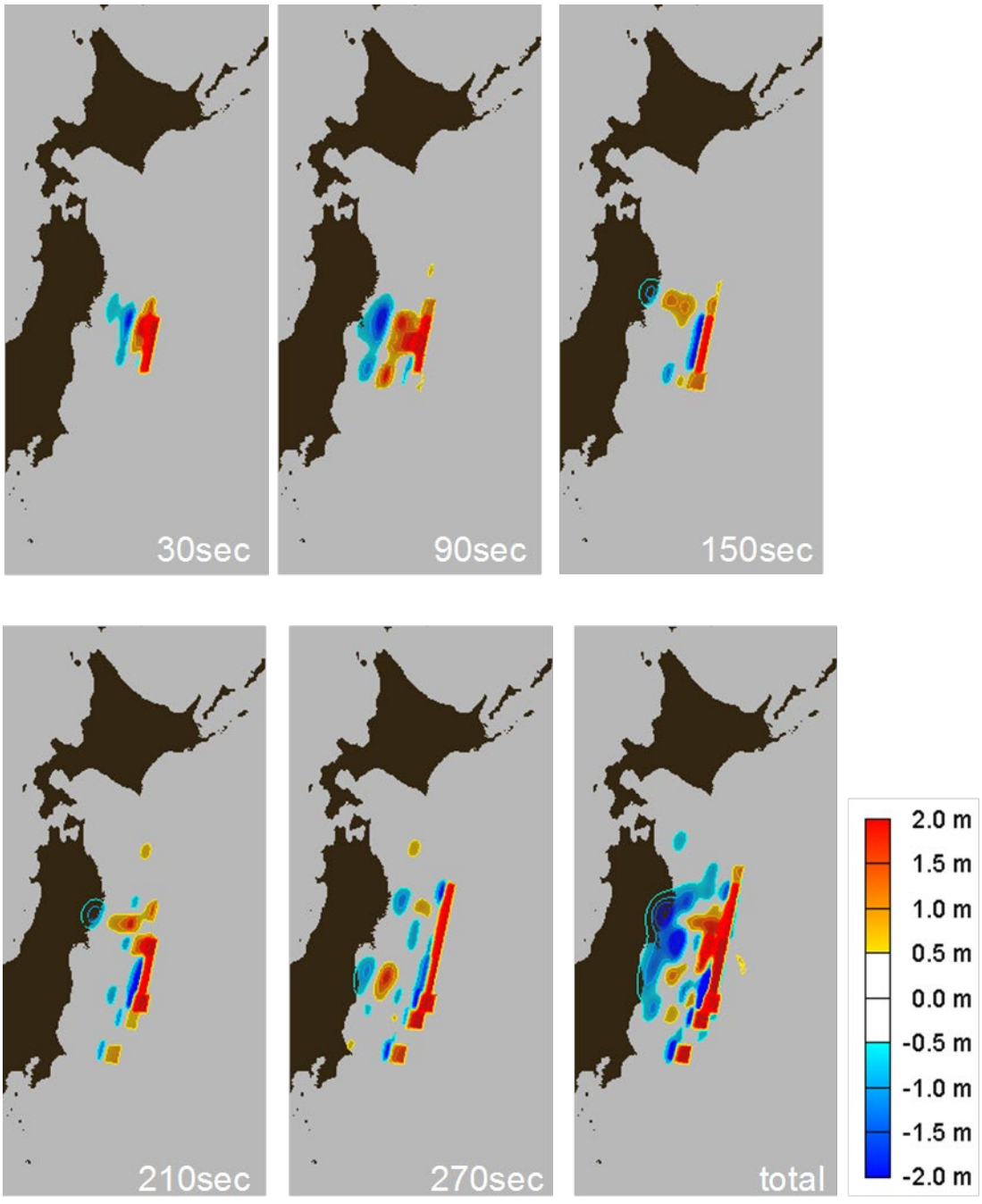

FIG. III–5. Ocean bottom deformations of Japan Nuclear Energy Safety Organization model [III–1].

III–1.7. Grid information

The bathymetric data are named ‘FT08’ according to [III-15]. The first line of the file is a comment line and the other lines are gridded bathymetric data. Positive values indicate water depth in the sea and negative values indicate altitude on the land in metres. Contour maps of the computational areas are shown in Fig. III–5. Table III–5 shows the classification of the mesh size of topographic data.

TABLE III–5. MESH SIZE OF TOPOGRAPHIC DATA FILE

Bathymetric and/or topographic data file name [III-15]	1350 m area	450 m area	150 m area	50 m area
FT08_AB3C6	A	B3	C6	—
FT08_AB3C7	A	B3	C7	
FT08_AB3C8	A	B3	C8	
FT08_AB4C9	A	B4	C9	
FT08_AB3C8D8	A	B3	C8	D8

Analysis: time step, boundary condition

Local tsunami analysis assumes that the initial velocity of fluid and the initial water level are 0. It also assumes open boundary conditions for free transmission and complete reflection at the coastline except for run-up areas. In the analysis, coastal structures such as breakwaters and sea walls need to be taken into consideration. The Homma formula shown in Fig. III–6 is used in order to judge whether water overflows the structure.

$$Q = \mu B h_1 \sqrt{2g h_1},\ h_2 \leq \frac{2}{3} h_1 \quad \text{(III–1)}$$

$$Q = \mu' B h_2 \sqrt{2g(h_2 - h_1)},\ h_2 > \frac{2}{3} h_1 \quad \text{(III–2)}$$

Where Q is the discharge overflowing the structure (m^3/sec), μ and μ' are the coefficients of discharge, h_1 is the water depth in front of the structure (m) and h_2 is the water depth behind the structure (m).

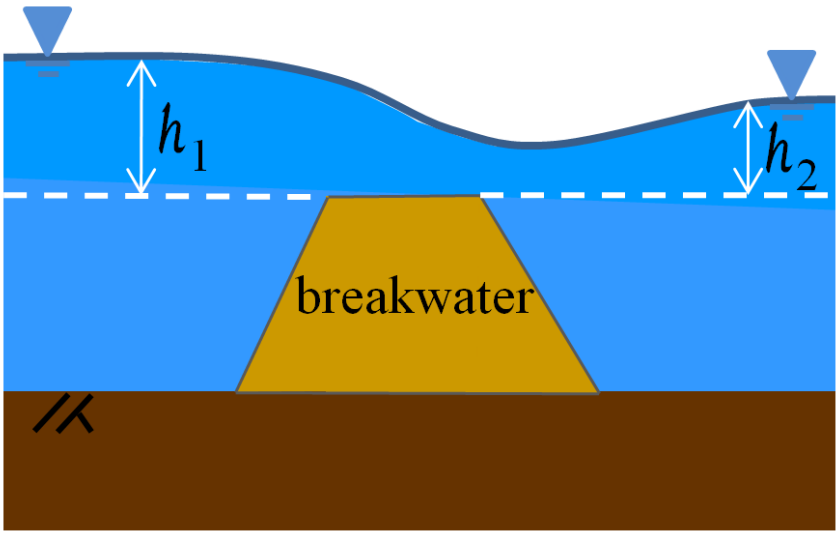

FIG. III–6. Calculation of discharge overflowing coastal structure by Hom-ma formula.

III–1.2.2. Recorded data for local tsunami

Users can compare their simulation results to recorded data such as tsunami waveform data and tsunami trace data. Table III–6 shows the file formats of tsunami wave form acquired by the GPS buoys and the coastal wave gauges of the Tohoku region.

TABLE III–6. EXAMPLE OF THE FILE FORMAT FOR TSUNAMI WAVEFORM (G801.CSV)

	time (s)	tsunami height (cm)
1	0	-87.7
2	5	-87.71
3	10	-87.52
4	15	-87.63
5	20	-87.44
6	25	-87.54
7	30	-87.65
8	35	-87.46

Table III–7 shows the file formats of tsunami trace data. The data are in a comma delimited text file and include the zone and location of an observation point, latitude and longitude, type of data, reliability, run-up distance and tsunami trace height. The units of location and height are degrees and metre respectively. It is noted that the tsunami height in the file is not the elevation from the mean sea level but the astronomical tide of that time. Type R denotes run-up and Type I denoted inundation height. Reliability rank A means that the mark

is clear, and the error of measurement is small. Figure III–7 shows the distribution map of tsunami trace data collected in the Onagawa area.

TABLE III–7. EXAMPLE OF THE FILE FORMAT FOR TSUNAMI TRACE

#	ZONE	Location	Lat	Lon	Type	Reliability	Run-up distance	Height corrected by ttjt
3141	Miyagi	Ogatsucho, Ishinomakishi	38.52289	141.54588	R	A	0	12.453
4999	Miyagi	Yoriisohama, Ishinomakishi	38.3855	141.53206	R	A	0	13.133
3142	Miyagi	Ogatsucho, Ishinomakishi	38.5368	141.52972	I	A	0	11.198
5001	Miyagi	Yoriisohama, Ishinomakishi	38.38958	141.5284	R	A	0	17.54

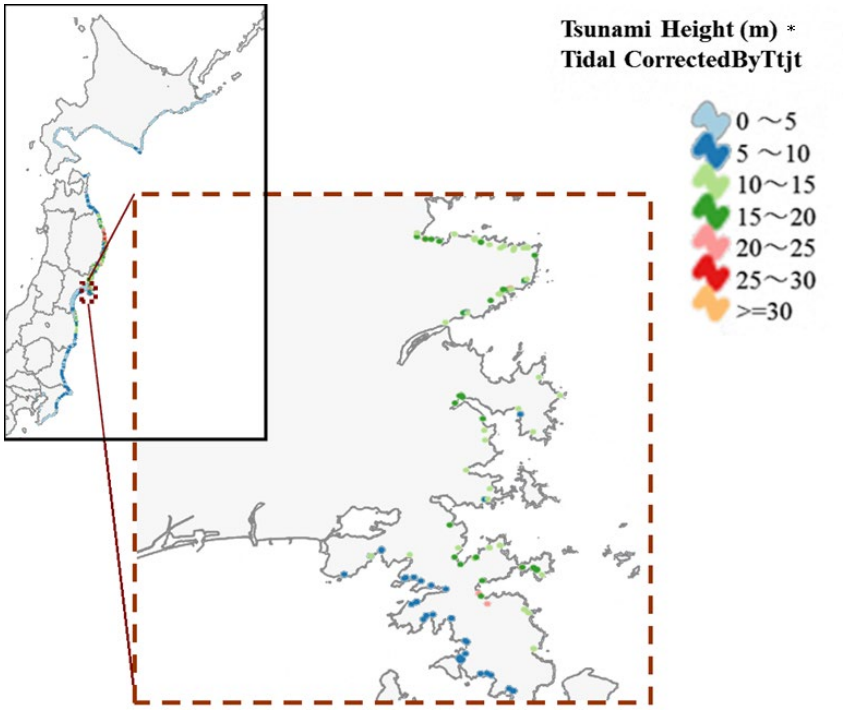

FIG. III–7. Distribution of tsunami height (run-up and inundation height) corrected by Ttjt (2011 Tohoku Earthquake Tsunami Joint Survey Group) in Onagawa area.

III–1.2.3. Results of simulation by different software

Numerical simulation of the Great East Japan tsunami was conducted using Tsunami Code, focusing on its effect on selected coastal areas, e.g. inundation in Onagawa, tsunami heights in Tohoku region.

The bathymetric data (FT08) covering the Tohoku area are shown in Fig. III–3. The Japan Nuclear Energy Safety Organization model was selected as the source condition and

imported from a file (FT10) containing water surface displacement. The mesh size was changed by 4 steps from 1350 m to 50 m (see Table III–2). Run-up was computed only in the area of the 50 m mesh size (see Fig. III–3, area D8).

The time duration for the analysis is the first two hours. One of the results of the computation is displayed in Fig. III–8. It is noted that the tidal effect to the observed tsunami waveform was compensated to compare the observed height with the computed one. Calculated contour maps for maximum water level are shown in Fig. III–9. Figure III–10 shows the maximum water level at tsunami observation points of tsunami trace data and Aida's K (geometric mean of the ratio of the measured height to computed height) and κ (geometric variance) values. K and κ are 0.97 and 1.27, respectively. According to Section 2.3.2, these values satisfy the acceptance criteria for tsunami simulation.

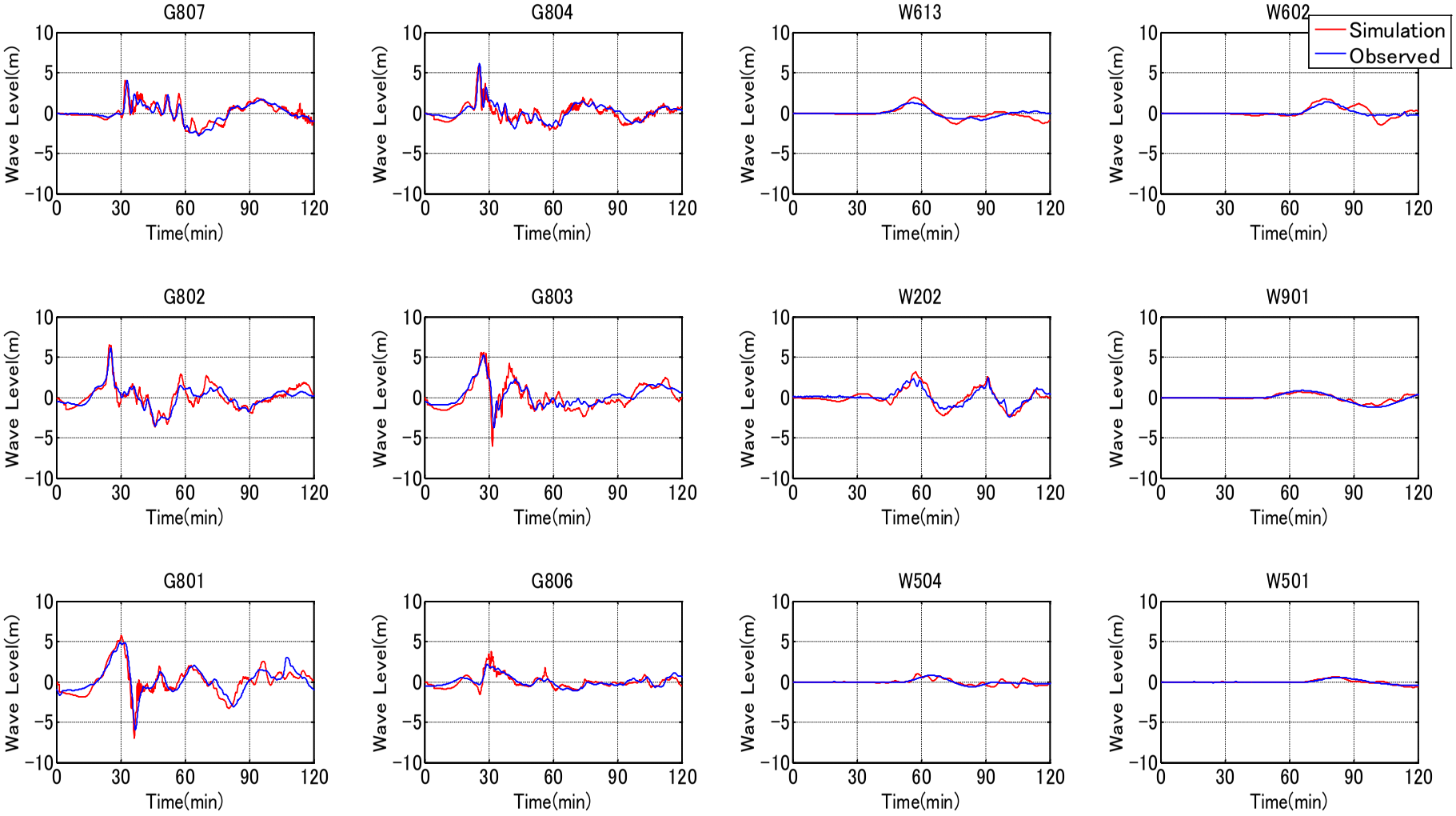

Red and blue lines indicate simulation and observation data, respectively.

FIG. III–8. Time series of water level (data from The Nationwide Ocean Wave Information Network for Ports and Harbours)

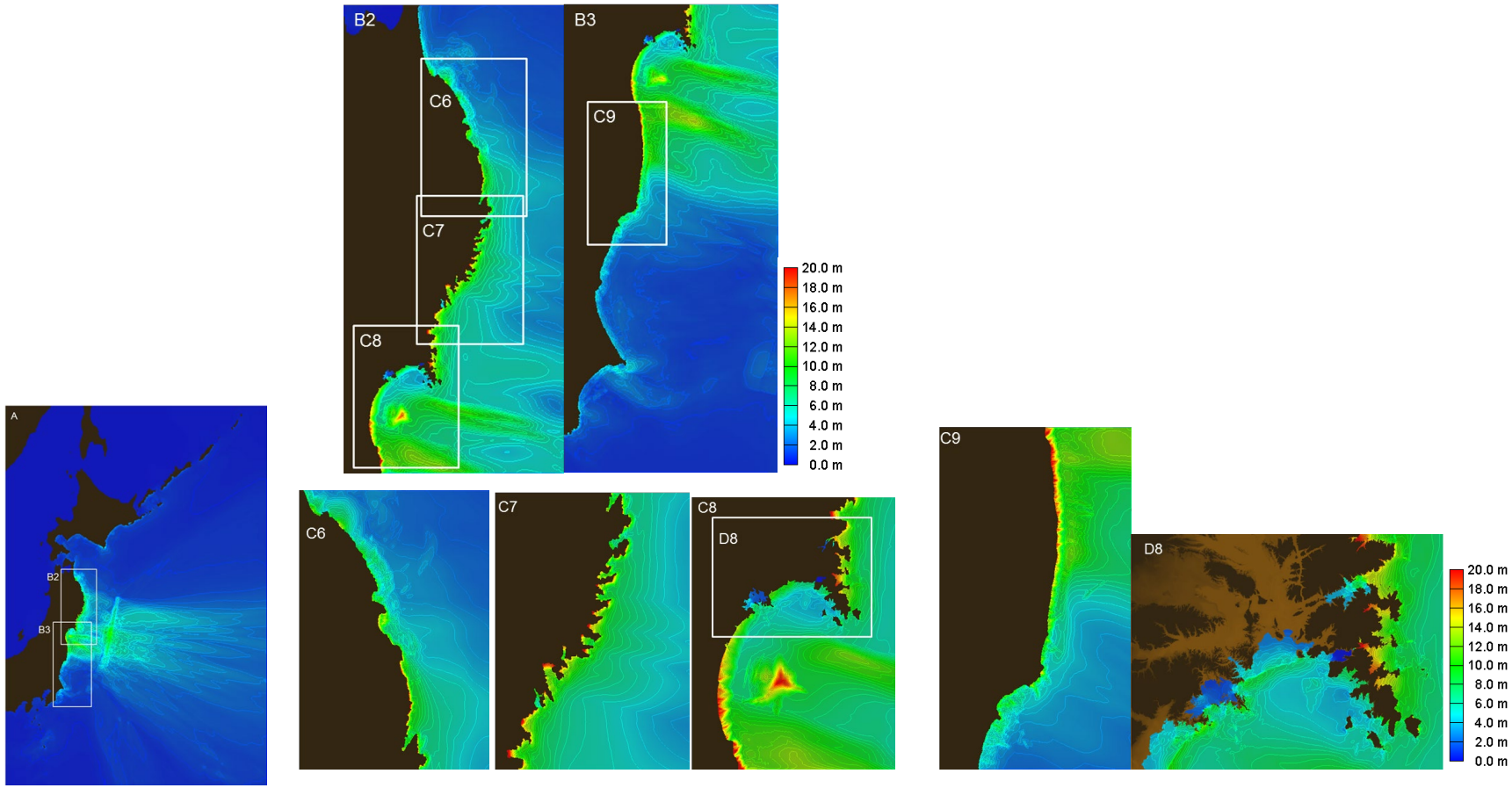

FIG. III–9. Contour maps for maximum water level (from A to D8) and inundation (D8) of Pacific coast area of Tohoku.

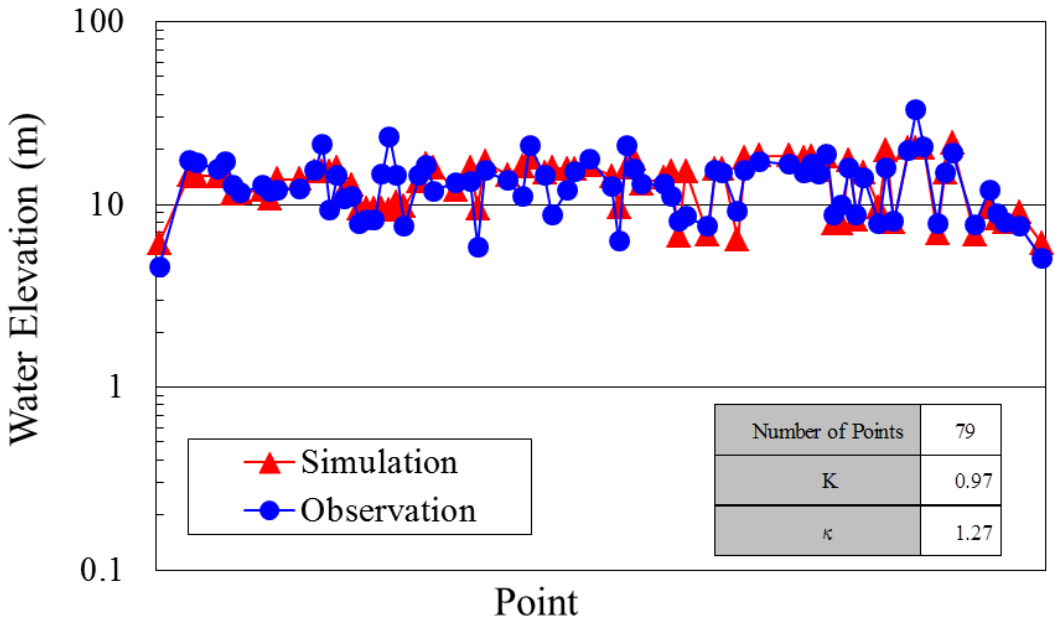

FIG. III–10. Maximum water level at tsunami observation points in Onagawa area.

In Fig. III–10, red and blue points indicate simulation and observation data, respectively. The table in the figure shows Aida's ***K*** (geometric mean of the ratio of the measured to computed height) and ***κ*** (geometric variance) values.

III–2. DISTANT TSUNAMI

The countries located along the rim of the Pacific Ocean have installed a variety of instruments capable of detecting or recording the tsunami wave forms. These include bottom pressure recorders, tsunami meters in Deep Ocean and tide gauges located in harbours. In addition, run-up values (observed or measured) during the 2011 event along the coasts (e.g. United States of America, Chile, Hawaii) located far away from the tsunami source are also available.

The recordings made in deep ocean by various instruments capture the propagation when the linear approximations to shallow water equations for tsunami propagation are still valid. The tide gauge data and run-up values measured along the coast captures shoaling and non-linear phenomena associated with tsunami propagation and evolution in shallow water region.

In view of the utility of both sets of data with respect to tsunami propagation, the following sections introduce the user to data that could be utilized for both phases, i.e. linear propagation (see Section III–2.1.1) and shoaling and run-up (see Section III–2.1.2). Section III–2.2 provides information on the application of specific numerical models to both phases of the tsunami.

III–2.1. Data

III–2.1.1. Distant tsunami: Linear propagation phase

Source model

As explained in Section 5, a number of source models have been proposed for the 2011 tsunami. For the simulation of propagation of distant tsunami, the instantaneous slip model from Fujii et.al [III–2] has been utilized. Table III–8 provides the details of the source model. The slip distribution estimated by this model is given in Fig. III–11.

TABLE III–8. FAULT PARAMETERS AS PER VERSION 4.2 (INSTANTANEOUS SLIP) OF FUJII AND SATAKE SOURCE MODEL FOR 2011 TSUNAMI

Fault segment number	Latitude	Longitude	Depth of top edge	Strike	Dip	Rake	Length (km)	Width (km)	Slip (m)
1	39.738	144.331	0	193	14	81	50	50	0
2	39.3	144.2	0	193	14	81	50	50	0
3	38.862	144.069	0	193	14	81	50	50	5.66
4	38.424	143.939	0	193	14	81	50	50	41.15
5	37.986	143.81	0	193	14	81	50	50	47.93
6	37.547	143.682	0	193	14	81	50	50	8.44
7	37.135	143.4	0	193	14	81	50	50	0
8	36.73	143.07	0	193	14	81	50	50	0
9	36.325	142.74	0	193	14	81	50	50	1.89
10	35.905	142.504	0	193	14	81	50	50	0.63
11	39.836	143.778	12.1	193	14	81	50	50	0
12	39.398	143.651	12.1	193	14	81	50	50	0.81
13	38.96	143.523	12.1	193	14	81	50	50	10.67
14	38.522	143.397	12.1	193	14	81	50	50	27.84
15	38.084	143.271	12.1	193	14	81	50	50	33.79
16	37.646	143.146	12.1	193	14	81	50	50	24.11
17	37.233	142.867	12.1	193	14	81	50	50	0
18	36.828	142.54	12.1	193	14	81	50	50	0
19	36.423	142.213	12.1	193	14	81	50	50	0
20	36.003	141.979	12.1	193	14	81	50	50	0
21	39.934	143.224	24.2	193	14	81	50	50	0
22	39.496	143.1	24.2	193	14	81	50	50	0
23	39.058	142.977	24.2	193	14	81	50	50	4.86
24	38.62	142.853	24.2	193	14	81	50	50	19.56
25	38.182	142.731	24.2	193	14	81	50	50	23.38
26	37.744	142.609	24.2	193	14	81	50	50	13.13
27	37.331	142.333	24.2	193	14	81	50	50	11.13
28	36.926	142.009	24.2	193	14	81	50	50	2.23
29	36.521	141.684	24.2	193	14	81	50	50	2.25
30	36.101	141.454	24.2	193	14	81	50	50	0.54
31	40.032	142.67	36.3	193	14	81	50	50	0
32	39.594	142.549	36.3	193	14	81	50	50	0
33	39.156	142.43	36.3	193	14	81	50	50	0
34	38.718	142.309	36.3	193	14	81	50	50	14.64
35	38.28	142.19	36.3	193	14	81	50	50	9.46
36	37.842	142.071	36.3	193	14	81	50	50	0
37	37.429	141.798	36.3	193	14	81	50	50	0
38	37.024	141.477	36.3	193	14	81	50	50	0
39	36.619	141.155	36.3	193	14	81	50	50	0
40	36.199	140.928	36.3	193	14	81	50	50	0

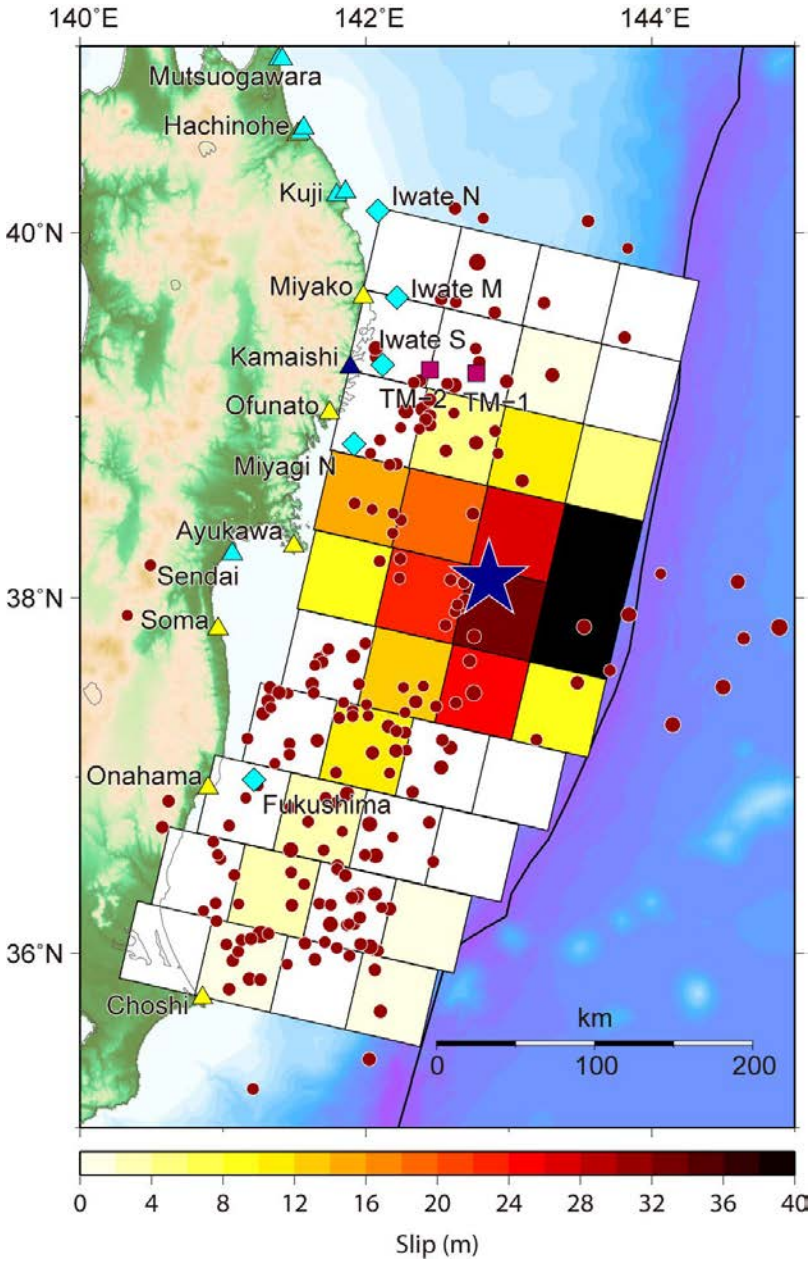

FIG. III–11. Slip distribution as estimated by Fujii and Satake ver. 4.2 (2011) model.[III-6—III-7]

Bathymetric data for distant tsunami simulations

This section covers the bathymetric datasets that could be used with respect to the evaluation of far-field propagation (across the Pacific Ocean) and run-up at far-field locations caused by the 2011 GEJE event. Considering the differences in specifications of bathymetric datasets needed for capturing various phases such as deep ocean propagation and subsequent shoaling and run-up, the description of the datasets is split into two parts.

This section describes the datasets (available in the public domain) that could be utilized for modelling of deep ocean propagation of tsunamis i.e. trans-oceanic propagation. In most of the scenarios of numerical modelling, the linear approximations of the governing equations depicted in spherical coordinates are used for simulating trans-oceanic propagation of tsunamis. While using these linear approximations, numerical models are unable to capture

run-up values and many models may also need manual corrections to water depths in regions with water depths shallower than approximately 100 m so as to be in line with the assumptions of the numerical model. Moreover, as run-ups are not of concern, the accuracy of topographic data does not have any bearing on the analysis. However, the shoreline needs to be represented with sufficient accuracy. In order to capture the far field propagation, these datasets need to cover wider areas and hence are generally depicted in spherical coordinates.

The details of bathymetric datasets needed for near-shore amplification and run-up values are described in Section III–2.1.2.

For modelling of far field propagation in deep ocean, the following sources of bathymetric data are available in public domain: ETOPO and general bathymetric chart of the oceans.

ETOPO

ETOPO is released by the National Geophysical Data Centre (NGDC) of NOAA in the United States of America. Over the years, the NGDC has released several datasets with increased resolution of grids. The first significant release was ETOPO5 that covered the Earth's surface at a resolution of 5-minute latitude/longitude grid or about 9 km spacing (ETOPO5, 1988). In 2006, the NGDC released an updated version, viz ETOPOv2 (2006). Recently, ETOPO2v2 was superseded by ETOPO1 (2009). ETOPO1 is a 1 arc-minute global relief model of the Earth's surface that integrates land topography and ocean bathymetry. The major inputs with regard to these global datasets include GLOBE, GTOPO30, (a 30arc second topographic grid developed by the United States Geological Survey), the Shuttle Radar Topography Mission data and the high-resolution coastline data (see Fig. III–12). The user needs to select the rectangular domain selection tool using the button located on the upper left-hand corner (window 1) of Fig. III–12. The type of data to be extracted is selected by window 2. In this example, XYZ format has been selected indicating that the downloaded data would be in longitude, latitude, depth form and would be in ASCII format.

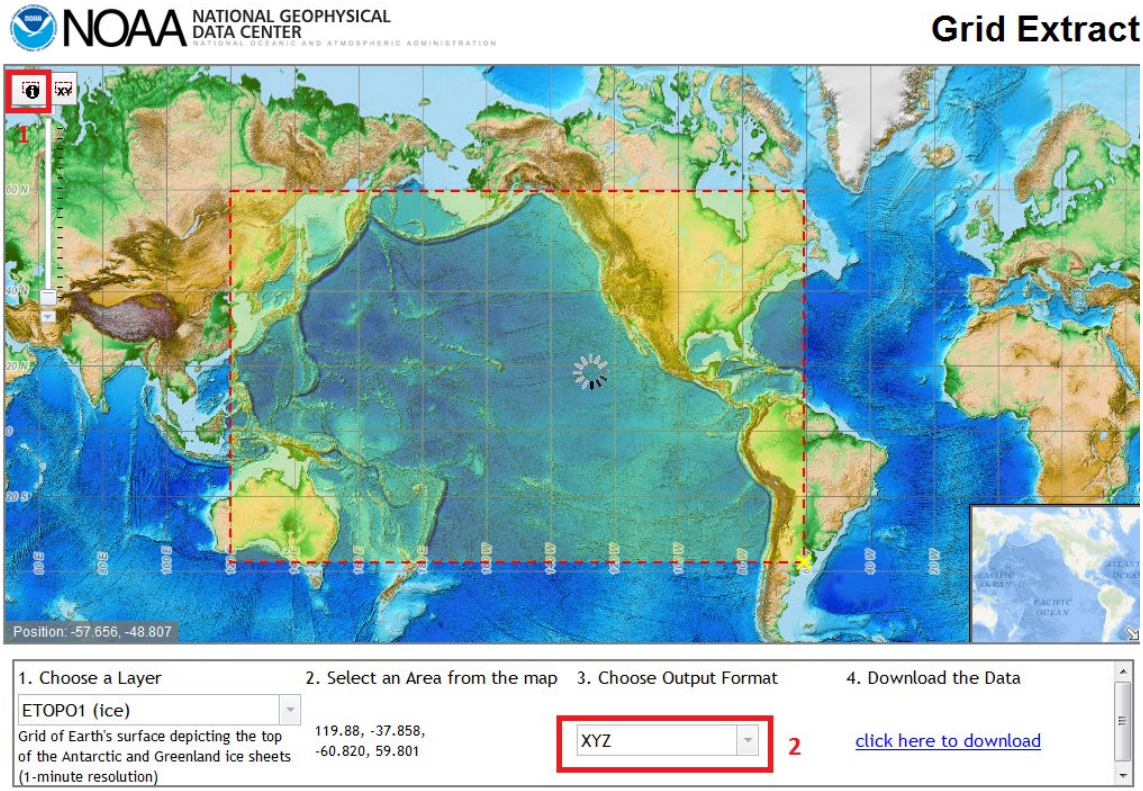

FIG. III–12. View of the grid data extraction window for ETOPO1 [III-8]

General bathymetric chart of the oceans

The General Bathymetric Chart of the Oceans grid, released in 2008 covers both topographic and bathymetric data at a grid spacing of 30 arc seconds, which is equivalent to about 900 metres. The grid is generated from several sources of data. For sea floor data, this included data from the NGDC, bathymetric data from the Scripps Institution of Oceanography, United States of America, the IBCAO and ship sounding data from French and Japanese agencies. Additionally, some shallow water data (<300 m depth) were also supplied by Member States of the International Hydrographic Organisation. The bathymetric grid was generated by combining ship depth soundings with interpolation between sounding points guided by satellite-derived gravity data[1].

A detailed discussion on publicly available bathymetric data sources and their evaluation is provided in [III–9].

Gauge data for distant tsunami simulation

As presented in Section 5, NOAA and other research organizations have deployed a set of bottom pressure recorders, Deep-ocean Assessment and Reporting of Tsunami (DART), in regions that are vulnerable to tsunamis, with the majority of them being in the Pacific Ocean. The tsunami wave propagation in deep ocean is picked up by DART buoys.

[1] The grid data are available from the National Oceanograpy Centre British Oceanographic Data Centre GEBCO gridded bathymetric data.

A listing of various DART stations deployed by NOAA/NGDC is given in Table III–9. Figure III–13 depicts an overlapping plot of the location of DART stations and contours of time of arrival of tsunami waves from the 2011 event. The records from the DART have been processed and made available by NOAA/NGDC. DART data include the sea depth at that location as well as the time and water level variations due to tidal fluctuations. The propagations of tsunami waves are seen as additional wave forms riding over the tidal fluctuations. A typical DART record of propagation of tsunami waves generated by the 2011 event is given in Fig. III–14.

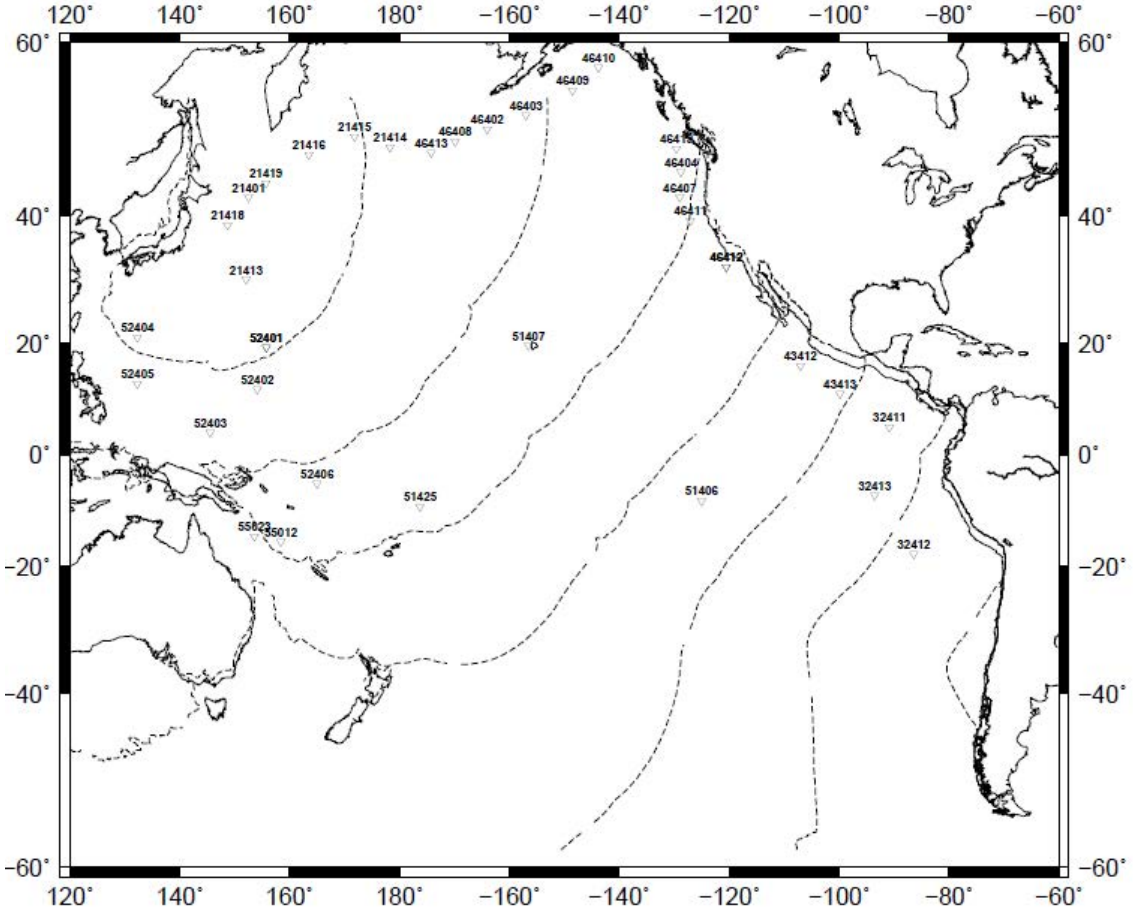

FIG. III–13 Spatial distribution of select DART array in Pacific Ocean including the DARTs that have recorded 2011 event.

TABLE III–9. LISTING OF DART STATIONS (data taken from National Oceanic and Atmospheric Administration's National Data Buoy Center historical DART data).

Station ID	Longitude	Latitude	Water Depth (m)	Start Date	Detection Threshold (mm)	Owner
21346	146.2	40.4	5126	06-Mar-13	99	INTERNATIONAL
21347	145.75	39.3	5247	06-Mar-13	99	INTERNATIONAL
21348	145.5833	38.0667	5292	06-Mar-13	99	INTERNATIONAL
21401	152.5833	42.6167	9999	08-Nov-10	99	INTERNATIONAL
21402	158.3433	46.4875	5150	01-Oct-12	99	INTERNATIONAL
21413	152.1103	30.52	5822	14-Jul-12	30	NDBC
21414	178.2658	48.9472	5375	05-Jul-11	30	NDBC
21415	171.8458	50.1803	4745	07-Jul-11	30	NDBC
21416	163.5153	48.0583	5744	09-Jul-11	30	NDBC
21418	148.6664	38.6939	5662	12-Jul-12	30	NDBC
21419	155.735	44.4547	5318	09-Jul-12	30	NDBC
23227	88.792	6.2547	3793	06-Oct-11	99	INTERNATIONAL
23228	65.3467	20.7986	2611	06-Oct-11	99	INTERNATIONAL
23401	88.5403	8.9044	9999	01-Jan-06	99	INTERNATIONAL
32066	-81.7686	-1.1297	1600	01-Aug-12	99	INTERNATIONAL
32401	-74.7264	-19.2903	9999	30-Apr-08	99	INTERNATIONAL
32402	-73.9831	-26.7439	4070	02-Apr-13	99	INTERNATIONAL
32411	-90.8381	5.0053	3312	13-Sep-12	30	NDBC
32412	-86.3133	-17.9806	4373	04-May-11	30	NDBC
32413	-93.4989	-7.4003	3893	17-Feb-12	30	NDBC
41420	-67.3256	23.4964	5739	10-May-12	30	NDBC
41421	-63.9747	23.4036	5802	09-May-12	30	NDBC
41424	-72.4758	32.932	5284	06-Aug-12	30	NDBC
42407	-68.1856	15.3067	4499	29-Apr-12	30	NDBC
42429	-85.6714	27.4011	3275	02-Feb-13	99	NDBC
43412	-106.9942	16.0142	3235	20-Sep-12	30	NDBC
43413	-99.8658	11.0628	3380	17-Sep-12	30	NDBC
44401	-50.0092	37.5642	5492	02-Jul-11	30	NDBC
44402	-70.945	39.4011	2443	08-Jul-11	30	NDBC
46402	-164.0233	51.0675	4760	28-Jun-12	30	NDBC
46403	-156.935	52.6389	4512	21-Jun-11	30	NDBC
46404	-128.78	45.8525	2793	08-Oct-12	30	NDBC
46407	-128.8136	42.6639	3322	05-Oct-12	30	NDBC
46408	-169.8778	49.6353	5400	29-Jun-12	30	NDBC
46409	-148.4995	55.3006	4244	23-Jun-12	30	NDBC
46410	-143.7992	57.6353	3783	14-Jun-11	30	NDBC
46411	-127.0208	39.3425	4266	31-May-11	30	NDBC
46412	-120.5536	32.4533	3720	12-Dec-11	30	NDBC
46413	-174.2042	48.2964	5385	03-Jul-11	30	NDBC
46419	-129.627	48.7686	2775	13-Jun-12	30	NDBC
51407	-156.5856	19.5778	4761	29-Sep-11	30	NDBC
51425	-176.2478	-9.5219	4960	18-Aug-11	30	NDBC
51426	-168.1389	-22.9736	5650	23-Aug-11	30	NDBC

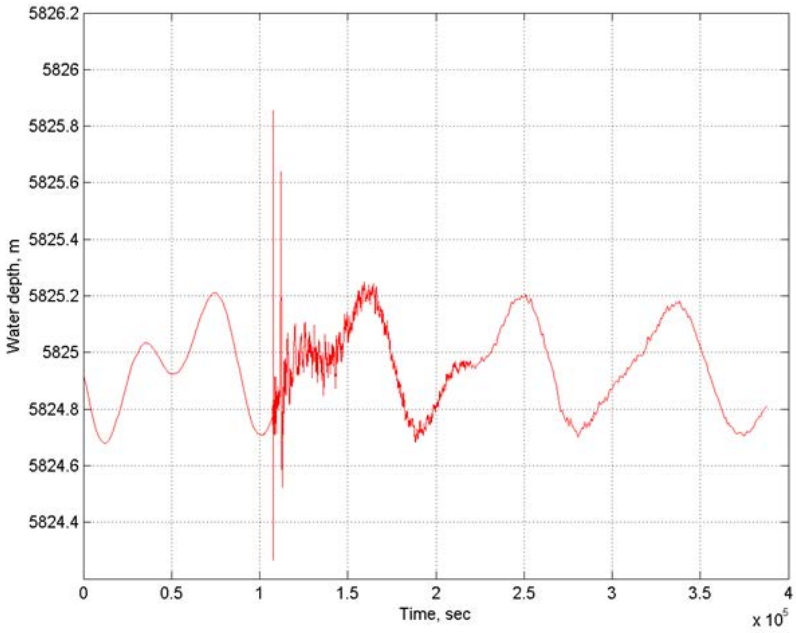

FIG. III–14. Dart data record at DART station 21413 showing the tidal variations and tsunami wave records imposed over the tidal variations. Zero refers to midnight of 10th March 2011 (in UTC).

De-tiding of data needs to be carried out before they are used for validation of tsunami propagation. NOAA has made available the de-tided and filtered data from DART stations[2]. The data are sampled at an interval of 1 minute. The layout of typical data is given in Table III–10.

[2] National Oceanic and Atmospheric Administration Pacific Marine Environmental Laboratory Tsunami Forecast Tool.

TABLE III–10. LAYOUT OF TYPICAL DATA FROM DART

Date	Time	Detected water levels
2011 03 11	00 00 00	1 5263.581 –0.0699 0.0188
2011 03 11	00 01 00	9 5263.578 –0.0727 0.0174
2011 03 11	00 02 00	9 5263.575 –0.0756 0.0161

Note. Data from DART 21401 is shown, left columns indicate year: month: date: hours: minutes: seconds and the detected water levels are indicated in right column (data taken from National Centers for Environmental Information March 11, 2001 DART Data).

Another source of these data is summarized by National Centres for Environmental Information. The files available include raw observations, fitted tidal components and residual tide values. Two types of data are provided with this database: (i) 15 s values as recorded by the Bottom Pressure Recorder and (ii) real time water level data as recorded by the bottom pressure Recorder in extended reporting mode containing measurement types of 15 minutes, 1 minute and 15 seconds.

The user may use the above sources of data for validation of far field propagation simulations during the 2011 GEJE event.

III–2.1.2. Distant tsunami: Linear propagation and non-linear shoaling

Source model

The same source model as that presented in [III–2] may be utilized for this phase of tsunami propagation.

Bathymetric and/or topographic data

As the waves propagating through the sea reach the coastline in distant areas, they are subjected to shoaling and run-up. During this phase of the tsunami, the governing equations and the numerical models used for simulation include non-linear terms as well as algorithms for capturing wetting and drying during run-up and inundation of dry land. Unlike the linear propagation phase where landmasses are treated as reflecting boundaries, near shore amplification/shoaling and run-up demand accurate depiction of terrain and/or topographic data as well.

This subsection describes the bathymetric and/or topographic data that could be utilized for modelling of near shore amplification and run-up. Unlike datasets for deep ocean propagation, the shallow water bathymetry needs to be captured with sufficient accuracy. In addition, to capture wave run-up values on to dry land, the topographic/terrain data also need to be represented in sufficient detail. The horizontal and vertical data of the bathymetric and/or topographic database have to be commensurate with the needs of the analysis. Since the majority of numerical simulations are carried out considering mean sea level conditions, it also needs to be verified that the coastline derived from the dataset (i.e. zero depth contour) at the region of interest has to match the mean sea level at site.

Due to the availability of both shallow water data and the tide records corresponding to the 2011 event, the Islands of Hawaii provide an ideal platform for verification for tsunami codes where in distant tsunami propagation and subsequent wave amplification near the coast is captured. The data recorded by the tide gauge station located inside the Kahului harbour in Maui island in the Mid Pacific Ocean is proposed for use for this analysis.

As for distant tsunami propagation, the data for simulation and verification include two types: the bathymetric and topographic data as well as measured data from the tide gauge.

Several sources of bathymetric data are available for Hawaii, including public freely available databases and the proprietary databases offered by commercial entities. Details on some of the publicly available databases are given below.

Main Hawaiian Islands multibeam bathymetry synthesis

This database contains the multibeam bathymetry synthesis for the main Hawaiian Islands, Fig. III–15 and covers terrain and bathymetry data at a spacing of 50 m.

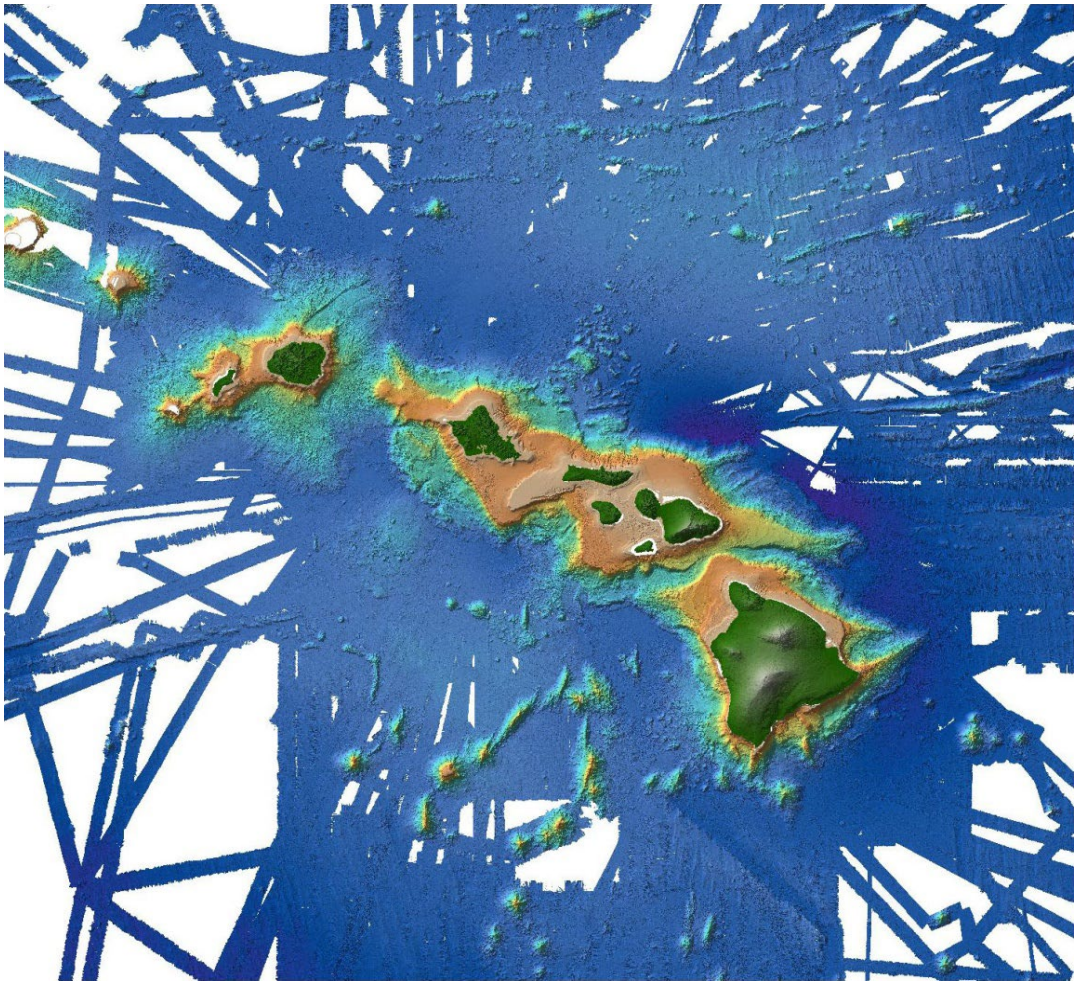

FIG. III–15. Coverage of multibeam data for Hawaiian archipelagos (data taken from Main Hawaiian Islands Multibeam Bathymetry and Backscatter Synthesis).

Though this database is among those having most exhaustive coverage with respect to the Islands of Hawaii, users need to be aware of existence of data voids e.g. Fig. III–16, while utilizing this data.

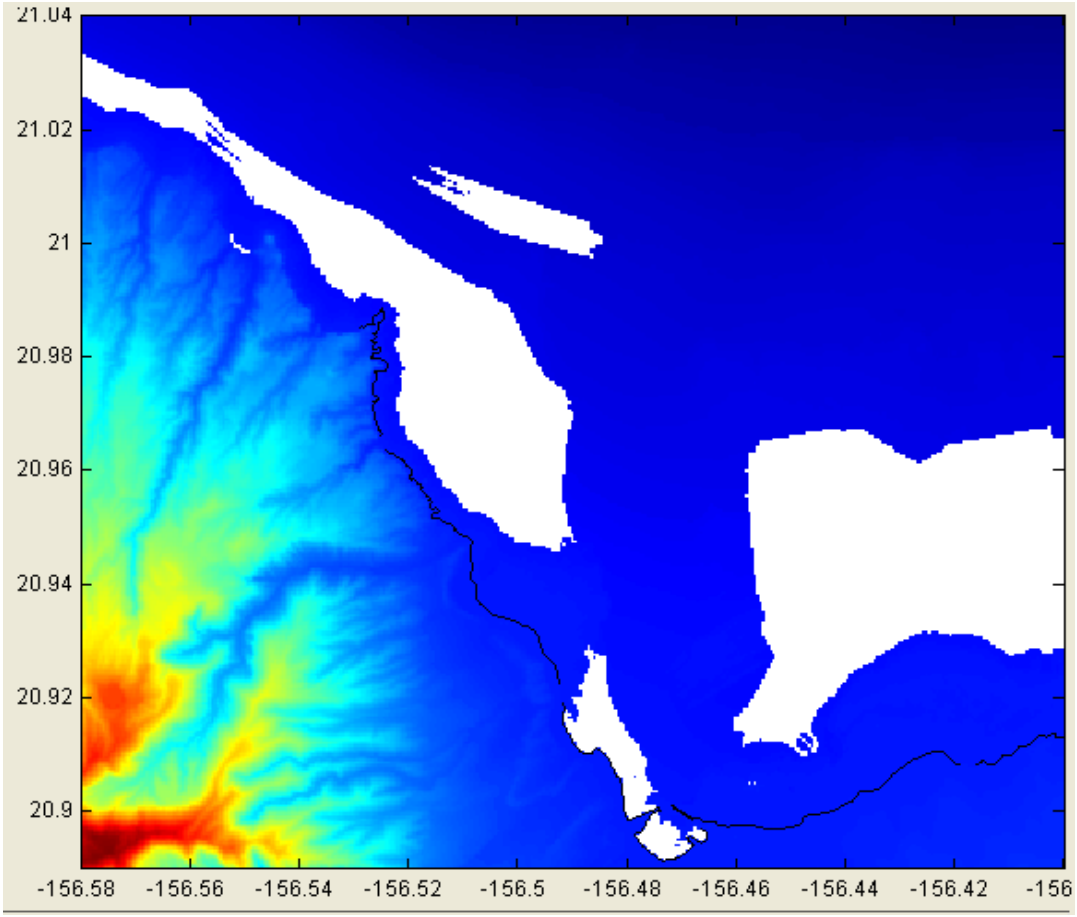

FIG. III–16. Existence of data voids in the multibeam bathymetry data.

Other sources of data could be used to augment this database include digital elevation models available at a grid spacing of ten metres from the University of Washington Geomorphological Research Group All Hawaii 10-meter Data.

Before combing datasets from different sources as well as during incorporation of data into numerical models, the user has to carry out a basic assessment of data to reconfirm the resolution as reported, the compatibility of horizontal and vertical data among different datasets, their adequacy with respect to the problem under consideration as well as any missing data.

National elevation dataset

The National Elevation Data set is available at the US Geological Survey National Geospatial Program Topographic Maps. All elevation values are provided in units of metre and are referenced to the North American Vertical Datum of 1988 (NAVD 88) over the conterminous United States. The vertical reference will vary in other areas. National Elevation Data set data are available nationally at resolutions of 1 arc-second (approx. 30 metres) and 1/3 arc-second (approx. 10 metres) and in limited areas at 1/9 arc-second (approx. 3 metres).

NOAA Tsunami inundation digital elevation models

Among the comprehensive resources that could be used by tsunami modellers for the evaluation of water levels (or tsunami heights) in the Hawaii region are the tsunami inundation

models developed by the National Centres for Environmental Information Coastal Elevation Models. The website allows for selecting the target state and region (both Hawaii for the current example). The data resolution ranges from 1/3 arc-second (~10 m) to 36 arc-seconds (~1 km). For the Kahului area, the data are available at a resolution of 1 arc-second (~30 m).

Tide gauge data

The arrival of the tsunami waves was recorded by a tide gauge station located inside the Kahului harbour. The first wave peak was seen after about 7.9 h of the tsunami initiation from the Japanese coast. Relevant information of the tide gauge station is provided in Table III–11. The data recorded by the tide gauge is available from NOAA. Figure III–17 below shows a step by step approach for the collection of the tide gauge data for the period of interest. A snapshot of the data retrieved (in text format) is given in Table III–12. Figure III–18 depicts the tide gauge data of the 2011 event recorded at the Kahului harbour.

TABLE III–11. INFORMATION ON THE TIDE GAUGE DATUM FOR THE NGDC TIDE GAUGE STATION # 1615680 AT KAHULUI. (Data taken from National Oceanic and Atmospheric Administration Center for Operational Oceanographic Products and Services)

21 Apr 2013 18:04 GMT ELEVATIONS ON STATION DATUM
National Ocean Service (NOAA)

Station:1615680 T.M.: 150 W
Name: Kahului, Kahului Harbor, HI Units: Meter
Status: Accepted (Apr 17 2003) Epoch:1983–2001
Datum: STND

Datum	Value	Description
MHHW	1.422	Mean Higher-High Water
MHW	1.313	Mean High Water
DTL	1.079	Mean Diurnal Tide Level
MSL	1.075	Mean Sea Level
MTL	1.074	Mean Tide Level
MLW	0.835	Mean Low Water
MLLW	0.736	Mean Lower-Low Water
STND	0 000	Station Datum
GT	0.686	Great Diurnal Range
MN	0.478	Mean Range of Tide
DHQ	0.109	Mean Diurnal High Water Inequality
DLQ	0.099	Mean Diurnal Low Water Inequality
HWI	0.24	Greenwich High Water Interval (in Hours)
LWI	6.64	Greenwich Low Water Interval (in Hours)
Maximum	1.798	Highest Observed Water Level
MAX Date	19681220	Highest Observed Water Level Date
MAX Time	00:00	Highest Observed Water Level Time
Minimum	0.244	Lowest Observed Water Level
Min Date	19550619	Lowest Observed Water Level Date
Min Time	00:00	Lowest Observed Water Level Time
HAT	1.678	Highest Astronomical Tide
HAT Date	19861231	Highest Astronomical Tide Date
HAT Time	13:24	Highest Astronomical Tide Time
LAT	0.481	Lowest Astronomical Tide
LAT Date	19900524	Lowest Astronomical Tide Date
LAT Time	17:42	Lowest Astronomical Tide Time

Tidal Datum Analysis Period:01/01/1983 - 12/31/2001

TABLE III–12 SNAPSHOT OF THE TIDE GAUGE DATA RETRIEVED FROM NOAA WEBSITE

Station Date Time Pred 6Vrfy 6
DCP#:1 1
Units: Meter
Data%:MSLGMT100.00100.00
Maximum: 0.156 1.883
Minimum:-0.316-1.958
------- -------- ----- ------- -------
1615680 20110311 00:00-0.152-0.153
1615680 20110311 00:06-0.141-0.119
1615680 20110311 00:12-0.131-0.107
1615680 20110311 00:18-0.121-0.116
1615680 20110311 00:24-0.110-0.087

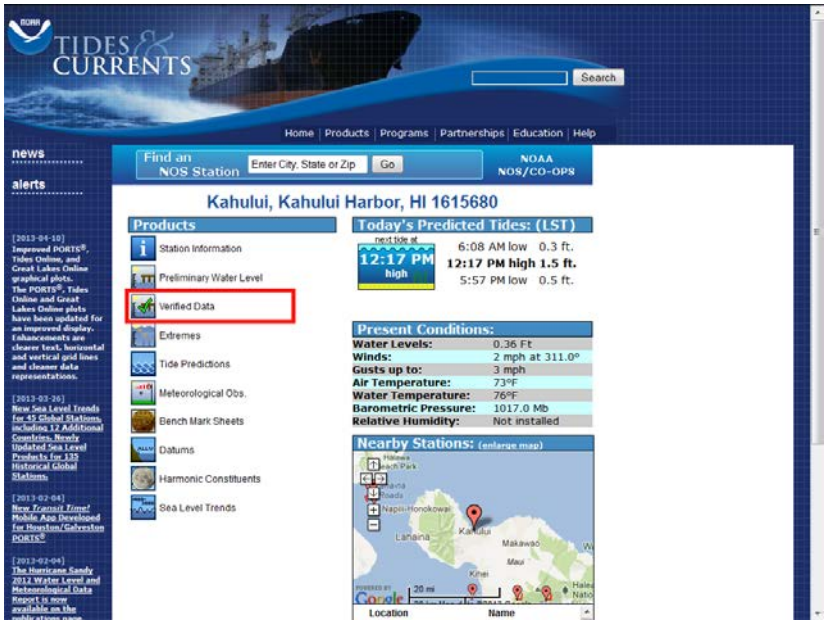

(a) Initial web page, tide gauge data for 2011 event can be obtained by clicking the link 'verified data', as seen inside red rectangular box

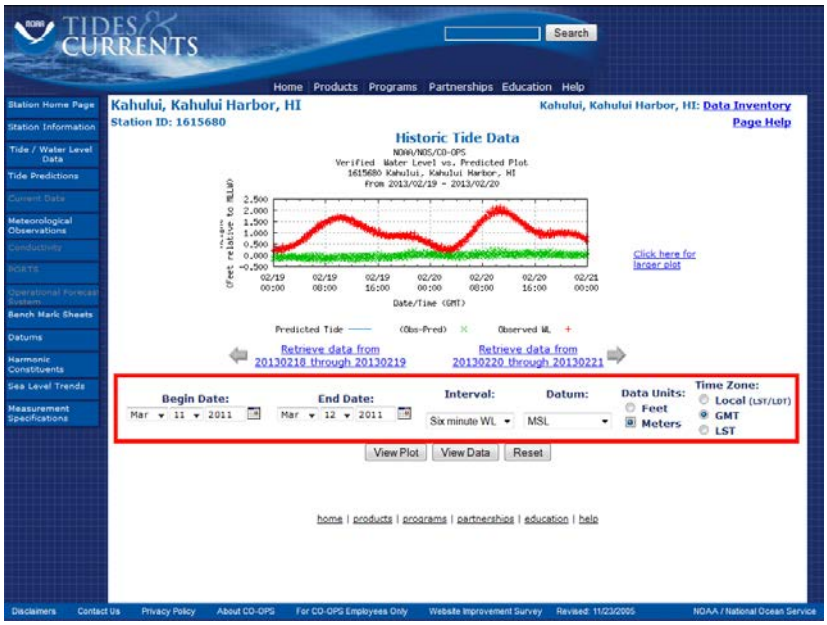

(b) A screen shot from 'verified data' page, the settings (start and end date, sampling interval, datum, data units and time zone) which need to be specified for appropriate retrieval of data is also included.

FIG. III–17. Pictorial representation of procedure for extraction of tide gauge data from NOAA database.

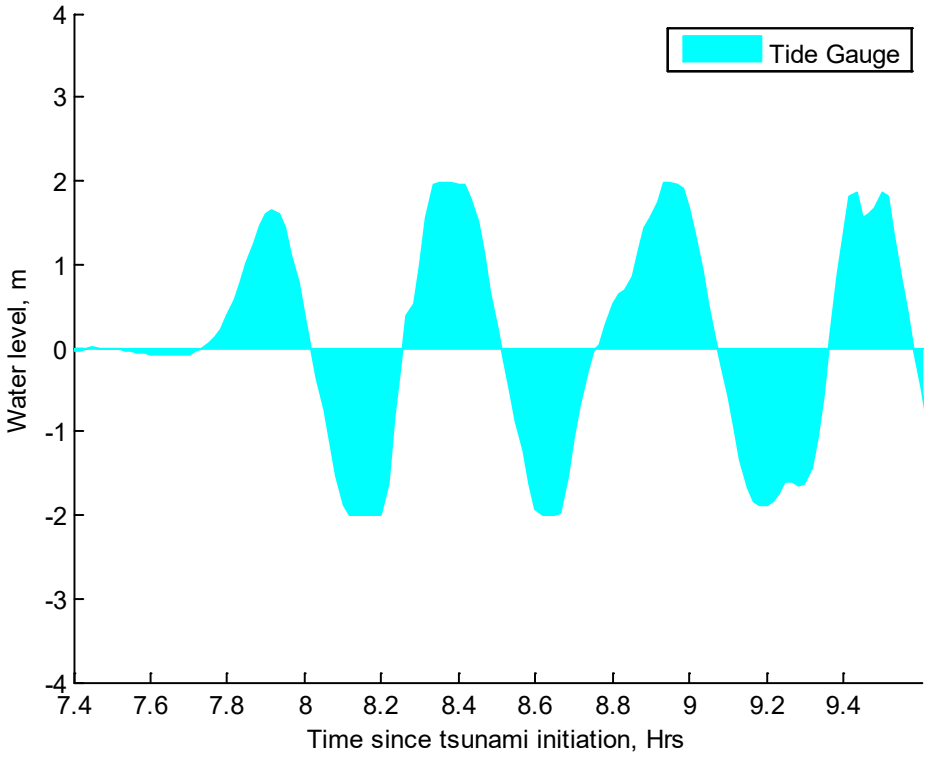

FIG. III–18. Tide gauge measurement at Kahului harbour of the 2011 tsunami event.

III–2.2. Application using specific software

As discussed in Section III–2.1, separate numerical simulations are carried out for evaluating the performance of numerical models during: (i) the linear propagation phase (see Section III–2.2.1) and (ii) the non–linear shoaling and run-up (see Section III–2.2.2). It may be noted that separate simulations were necessitated by combined limitations of the operating system (windows 32 bit) and the numerical models. In an ideal scenario, both analyses could be carried out on a single model.

Several numerical models are available in the public domain as well as in academic circles for the solution of shallow water equations and estimation of run-up. Some of these are TUNAMI-N2 [III–10], MOST [III–11], Cornell Multi-grid Coupled Tsunami Model (COMCOT) [III–12], NAMI DANCE [III–13], Tsunami Code [III–15]. The current assessment has been carried out following these codes. It may be noted that several other comprehensive sets of numerical models are available for simulation of propagation of tsunami waves and the IAEA does not specify the use of any particular numerical model.

A short description on Tsunami Code, NAMI DANCE and COMCOT is given in the following sections.

III–2.2.1. Tsunami code

The details on the validation of Tsunami Code as well as comparison of its performance with other codes are covered elsewhere [III–14, III–16, III–17].

Description of distant tsunami code

Distant tsunami analysis code is generally used for an event with a propagation distance over 1 000 km, such as the Sumatra-Andaman earthquake tsunami in 2004 and the Chile earthquake tsunami in 1960. Mesh size from several kilometres to several tens of kilometres is used in this kind of analysis in order to cover the large target area. Tsunami Code is made considering the latest knowledge of the tsunami simulation technology in reference to a TUNAMI Code open in the TIME project of Tsunami Engineering Laboratory at the Tohoku University in Japan. Tsunami Code can predict data such as maximum water level, range of run-up areas, first-wave time of arrival in coastal areas. The code calculates water level and discharge flux at a time interval of Δt by using the equation of fluid motion and the equation of continuum for given parameters such as bathymetric data, still water depth, source conditions. The wavelength of distant tsunamis (several hundreds of kilometres) is larger than its water depth (several kilometres) and its water level is even smaller (several metres). Therefore, the distant tsunami analysis code is based on the linear theory. The governing equations are described in the spherical coordinate system (see Fig. III–19) with its origin at the centre of the earth since a distant tsunami is a large scale phenomenon.

Equation of Motion

$$\frac{\partial M}{\partial t} = -\frac{gh}{a\cos\varphi}\frac{\partial \xi}{\partial \lambda} + fN \tag{III–3}$$

$$\frac{\partial N}{\partial t} = -\frac{gh}{a}\frac{\partial \xi}{\partial \varphi} - fM \tag{III–4}$$

Equation of continuum

$$\frac{\partial \xi}{\partial t} = -\frac{1}{a\cos\varphi}\left\{\frac{\partial M}{\partial \lambda} + \frac{\partial}{\partial \varphi}(N\cos\varphi)\right\} \tag{III–5}$$

Where: M is the discharge flux integrated along the depth in the longitude (λ) direction (m^2/s), N is the discharge flux integrated along the depth in the latitude (φ) direction (m^2/s), t is time (s), g is the gravitational acceleration (m/s^2), h is the water depth (m), ξ is the water level (m), f is the Coriolis factor ($= 2\omega sin\varphi$), λ is the longitude (rad.) and φ is the latitude (rad.).

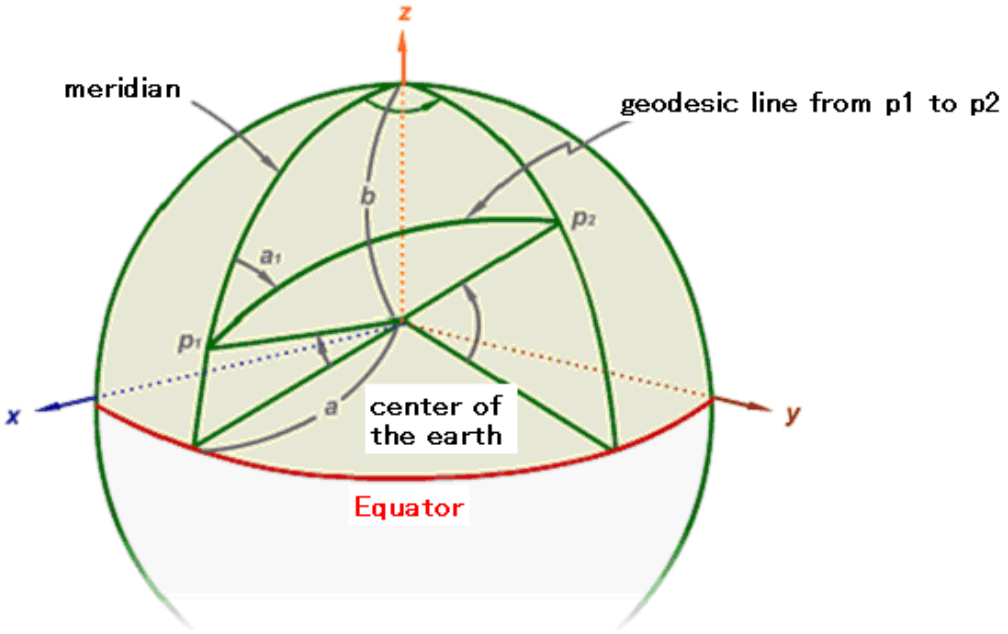

FIG. III–19. Coordinate system of distant tsunami analysis code (reproduced with permission of Regulatory Standard and Research Department Secretariat of Nuclear Regulation Authority [III–18]).

In order to mimic the truncation error caused by discretizing the linear long wave equation using the finite difference method to the physical dispersion effect, the parameter $R.D.$ is kept as 1.0 where:

$$R.D. = \frac{\Delta l}{2h}\sqrt{1 - \left(C_0\frac{\Delta t}{\Delta l}\right)^2} \tag{III–6}$$

And: Δt is the time difference step (s), Δl is the mesh size (m), C_0 is the velocity of the linear long wave (m/s) and h is the average static water depth (m).

The seabed is elastically distorted by the change of the total weight of sea water loaded on the seabed due to the sea level change by the tsunami. This is called the ocean self-attraction and loading effect (SAL) and the phenomenon changes the apparent sea level and affects the tsunami velocity [III–19] especially in trans-oceanic tsunami propagation as in the case of the GEJE and the Chilean tsunami of 2010. The distant tsunami analysis code 'Tsunami_FAR' introduces this effect as a scale parameter shown in the following equations.

$$\frac{\partial M}{\partial t} = -\frac{gh}{a\cos\varphi}\frac{\partial}{\partial \lambda}\xi(1-\beta) + fN \qquad \text{(III–7)}$$

$$\frac{\partial N}{\partial t} = -\frac{gh}{a}\frac{\partial}{\partial \varphi}\xi(1-\beta) - fM \qquad \text{(III–8)}$$

Where: β is the SAL scale parameter.

The value of scale parameter β can be set in FT07, which is the input data of the distant tsunami analysis. In general, the value of β is set to be 0.01.

Analysis procedure

The flowchart of the calculation process is shown in Fig. I–2 of Annex I. First, the code reads analysis conditions, bathymetric data and water surface displacement. The analyser can choose whether to give the value of the water surface displacement directly, or to compute the ocean bottom deformation from fault parameters. Then the code calculates the water level and discharge flux at each selected time on the basis of the equation of motion and the equation of continuum. Water level and fluid velocity at each selected time are given as output data.

The explicit leap-frog finite difference method is adopted to solve linear shallow water equations. The evaluation of the water surface elevation ξ and volume fluxes M and N is staggered in time and space. The water surface elevation ξ is evaluated at the centre of a grid cell and volume fluxes M and N (product of velocity and water depth) are evaluated at the edge centres of the grid cell.

Input data

Tsunami Code uses three types of data:

(a) FT07: conditions for analysis (e.g. time duration, region data, output interval, fault dimensions, output gauge locations, connection to local domain, if any).

(b) FT08: bathymetry data, with sea depths considered as positive values.

(c) FT10: spatial sea bottom and surface deformation file, with matching dimensions of FT08. This file is needed, if fault dimensions and other details are not provided in FT07.

Source modelling

The instantaneous slip model by Fujii and Satake [III–2] has been used for assessment. The details of the source model are covered in Section III–2.1. The initial displaced profile

estimated by Tsunami Code using the fault parameters depicted in Table III–8 is given in Fig. III–20. The same data has also been used as input to the other numerical model, COMCOT.

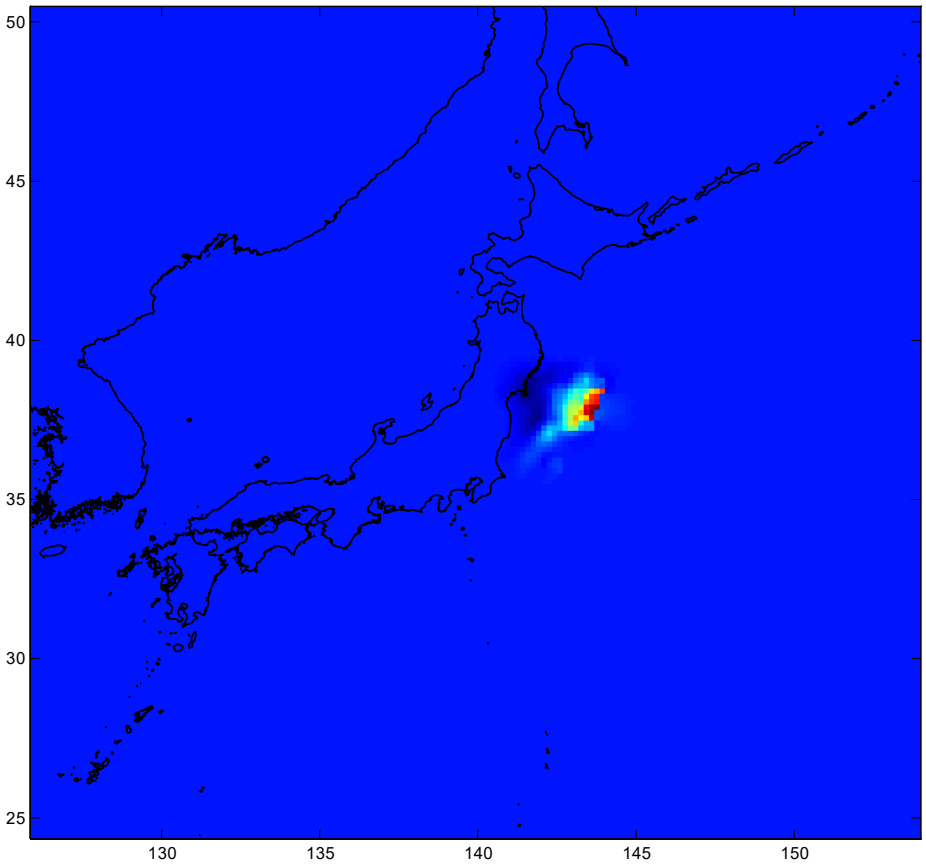

FIG. III–20. Plot of initial wave profile used for analysis.

Grid information

For the simulation of the propagation of the tsunami across the Pacific Ocean, a 10-minute data based on ETOPOv2 is used. The grid extents are chosen so as to encompass all relevant land masses that could guide and/or reflect the waves as well as to cover all DART stations of interest. The plot of the 10-minute bathymetric grid used is given in Fig. III–21. The user may also take note of the need for use of a continuous longitude (0 to 360 degree) as against change in values from +180 degrees to -180 degrees near the international date line. Needs such as these, specific to each numerical modelling system have to be taken into account while developing the numerical grid.

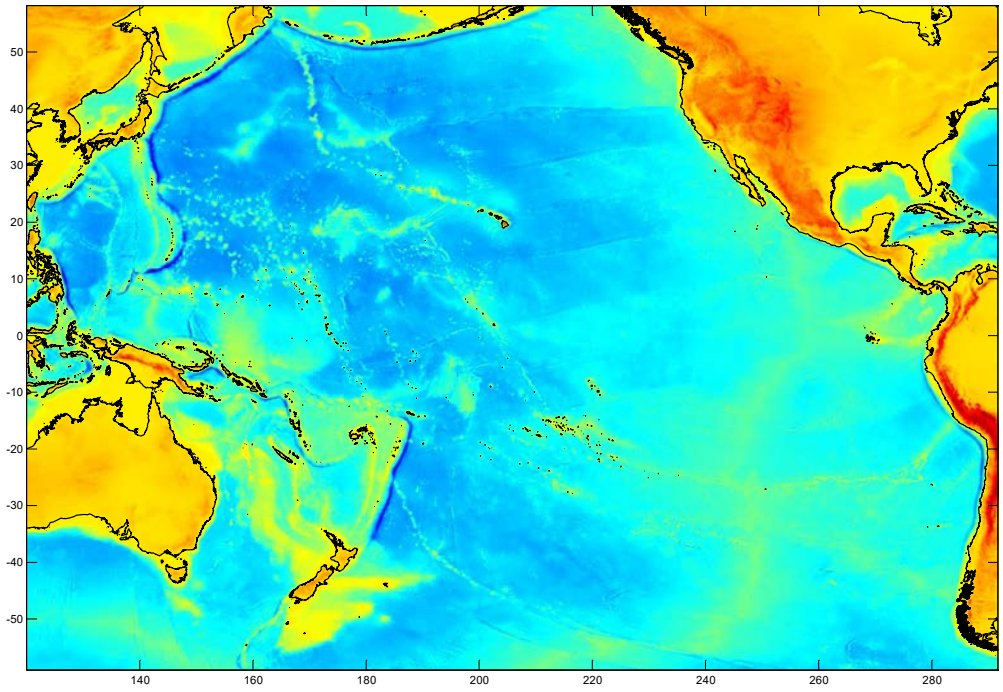

FIG. III–21. Plot of bathymetric data as used by TSUNAMI CODE and COMCOT.

For Tsunami Code the bathymetric data are named 'FT08'. The first line of the file is a comment line and the other lines are gridded bathymetric data. Positive values indicate water depth in the sea and negative values indicate altitude on the land in (m).

Analysis: time step, boundary condition

Distant tsunami analysis assumes that the initial velocity of the fluid and the initial water level are 0. It also assumes open boundary conditions for free transmission and perfect reflection by land. A time step size of 25 seconds was used during numerical simulations.

III–2.2.2. NAMI DANCE tsunami numerical model

As described in Annex I, tsunami numerical model NAMI DANCE is developed based on the solution of the non-linear form of the long wave equations with respect to related initial and boundary conditions. NAMI DANCE has the capability to solve trans-oceanic propagation of tsunamis in nested domains. In the solution procedure the user can also indicate the code to solve the linear or non-linear form of long wave equations in either Cartesian or spherical coordinates with a specified or spatial distribution manning friction coefficient.

NAMI DANCE can compute the tsunami source from rupture parameters by considering segmented rupture with the time lag between successive ruptures according to the rupture propagation speed. The initial wave form can also be defined by the user. The grid size ration from parent to next child nested domain is 1/3. Details of the analysis procedure are available in the user manual for NAMI DANCE [III–13].

III–2.2.3. Cornell multi-grid coupled tsunami model, COMCOT

Description of distant tsunami code

COMCOT version 1.7 [III–12] was developed by Wang at the Institute of Geological & Nuclear Science, New Zealand. Part of the current version and all earlier versions were developed by the Wave Group led by Liu at the Cornell University in the United States of America.

As is the case with Tsunami Code, COMCOT also uses shallow water equations for modelling tsunami wave propagation. COMCOT adopts staggered leap-frog finite difference schemes to solve shallow water equations in both spherical and Cartesian coordinates. For enabling refinement of the predictions near the region of interest, a nested grid system, dynamically coupled up to 12 levels with different grid resolution, is also available in the model. In one grid region, a uniform grid size is adopted in COMCOT. In COMCOT, a spherical or Cartesian coordinate system, as well as either a linear or non-linear version of the governing equations can be specified for each region. In addition to seismogenic tsunami initiation, COMCOT has provisions to simulate dynamic movement of the sea bottom, thus capturing scenarios such as sub-sea landslides. Information on the basic formulation of the code as well as a numerical solution scheme is available in the user manual for COMCOT [III–20].

Analysis procedure

Based on the analysis conditions including those at boundary, bathymetric data and water surface displacement, COMCOT carries out the numerical simulation of propagation of tsunami waves. Details of the analysis procedure are available in the user manual of COMCOT [III–20].

Input data

The basic information needed for earthquake induced tsunami simulation using COMCOT is to be provided in the control file ‘comcot.ctl’. The file, which is self-descriptive in nature, has separate sections covering general parameters for simulation, parameters for fault model, configurations for all grids covering grid type (spherical/Cartesian), extents, type of bathymetric data file corresponding to the grid (e.g. xyz, most, ETOPO), andvariable output specifications. The bathymetric data for the corresponding grid is read from the name of bathymetry data file provided for that grid in the control file. For the current analysis, bathymetry data (in 10 minute spacing) are provided in in.most format.

Source modelling

COMCOT has specific tools capable of modelling the sea floor deformation due to tsunamigenic earthquakes, given information about fault parameters as well as dynamic sea floor deformation due to sub-marine landslides. Pre-computed sea floor deformation in ASCII xyz format can also be used as input. The instantaneous slip model by Fujii and Satake (2011) has been used for assessment. In the current exercise, so as to have exactly similar deformation files, the sea floor deformation as computed by Tsunami Code is input in the form of ASCII xyz (i.e. longitude, latitude and value) file to COMCOT.

The details about the source model are covered in Section III–2.1. The initial displaced profile estimated by Tsunami Code using the fault parameters depicted in Table III–8 is given in Fig. III–20.

Grid information

For the simulation of the propagation of a tsunami across the Pacific Ocean, a 10-minute data based on ETOPOv2 is used, see Fig. III–21.

Analysis: time step, boundary condition

For the analysis using COMCOT the initial velocity of fluid and the initial water level are assumed to be zero. Open boundary conditions for free transmission are assumed in water and perfect reflection by the land. A time step size of 15 seconds was used during numerical simulations.

III–2.2.4. Distant tsunami: Linear propagation phase

Simulations

Using the deformed water profile as initial conditions and bathymetry data for the computational domain, the propagation of the tsunami across the Pacific Ocean is simulated using both numerical models. Exactly the same initial wave profile and bathymetric data are used by both codes.

Considering the large extent of the domain in which the simulations need to be conducted, the user needs to adopt a numerical model that resolves tsunami propagation in a spherical coordinate system. Effects due to tsunami wave dispersion might also contribute to modification of wave profile while it is propagating across the Pacific. This phenomenon also needs to be captured.

The data on wave trains at each DART station as well as the maximum water levels observed in the domain during the time of computation were stored for comparison with the observed data.

The input files used for propagation runs are available in the link with the supplementary material.

Figure III–22 provides the maximum water levels computed by COMCOT, Tsunami Code and NAMI DANCE. Comparison of computed maximum water levels and the levels recorded at location of 29 DART stations is given in Fig. III–23. Based on the values evaluated from the simulation, a statistical comparison of the maximum water levels has been conducted. Table III–13 provides the mean deviations from the observed data with the predicted ones as well as the range of deviations observed.

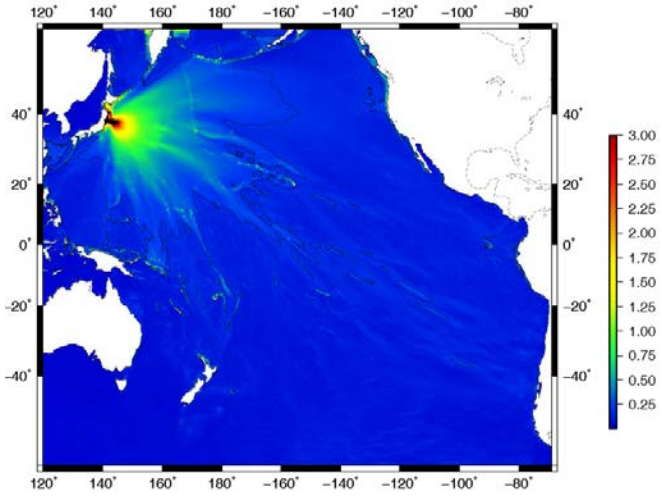

(a) COMCOT

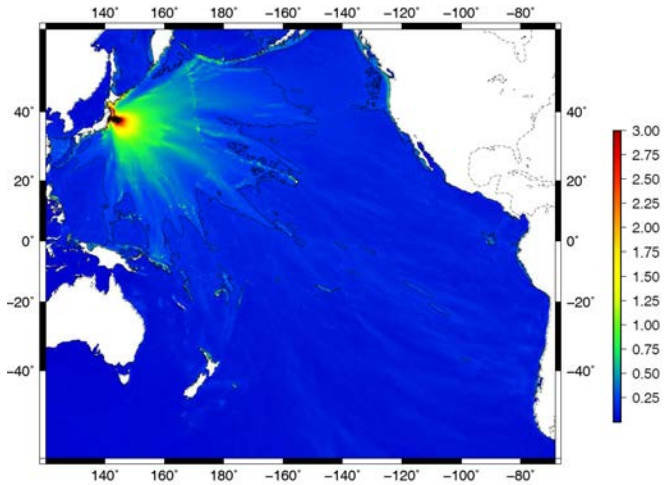

(b) Tsunami Code

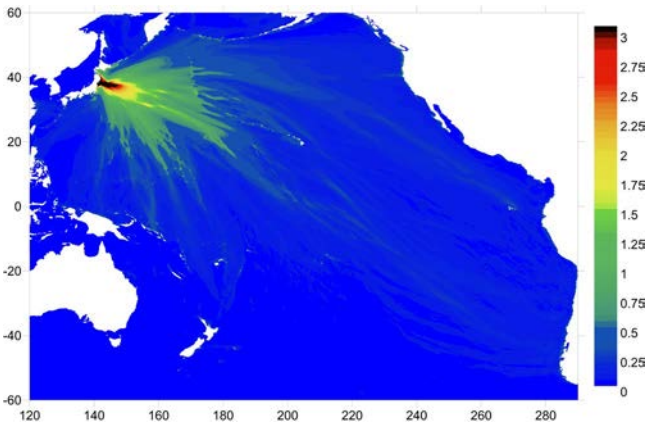

(c) NAMI DANCE

FIG. III–22. Comparison of maximum water levels (m) in the computational domain by COMCOT, Tsunami Code and NAMI DANCE.

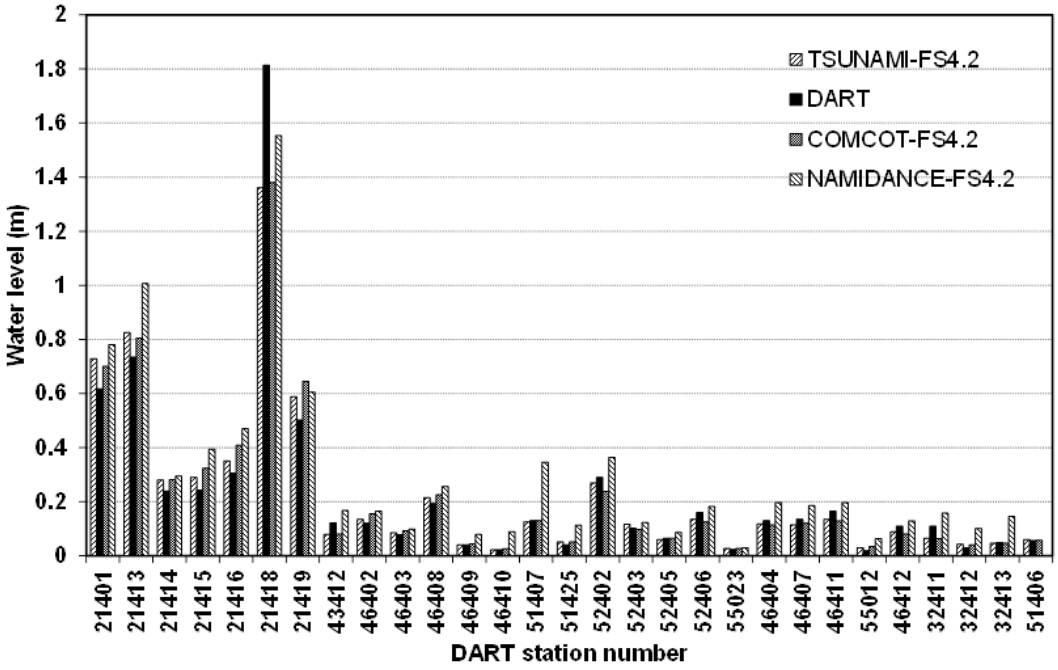

FIG. III–23. Comparison of maximum water level (m) by each DART.

TABLE III–13. COMPUTED VARIATIONS MAX ERRORS IN THE ESTIMATED VALUES VS OBSERVED WATER LEVELS FROM ALL DART STATIONS

	Tsunami-FS Rev4.2	COMCOT-FS Rev4.2	NAMI DANCE
Average	-3.2	-6.0	7.7
Minimum	-57.9*	-84.2*	-56.0
Maximum	40.9[a]	41.8*	45.0

[a] Larger errors are observed from those DARTs where absolute value of maximum water levels is small. Please see paragraph below.

It is noted that the distribution of maximum water levels by COMCOT, Tsunami Code and NAMI DANCE follows a similar trend. On average, the water levels are under predicted by about 8% by both codes; these values fall within the error range (20%) specified as acceptance limits for validation of field data (see Section 2.3.3).

It is also observed that in 11 stations that recorded water levels larger than 0.15 m, the range of errors are also within 30%. With the use of better source models (e.g. with dynamic rupture propagation), it is expected that these differences would be further reduced.

The times of arrival of waves is also an important parameter that characterizes the tsunami propagation. A comparison of time arrivals as estimated by numerical models vs the observed data is given in Fig. III–24 and the corresponding statistical comparison is given in Table III–14. It is seen that both codes predict earlier arrival of waves compared to actual observations. This issue has also been reported by other researchers [III–21]. The estimated average deviation in time of arrival is about 1% by COMCOT and NAMI DANCE and less than 0.5% by Tsunami Code.

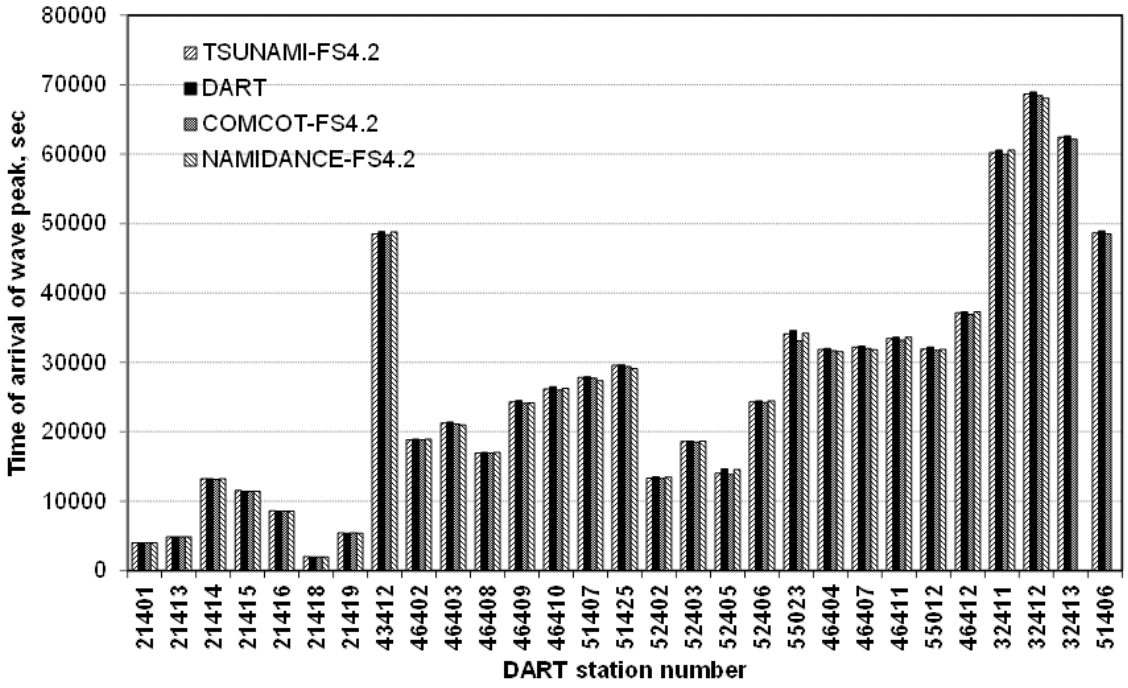

FIG. III–24. Estimated times of arrival (sec) based on Fujii-Satake model by Tsunami Code, COMCOT and NAMI DANCE vs observed ones from DART.

TABLE III–14 STATISTICAL COMPARISON OF MAX ERROR IN TIME OF ARRIVAL AS ESTIMATED BY NUMERICAL MODELS WITH DART

	Tsunami-FS Rev4.2	COMCOT-FS Rev4.2	NAMI DANCE
Average	0.46	1.05	0.95
Minimum	-2.20	-0.99	-2.10
Maximum	4.29	5.52	3.10

Plots are also made with reference to the wave trains at each DART station (see Figs. III–25 to III–26). It can be observed that apart from the earlier arrival of wave peaks, the characteristics of wave trains are simulated well by both numerical models. However, it is also observed that in some DART stations closer to the source, Tsunami Code predicts a second set of predominant wave peaks which is not observed in DART stations.

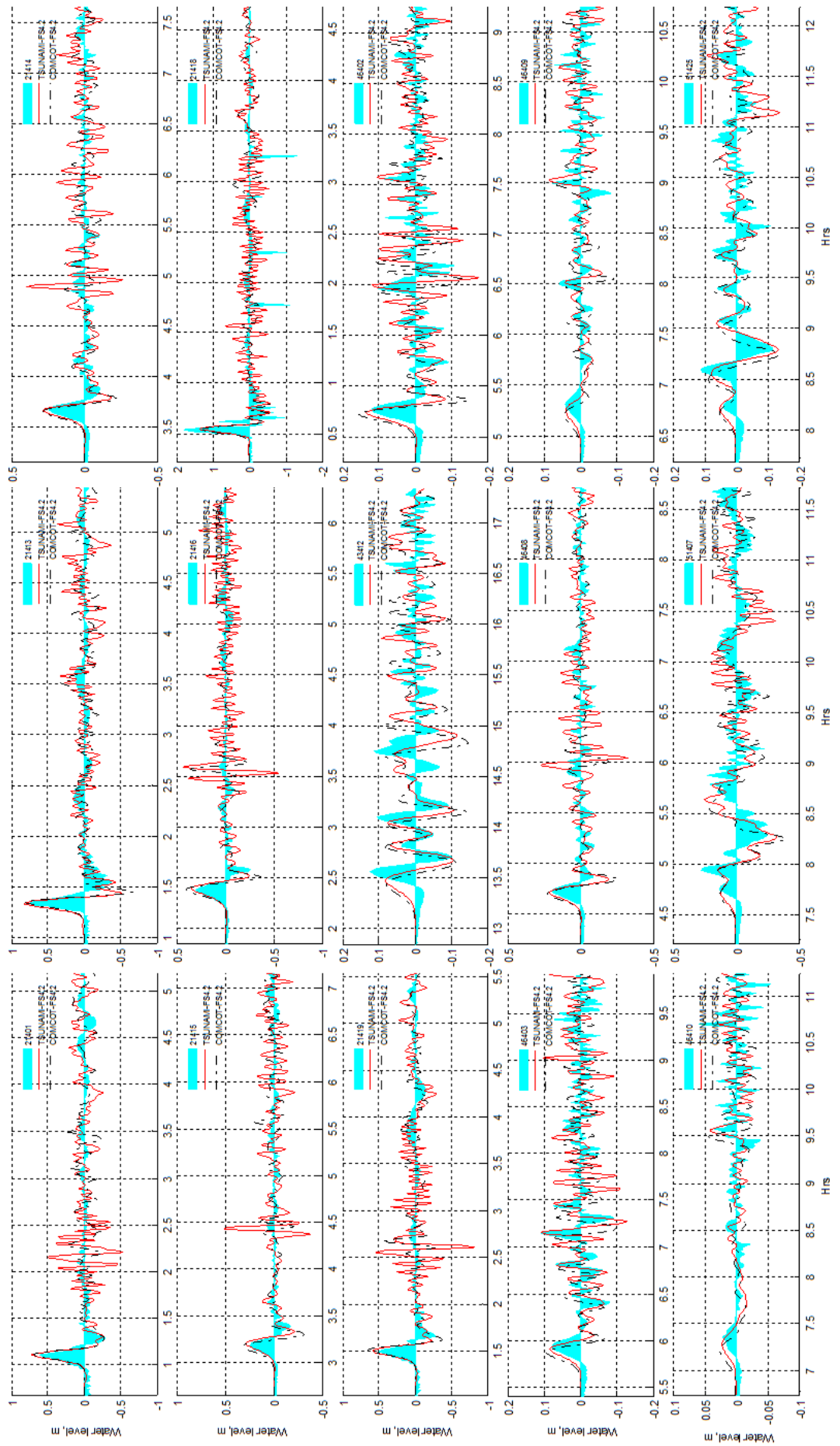

FIG. III–25. Comparison of wave trains as estimated by numerical models Tsunami Code and COMCOT with the recorded tsunami wave forms by DART.

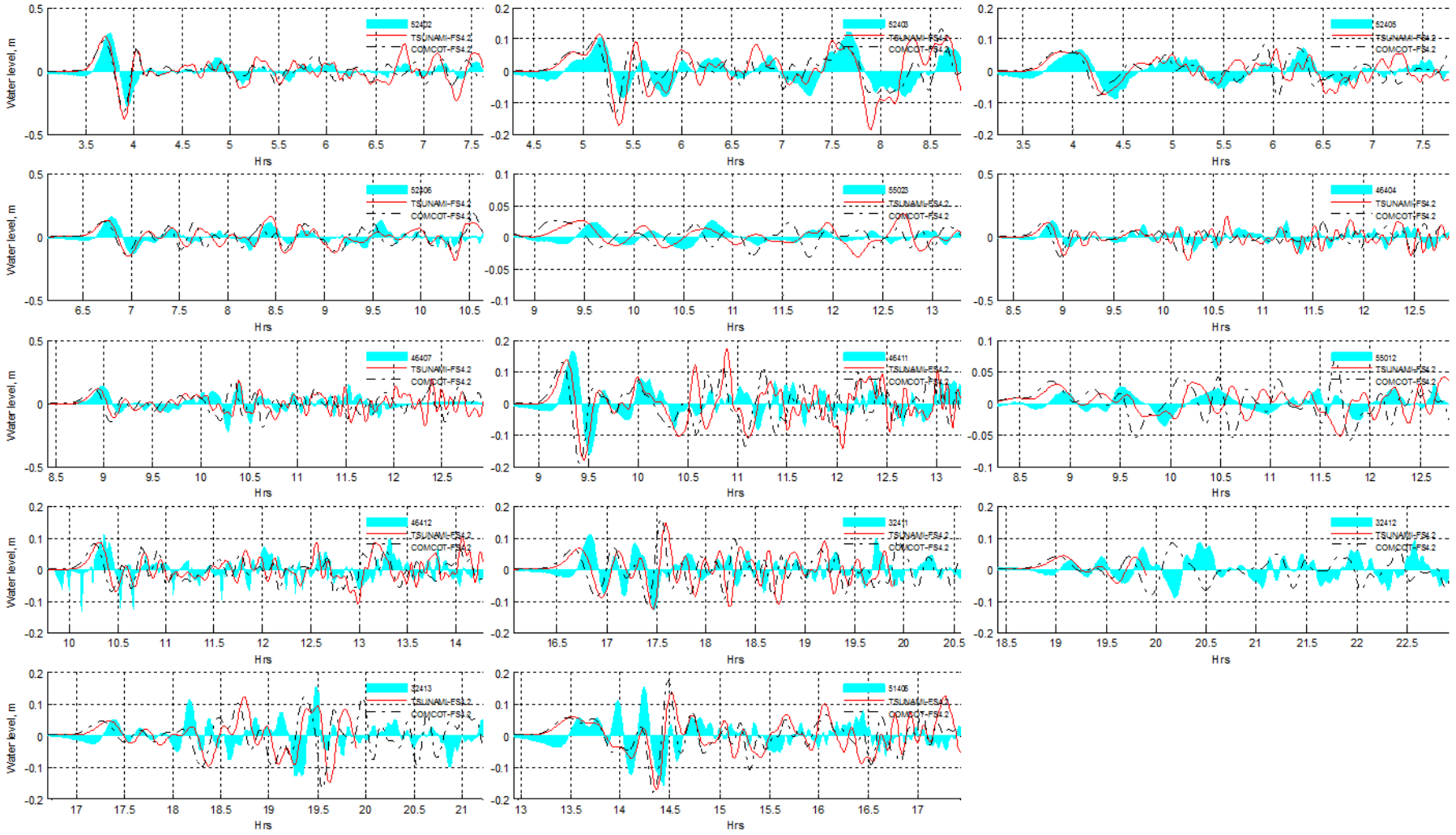

FIG. III–25. Comparison of wave trains as estimated by numerical models Tsunami Code and COMCOT with the recorded tsunami wave forms by DART (Cont.).

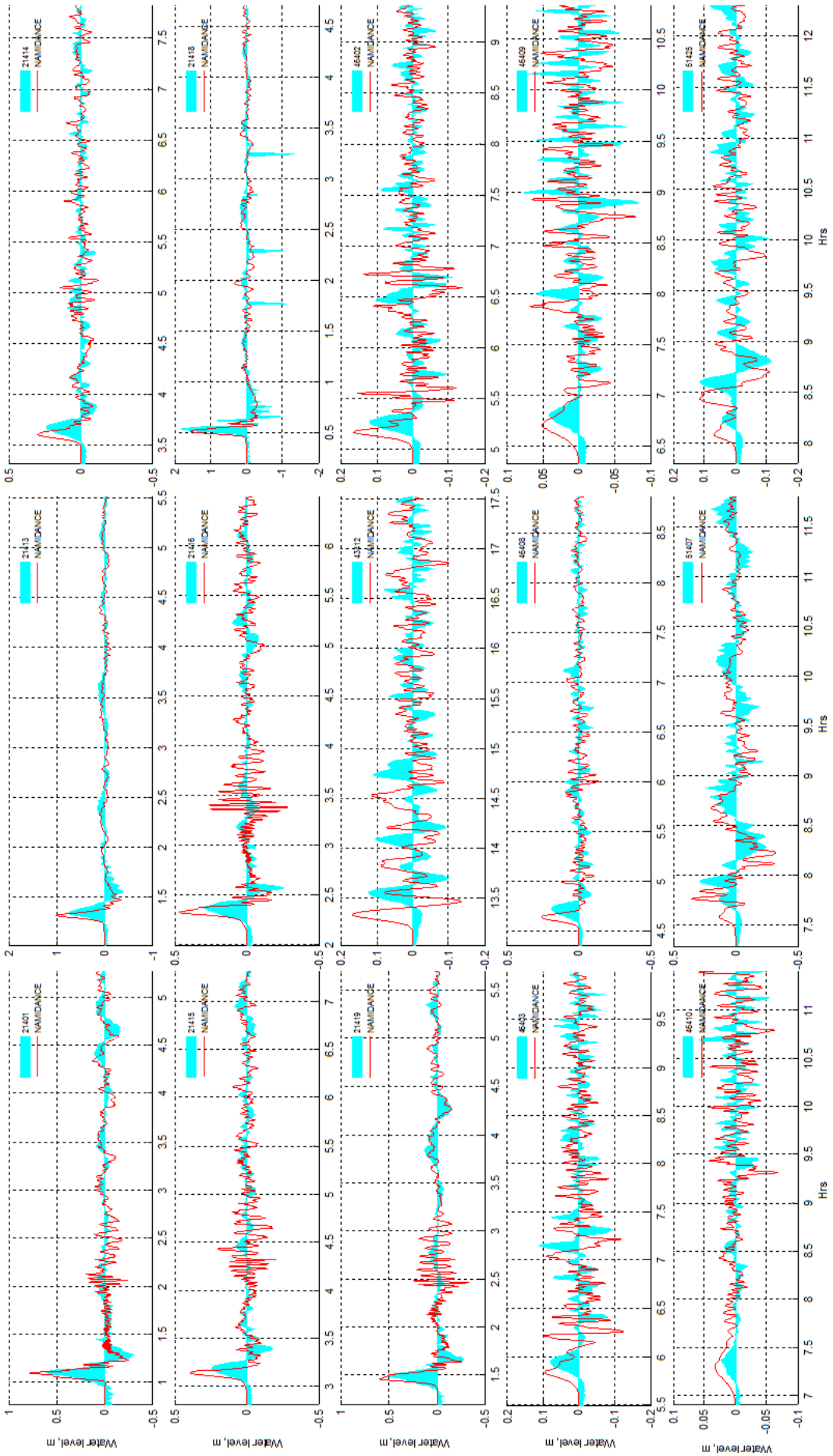

FIG. III–26. Comparison of wave trains as estimated by numerical model NAMI DANCE with the recorded tsunami wave forms by DART.

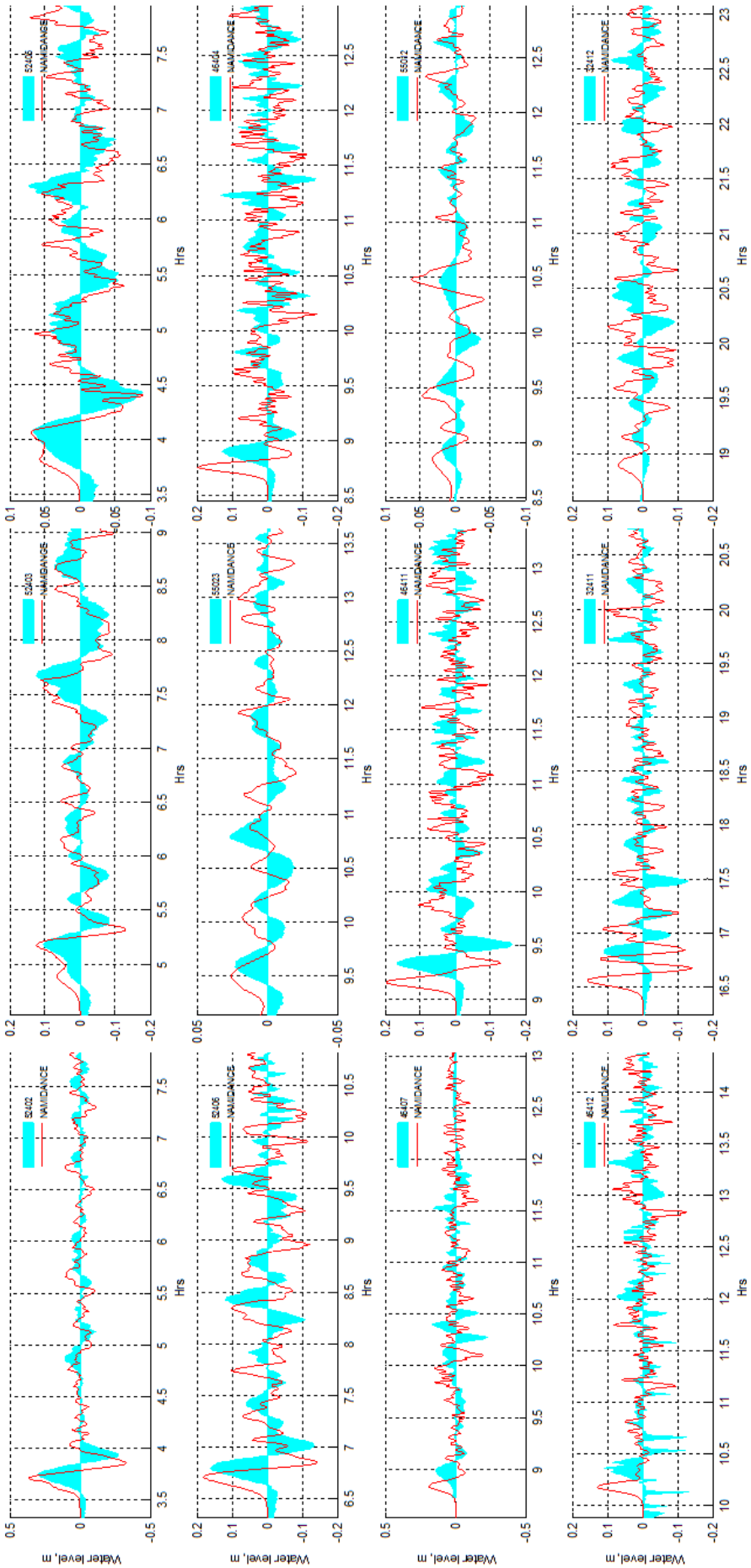

FIG. III–26. Comparison of wave trains as estimated by numerical model NAMI DANCE with the recorded tsunami wave forms by DART (Cont.).

Simulations

The previous sub-section detailed simulations covering the deep ocean propagation phase (i.e. distant tsunami) and a comparison with several recording stations (i.e. DART) in deep regions of the Pacific Ocean. The second set of simulations is conducted to capture distant tsunami propagation and its subsequent shoaling/amplification near the coast for a specific region, the Kahului harbour, Hawaii, in this case. As explained earlier, tide gauge record at the Kahului harbour for the 2011 event is considered for comparison with numerical estimates using Tsunami Code and COMCOT. The same source model (viz. Fujii-Satake source model, version 4.2), for use for linear propagation evaluation as covered in previous sub-section (see Table III–8) is also used for the current set of simulations.

A 2-minute bathymetry, ETOPOv2, has been unitized for depicting the Pacific Ocean, in deep ocean propagation models. A 1 second integrated topography-bathymetry DEM (tsunami inundation map) available from the NOAA National Geophysical Data Center has been utilized for representing the local shore bathymetry and topography of Kahului.

In Tsunami Code, the facility of 'connection' in the distant tsunami analysis module is used to generate the wave trains along the boundary of the local tsunami analysis code. The distant tsunami analysis code is run for the specified duration using the displaced fault profile as initial condition and corresponding wave trains (with respect to time) along local field boundary are generated. These wave trains are subsequently used as boundary inputs to local tsunami analysis code. The local tsunami model has a total of four grids (including three nested grids) and further propagation including shoaling is simulated by this non-linear model (see Fig. III–27). The wave trains at the point of interest (tide gauge station at Kahului Harbour) is saved (FT02 file in Tsunami Code).

In case of COMCOT, an integrated model with a total of five grids is used for simulation. Table III–15 provides details of numerical grids used for simulation along with other related information including sources of bathymetric and/or topographic data.

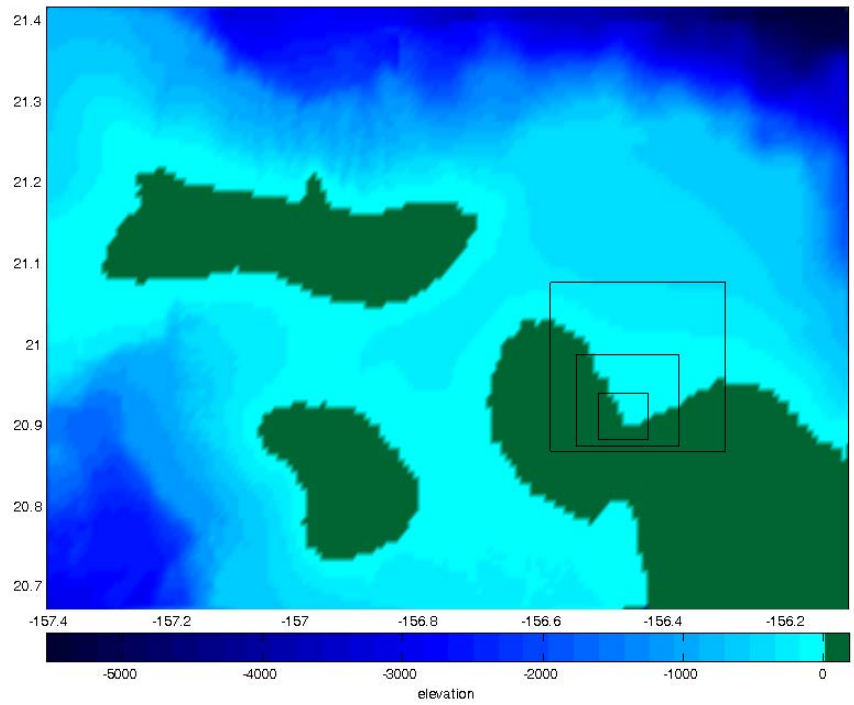

(a) View of nested grids used by Tsunami Code (Please note that far field grid is not shown)

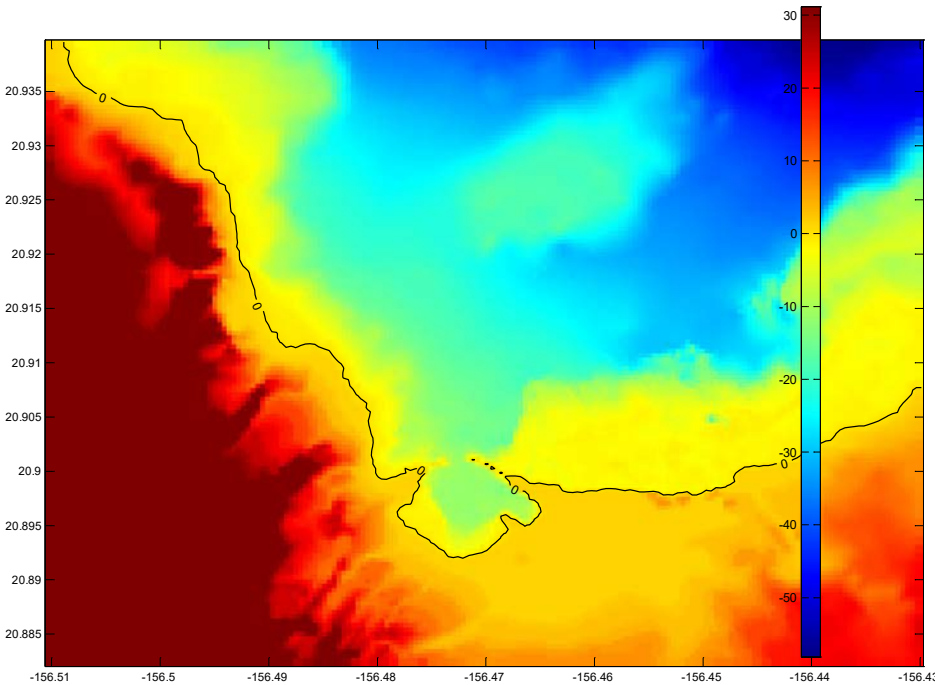

(b) Bathymetry/topography of the innermost nested grid (with 45 m resolution).

FIG. III–27. Overview of (a) nested grids and (b) Bathymetry and Topography used for local tsunami analysis.

TABLE III–15. DESCRIPTION OF GRIDS USED FOR TSUNAMI CODE, COMCOT AND NAMI DANCE

Grid	Tsunami	COMCOT	NAMI DANCE	Propagation model	Bathymetric data source
Grid A	6 min (distant tsunami analysis module, spherical)	2 min (spherical)	2 min (spherical)	Linear	ETOPOv2
Grid B	810 m (Cartesian)`	40 s (~1215 m)	40 s (~1215 m) (spherical)	Non-linear	
Grid C	270 m (Cartesian)	13.3 s (~405 m)	13.3 s (~405 m) (spherical)	Non-linear	NOAA Tsunami Inundation Digital Elevation Model
Grid D	90 m (Cartesian)	4.44 s (~135 m)	4.44 s (~135 m) (spherical)	Non-linear	
Grid E	45 m (Cartesian)	1.48 s (~45 m)	1.48 s (~45 m) (spherical)	Non-linear	

Comparison of wave trains simulated by Tsunami and COMCOT with the tide gauge record is given in Fig. III–28. Table III–16 depicts the time of arrival as well as the crest amplitudes of first three waves along with the estimated errors with respect to observed data.

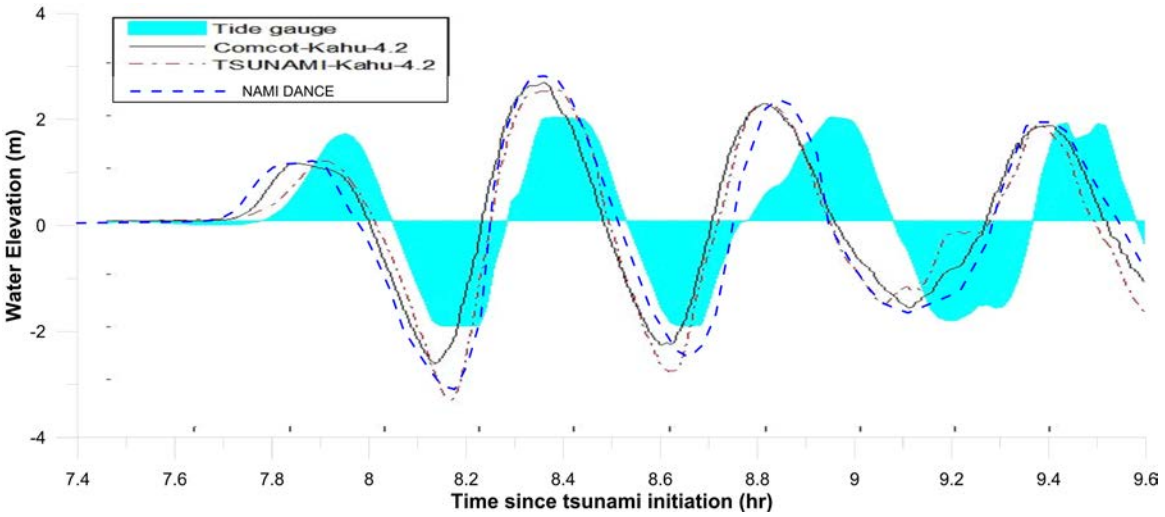

FIG. III–28. Plot of wave trains estimated by Tsunami Code, COMCOT and NAMI DANCE with the recorded data by Tide gauge.

TABLE III–16. ERRORS (MAX ERROR) IN ESTIMATION OF TSUNAMI PROPAGATION BY TSUNAMI CODE, COMCOT AND NAMI DANCE

-	Time of arrival (h)	% Error	Wave crest elevation (m)	% Error
1st Wave Crest				
Tide gauge[a]	7.92		1.66 (1.66)	
COMCOT-FS Rev4.2	7.81	1.30	1.10	34.04
Tsunami-FS Rev4.2	7.88	0.48	1.14	31.63
NAMI DANCE	7.85	0.90	1.15	32.04
2nd Wave Crest				
Tide gauge[a]	8.38		1.95 (2.5)	
COMCOT-FS Rev4.2	8.34	0.53	2.63	-5.16
Tsunami-FS Rev4.2	8.35	0.41	2.47	1.28
NAMI DANCE	8.35	0.41	2.70	1.34
3rd Wave Crest				
Tide gauge[a]	8.95		1.97 (2.35)	
COMCOT-FS Rev4.2	8.80	1.68	2.23	5.15
Tsunami-FS Rev4.2	8.80	1.68	2.24	4.85
NAMI DANCE	8.80	8.80	2.26	5.45

[a] The wave crest elevation in brackets for tide gauge readings indicates the extrapolated values to account for flat peaks (possibly due to under sampling) of wave crest. Errors in wave crest elevation are estimated with respect to extrapolated values.

TABLE III–17. RMS ERRORS IN ESTIMATION OF TSUNAMI PROPAGATION BY TSUNAMI CODE, COMCOT AND NAMI DANCE, TIME WINDOW 7.4 TO 9.6 HRS AT A TIME SPACING OF DT = 10 SECONDS

Code	% RMS error	% RMS error with a time shift of +200 seconds
COMCOT-FS Rev4.2	29.6	14.6
Tsunami-FS Rev4.2	29.8	19.2
NAMI DANCE	29.8	16.9

Comparison of wave trains simulated by Tsunami and COMCOT with the tide gauge record is given in Fig. III–28. Table III–16 depicts the time of arrival as well as crest amplitudes of the first three waves along with the estimated errors with respect to observed data. The RMS error estimates of the wave train are given in Table III–17. The following can be summarized from the analysis:

(a) Despite using a relatively simple form of source model, both codes are generally able to capture the wave amplitudes and the wave periods of the incoming tsunami.

(b) 'Earlier' arrival of waves is predicted by both the codes. For the first wave, the difference with respect to the observed values for Tsunami and COMCOT are 0.48% and 1.3% respectively whereas for the second wave the corresponding errors are 0.41 and 0.53%. Even after about 9 hours of travel, the differences in the times of arrival are seen to be minimal. Better matching with travel time could be obtained once additional phenomena, such as wave dispersion are captured in a more accurate manner.

(c) The amplitude of the first wave crest is underestimated by about 30–35% by both Tsunami and COMCOT whereas for the subsequent waves, which are also governing the maximum observed heights, the error is much lower (1–5%). It is also noted that possibly due to use of under-sampled tide gauge data, flattened peaks of wave crests are observed, especially for the second and third waves. Hence the error estimates are made after visual extrapolation of the flattened peaks (see Table III–16).

(d) It is seen from RMS error estimates spanning four wave crests covering a duration of more than 2 hours that, RMS error is within 20% after application of time offset of about 200 seconds (after eight hours of tsunami travel time), which is considered a good numerical prediction as per applicable acceptance criteria (see Section 2.3.2).

(e) It can be summarized that in general, the estimated times of arrival of the wave as well as amplitudes are in line with the acceptance criteria error band (20% for field data) as defined in Section 2.3.2. It is expected that with the use of elements such as refined source models, higher resolution numerical models, bathymetric data and interaction of tsunamis with tide, it might be possible to achieve better results including results for wave troughs.

REFERENCES TO ANNEX III

[III-1] SUGINO, H., WU, C., KORENAGA, M., NEMOTO, M., IWABUCHI, Y., EBISAWA, K., Analysis and verification of the 2011 Tohoku earthquake tsunami at nuclear power plant sites, The Journal of JAEE, **13** 2 (2013) 2–21 (in Japanese).

[III-2] FUJII, Y., SATAKE, K., SAKAI, S., SHINOHARA, M., KANAZAWA, T., Tsunami source of the 2011 off the Pacific coast of Tohoku Japan earthquake, Earth Planets Sp. **63** 7 (2011) 815–820.

[III-3] MANSINHA, L., SMYLIE, D.E., The displacement fields of inclined faults, Bull. Seismol. Soc. Am. **61** 5 (1971) 1433–1440.

[III-4] SUGINO, H., IWABUCHI, Y., EBISAWA, K., NEMOTO, M., KORENAGA, M., Investigation of mechanisms causing ground motion and tsunami due to the 2011 Tohoku earthquake at nuclear power plant sites, Fifteenth World Conference on Earthquake Engineering, Lisbon (2012).

[III-5] MORI N., TAKAHASHI T. and the 2011 Tohoku Earthquake Tsunami Joint Survey Group, Nationwide post-event survey and analysis of the 2011 Tohoku earthquake tsunami, Coastal Engineering J., **54** 1 (2018) 1-27.

[III-6] OKADA, Y., Surface deformation due to shear and tensile faults in a half-space, Bull. Seismol. Soc. Am., **75** (1985) 1135-1154.

[III-7] SATAKE, K., Linear and nonlinear computations of the 1992 Nicaragua earthquake tsunami, Pure and Appl. Geophys., **144** (1995) 455-470.

[III-8] AMANTE, C., EAKINS B. W., ETOPO1 1 Arc-Minute Global Relief Model: Procedures, Data Sources and Analysis, NOAA Technical Memorandum NESDIS NGDC-24, NOAA (2009).

[III-9] MARKS, K.M., SMITH, W.H.F., An evaluation of publicly available global bathymetry grids, Marine Geophys. Researches **27** 1 (2006) 19–34.

[III-10] IMAMURA, F., YALCINER, A.C., OZYURT, G., Tsunami modelling manual (2006).

[III-11] TITOV, V.V., GONZALEZ, F.I., Implementation and testing of the Method of Splitting Tsunami (MOST) model, NOAA Technical Memorandum ERL PMEL-112, NOAA, Seattle, WA (1997).

[III-12] LIU, P.L.F., WOO, S.B., CHO, Y.S., COMCOT Computer Programs for Tsunami Propagation and Inundation (1998).

[III-13] YALCINER, A.C., PELINOVSKY, E., ZAYTSEV, A., KURKIN, A., OZER, C., KARAKUS, H., NAMI DANCE Manual, Middle East Technical University, Civ. Eng. Dep., Ocean Eng. Res. Cent., Ankara (2006).

[III-14] INTERNATIONAL ATOMIC ENERGY AGENCY, IAEA Extra Budgetary Project (EBP) on Protection of Nuclear Power Plants against Tsunamis and Post Earthquake Considerations in The External Zone (TiPEEZ), Final Report, IAEA-EBP-TS-004, IAEA, Vienna (2010).

[III-15] JAPAN NUCLEAR ENERGY SAFETY ORGANIZATION, Tsunami Code Manual, JNES, Tokyo (2014).

[III-16] ROSHAN, A.D., Benchmark analysis of JNES software: Experience feedback from AERB, Kick-off Meeting of Tsunami Hazards Work Area, Vienna (2011).

[III-17] ROSHAN, A.D., BASU, P.C, JANGID, R.S., Performance evaluation of some tsunami numerical models for far field propagation of 2011 tsunami, International Tsunami Symposium (ITS), Göcek and Rodos (2013).

[III-18] JAPAN NUCLEAR ENERGY SAFETY ORGANIZATION, Tsunami Simulation Code, Tsunami Manual, JNES, Tokyo (2012).

[III-19] INAZU, D., SAITO, T., Simulation of distant tsunami propagation with a radial loading deformation effect, Earth Planets Space **65** (2013) 835–842.

[III-20] WANG, X., User manual for COMCOT version 1.7 (2009).

[III-21] WATADA, S., KUSUMOTO, S., SATAKE, K., Cause of Travel-Time Difference between Observed and Synthetic Waveforms of Distant Tsunami, International Tsunami Symposium (ITS), Göcek and Rodos (2013).

ANNEX IV: SUPPLEMENTARY FILES

The supplementary files for this publication can be found on the publication's individual web page at www.iaea.org/publications.

The files provided in the supporting material are related to the input of the analytical benchmark – 1 and 2, respectively, and to the data collected in the laboratory test that were used for comparison with the numerical results.

The details on the file content available in the supporting material are provided in tables embedded in the text and listed below:

1. Input data for analytical benchmark – 1: Table I–1
2. Input data for analytical benchmark – 2: Table I–2
3. Data from laboratory experiments: Table II–1

CONTRIBUTORS TO DRAFTING AND REVIEW

Abe, H.	Nuclear Regulation Authority, Japan
Azuma, K.	Nuclear Regulation Authority, Japan
Bugaev, E. G.	Federal Environmental, Industrial and Nuclear Supervision Service, Russian Federation
Chaytor, J.	United States Geological Survey, United States of America
Comerci, V.	Instituto Superiore per la Protezione e la Ricerca Ambientale, Italy
Contri, P	International Atomic Energy Agency
Costa, A.	Instituto Nazionale di Geofisica e Vulcanologia, Italy
Di Manna, P.	Instituto Superiore per la Protezione e la Ricerca Ambientale, Italy
Ebisawa, K.	Central Research Institute of Electric Power Industry, Japan
Fujii, N.	Tokyo Electric Power Services, Japan
Geist, E.	United States Geological Survey, United States of America
Ghosh, A. K.	Bhabha Atomic Research Centre, India
Godoy, A. R.	Consultant, Argentina
Hibino, K.	International Atomic Energy Agency
Hebert, H.	Commissariat à l'énergie atomique et aux énergies alternatives, France
Henkel, F. O.	WOELFEL Beratende Ingenieure GmbH + Co. KG, Germany
Hussain, J.	Pakistan Atomic Energy Commission, Pakistan
Hyun, S. G.	Korea Institute of Nuclear Safety, Korea, Republic of
Imamura, F.	Tohoku University, Japan
Iwabuchi, Y.	Nuclear Regulation Authority, Japan
Jin, S.	Korea Institute of Nuclear Safety, Korea, Republic of
Jones, H.	Nuclear Regulatory Commission, United States of America
Kanoğlu, U.	Middle East Technical University, Turkey

Khan, Z. A.	Pakistan Atomic Energy Commission, Pakistan
Kim, M. K.	Korea Atomic Energy Research Institute, Korea, Republic of
Lynett, P.	University of Southern California, United States of America
Matsuyama, M.	Central Research Institute of Electric Power Industry, Japan
Mian, M. T.	Pakistan Atomic Energy Commission, Pakistan
Mori, K.	Nuclear Regulation Authority, Japan
Morita, S.	International Atomic Energy Agency
Nishizaki, S.	International Atomic Energy Agency
Noguchi, Y.	International Atomic Energy Agency
Nomura, S.	International Atomic Energy Agency
Park, S. H.	Korea Hydro & Nuclear Power Co., Korea, Republic of
Pisharady, A. S.	Atomic Energy Regulatory Board, India
Rastogi, R.	Bhabha Atomic Research Centre, India
Roshan, A. D.	Atomic Energy Regulatory Board, India
Samaddar, S. K.	International Atomic Energy Agency
Satake, K.	University of Tokyo, Japan
Sato, T.	Nuclear Regulation Authority, Japan
Schindele, F.	Commissariat à l'énergie atomique et aux énergies alternatives, France
Sharma, P. K.	Bhabha Atomic Research Centre, India
Sugino, H.	Nuclear Regulation Authority, Japan
Suzuki, Y.	Japan Nuclear Safety Institute, Japan
Takao, M.	Tokyo Electric Power Company, Japan
Titov, V.	United States National Ocean and Atmospheric Administration, United States of America
Vasilievich, Y. V.	ROSENERGOATOM, Russian Federation

Viallet, E.	Electricité de France, France
Viana-Baptista, M. A.	Instituto Superior de Engenharia de Lisboa, Portugal
Vittori, E.	Instituto Superiore per la Protezione e la Ricerca Ambientale, Italy
Watanabe, K.	International Atomic Energy Agency
Wu, C.	Nuclear Regulation Authority, Japan
Yalcıner, A. C.	Middle East Technical University, Turkey
Yanagisawa, H.	Tohoku Gakuin University, Japan
Yanagisawa, K.	Tokyo Electric Power Company, Japan

Consultants Meetings

Vienna, Austria: 10 April 2013, 15 April 2015

Antalya, Turkey: 30 April – 1 May 2013

Göcek, Turkey: 1–3 October 2013

Mumbai, India: 8–10 December 2014

IAEA
International Atomic Energy Agency

No. 26

ORDERING LOCALLY

IAEA priced publications may be purchased from the sources listed below or from major local booksellers.

Orders for unpriced publications should be made directly to the IAEA. The contact details are given at the end of this list.

NORTH AMERICA

Bernan / Rowman & Littlefield

15250 NBN Way, Blue Ridge Summit, PA 17214, USA
Telephone: +1 800 462 6420 • Fax: +1 800 338 4550

Email: orders@rowman.com • Web site: www.rowman.com/bernan

REST OF WORLD

Please contact your preferred local supplier, or our lead distributor:

Eurospan Group

Gray's Inn House
127 Clerkenwell Road
London EC1R 5DB
United Kingdom

Trade orders and enquiries:

Telephone: +44 (0)176 760 4972 • Fax: +44 (0)176 760 1640
Email: eurospan@turpin-distribution.com

Individual orders:

www.eurospanbookstore.com/iaea

For further information:

Telephone: +44 (0)207 240 0856 • Fax: +44 (0)207 379 0609
Email: info@eurospangroup.com • Web site: www.eurospangroup.com

Orders for both priced and unpriced publications may be addressed directly to:

Marketing and Sales Unit
International Atomic Energy Agency
Vienna International Centre, PO Box 100, 1400 Vienna, Austria
Telephone: +43 1 2600 22529 or 22530 • Fax: +43 1 26007 22529
Email: sales.publications@iaea.org • Web site: www.iaea.org/publications

21-02316E

International Atomic Energy Agency
Vienna